POLYOXOMETALATES

Open Access
REVIEW ARTICLE

Recent advances and future research directions in polyoxometalate-based water electrolysis for hydrogen production

Houen Zhu[1,§], Shumao Yuan[1,§], Yafu Wang[1,§], Zhihua Zhang[1], Zhenlin Zhao[2], Ke Yang[1], Zhencheng Feng[1], Jianqi Lu[1], Xiangyu Liu[1], Fanchentao Sun[1], and Jiangwei Zhang[1,3]

[1] *College of Energy Material and Chemistry; Inner Mongolia Key Laboratory of Low Carbon Catalysis; Inner Mongolia Advanced Research Institute; Inner Mongolia University, Hohhot 010021, China*
[2] *WellRun Technology Co., Ltd, Beijing 100000, China*
[3] *Key Laboratory of Advanced Energy Materials Chemistry, Nankai University, Tianjin 300071, China*
[§] *Houen Zhu, Shumao Yuan, and Yafu Wang contributed equally to this work.*

Cite This: *Polyoxometalates*, **2026**, *5*, 9140112

Read Online

ABSTRACT: Hydrogen energy, as a clean, efficient, and renewable secondary energy carrier, plays a pivotal role in the global energy transition and the achievement of "dual carbon" goals. Among the various hydrogen production pathways, water electrolysis has emerged as the most promising approach for green hydrogen generation owing to its zero carbon emissions during operation and the high purity of the hydrogen produced. However, conventional electrolysis technologies depend heavily on noble-metal catalysts, such as platinum and iridium oxide, whose high cost and limited abundance severely restrict large-scale industrial deployment. Therefore, the development of high-performance, durable, and cost-effective catalysts for water electrolysis remains a critical challenge for the advancement of hydrogen energy technologies. Polyoxometalates (POMs), a class of nanoscale metal–oxygen clusters composed of transition metals such as molybdenum and tungsten, have emerged as promising alternatives owing to their diverse redox states, molecular-level tunability, high negative charge density, and excellent structural stability. This review systematically elucidates the advantages of POM-based materials for both the hydrogen evolution reaction and the oxygen evolution reaction in water electrolysis. By integrating recent advances, it summarizes diverse strategies aimed at overcoming the current limitations of POM electrocatalysts. Finally, the review discusses the opportunities and challenges associated with using POM compounds to enhance water electrolysis performance for hydrogen production and, by synthesizing state-of-the-art research directions, and provides an outlook on future trends in this rapidly developing field.

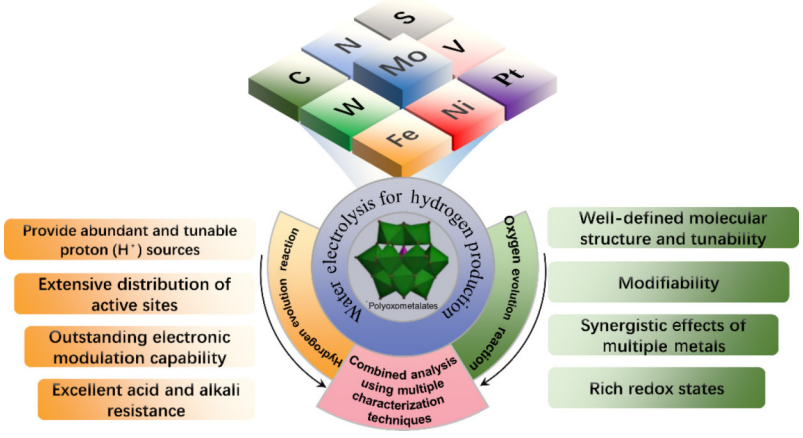

KEYWORDS: polyoxometalate, water electrolysis, hydrogen evolution reaction, oxygen evolution reaction, sustainable energy

1 Introduction

As the global energy system accelerates its transition toward green and low-carbon development, water electrolysis technology for the hydrogen evolution reaction (HER) and oxygen evolution reaction (OER) has been widely recognized as a key strategy for achieving carbon neutrality, serving as a crucial platform for renewable energy conversion and storage [1–4]. However, the heavy reliance on traditional noble-metal catalysts, such as Pt/C and IrO_2, has become a major bottleneck for large-scale application owing to their high cost and limited natural abundance [5, 6]. Therefore, the development of non-precious-metal catalysts that combine high efficiency, long-term stability, and cost-effectiveness has emerged as an urgent research priority in this field [7, 8].

Nanoclusters, as polynuclear aggregate structures that bridge atoms, molecules, and macroscopic solids, possess well-defined atomic compositions and chemical architectures, representing an early stage of condensed matter [9, 10]. As ideal model systems for correlating macroscopic properties with microscopic structures, nanoclusters are of fundamental importance for deepening the

Received: October 28, 2025; **Revised:** December 21, 2025
Accepted: December 31, 2025

Address correspondence to zjw11@tsinghua.org.cn, jwz@imu.edu.cn

https://doi.org/10.26599/POM.2026.9140112

understanding of material transformation mechanisms and constitute a pivotal concept in the size regime of nanomaterials [11, 12]. Among the diverse classes of nanocluster materials, polyoxometalates (POMs) and noble-metal nanoclusters are particularly prominent, representing two major research pillars in this field [13, 14]. POMs are nanoscale metal–oxygen clusters composed of transition metals (such as W, Mo, and V) interconnected by oxygen atoms through covalent bonds. Their distinctive and highly tunable structures, rich redox chemistry, and molecular-level functionalization capability collectively endow POM-based materials with considerable potential for electrocatalytic applications (Fig. 1) [15–17]. In recent years, accurate modulation of the chemical composition of POMs (such as heteroatom incorporation), rational design of their spatial architectures (e.g., Keggin- and Dawson-type structures), and optimization of the interfacial environment (e.g., integration with carbon-based materials or metal–organic frameworks, MOFs) have collectively enabled remarkable catalytic performance. Extensive studies have demonstrated their outstanding activity in acid catalysis (including hydrolysis, dehydration, and cyanohydrination reactions), oxidation catalysis (such as desulfurization and epoxidation), as well as photo- and electrocatalysis, encompassing the HER, OER, nitrogen reduction reaction, and carbon dioxide reduction reaction (CO_2RR) [18–22]. Meanwhile, owing to their role as "electron sponges," POMs can modulate the adsorption strength of reaction intermediates via reversible electron-transfer processes during catalysis, thereby effectively alleviating the kinetic limitations associated with conventional catalysts [23]. Thus, POMs serve as a versatile and tailorable catalytic platform, offering substantial research value in energy conversion and environmental catalysis.

However, despite the substantial progress achieved with POMs in water electrolysis, their practical application still faces several critical bottlenecks. (1) Structural stability challenges: During water electrolysis, POM clusters used as catalysts may suffer from stability issues, particularly under prolonged operating conditions, where degradation or deactivation can occur, considerably limiting their practical viability [9, 24]. (2) Charge transport limitations: Although POMs offer abundant active sites, their intrinsically low electrical conductivity can impede efficient electron transfer, thereby constraining overall electrocatalytic performance [25]. (3) Catalytic activity limitations: Compared with platinum-based catalysts, POMs generally exhibit lower intrinsic catalytic activity, especially at high current densities, where their HER performance remains relatively modest [26]. Unclear catalytic mechanisms: The dynamic structural evolution of POMs during electrocatalysis, as well as the accurate nature of their true active sites in complex electrolyte environments, remains insufficiently understood [27]. Therefore, a comprehensive understanding of POM catalytic behavior requires in-depth investigations combining *in situ* characterization techniques with theoretical calculations to elucidate reaction pathways, thereby guiding rational structural design and performance optimization [28]. In response to these challenges, recent research has exhibited two major trends. On the one hand, molecular engineering strategies and nanocomposite approaches have been used to enhance the intrinsic activity and stability of POM-based catalysts. On the other hand, advanced *in situ* and operando analytical techniques have been increasingly applied to elucidate structure–performance relationships, providing critical theoretical insights for the rational design of efficient and cost-effective POM-based electrocatalysts [29–31].

This review aims to provide a comprehensive overview of recent advances and development trends in POM-based materials for water electrolysis, with particular emphasis on the following key aspects: (1) design principles of POM-based catalysts and the fundamental mechanisms governing their activity and stability in the OER and HER [3, 32]; (2) interfacial engineering strategies involving POMs and advanced support materials, along with the associated synergistic enhancement mechanisms [33]; (3) performance optimization strategies for POM-based water

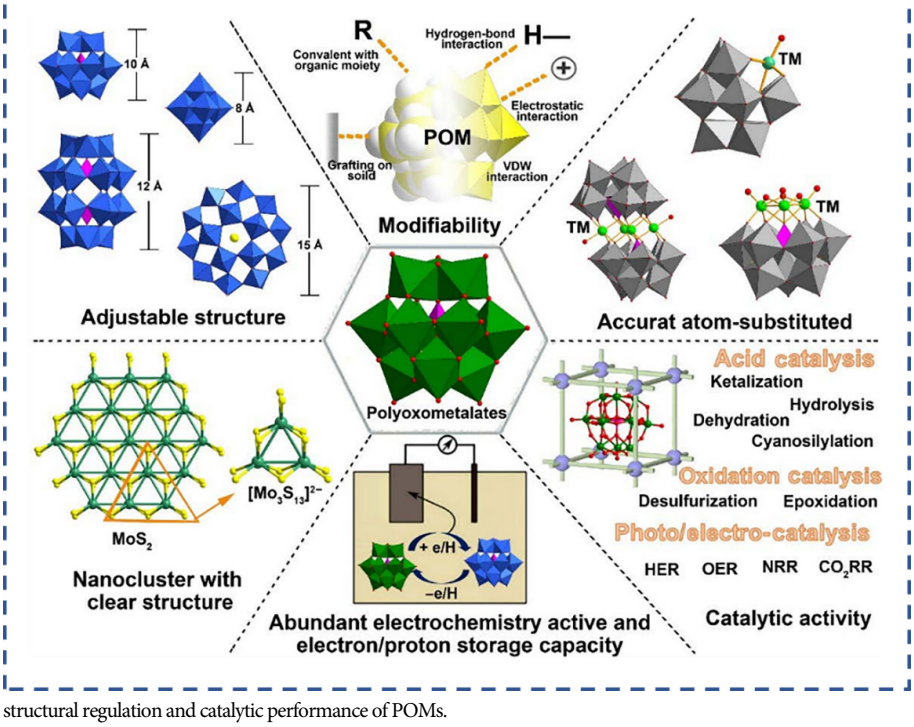

Figure 1 Schematic of the structural regulation and catalytic performance of POMs.

electrolysis systems in practical application scenarios [34]; (4) current research challenges and future development directions (e.g., analysis of dynamic mechanisms) [17, 35]. By combining experimental advances with theoretical insights, this review aims to offer new perspectives on the electrocatalytic functionalization of POM-based materials and to accelerate the practical deployment of green hydrogen energy technologies.

2 Overview of POMs

POMs exhibit diverse and complex architectures. Their chemical composition is primarily based on transition metals such as Mo, W, V, Nb, and Ta, which serve as fundamental building blocks to form metal–oxide clusters coordinated by oxygen atoms. These frameworks can incorporate a variety of heteroatoms (e.g., P, As, B, Al, Si, Ge, and S) as central templates around which the clusters are organized [36, 37]. POMs are made from earth-abundant and cost-effective metal ions. In their complex anionic frameworks, each cluster consists of corner-sharing and edge-sharing pseudo-octahedral MO_6 units (where M = Mo, W, V, or Nb), which act as the core building blocks of the assembly [38, 39]. POMs exhibit diverse dimensions and distinct architectural configurations [40]. To date, six primary POM configurations have been identified, as shown in Fig. 2 [41]: Keggin-type [42], Dawson-type [43], Lindqvist-type [44], Anderson-type [45], Waugh-type [46], and Silverton-type [47]. This structural diversity enables tunable metal nuclearity, oxygen coordination, and ligand-field environments, allowing accurate control over the electronic structures and redox properties of POM clusters. Such configurational flexibility is difficult to achieve in conventional inorganic solids, highlighting the unique design versatility of POM-based systems. A key feature of POMs is their reversible multi-electron transfer capability. For instance, the Keggin-type $[PW_{12}O_{40}]^{3-}$ anion exhibits a W^{6+}/W^{5+} redox couple that can undergo stepwise multi-electron reduction over a wide potential range (from −0.8 to −0.2 V vs. RHE), with each molecule capable of accepting up to six electrons without structural collapse [48]. This "electron sponge" property allows POMs to effectively modulate electron density at the electrode interface, alleviate charge accumulation during reactions, reduce overpotential, and enhance the kinetics of multi-electron reactions. Acting as an electron relay, POMs facilitate electron transfer from the electrode to active sites in heterogeneous catalytic systems, making them highly promising and robust electrocatalysts for various multi-electron processes [49, 50]. Each distinct POM structure exhibits unique electronic configurations and bonding patterns, imparting tunable physicochemical properties [3, 51]. The surfaces of POMs are rich in bridging oxygen (μ_2-O) and terminal oxygen (M=O) atoms, which can act as efficient proton acceptors and transport channels. During the HER, POMs can form hydrogen-bonding networks with protons via their surface oxygen atoms, thereby lowering the proton-binding energy barrier and promoting the Volmer step ($H^+ + e^- \rightarrow H^*$) [52]. Owing to their intrinsic Brønsted acidity and tunable pKa values, POMs retain structural integrity and catalytic activity in acidic, neutral, and alkaline electrolytes [53]. Moreover, POMs possess highly ordered molecular structures, with well-defined atomic compositions and spatial configurations that can be accurately resolved by single-crystal X-ray diffraction analysis [54].

POMs possess multiple atomic-scale active sites, and their composition and confinement strategies can be adapted to various material systems, including porous materials (organic, inorganic, and hybrid), layered materials with different charge characteristics, and nanotube architectures (Fig. 3) [55]. Tubular materials, such as carbon nanotubes (CNTs), with their hollow structures, can confine POMs in their inner cavities through electrostatic interactions, thereby improving both electrical conductivity and dispersion stability [3, 56–58]. Layered materials, such as layered double hydroxides (LDHs) and graphene, can accommodate POMs through intercalation into interlayer spaces, which enhances active-site exposure and prevents aggregation [59–62]. Porous materials, including molecular sieves with ordered pore structures, can confine POMs in channels via physical adsorption or chemical bonding, thereby improving both stability and catalytic efficiency [63–65]. The intrinsic structural diversity of POMs provides pronounced chemical tunability and excellent electron-accepting capacity, which underlies their suitability for constructing a wide range of functional electrocatalytic systems [49]. To fabricate POM-based composites, researchers have developed multiple synthetic strategies, including molecular bridging, hybridization with micro- or nanosized particles, and incorporation of nanolayered or bulk

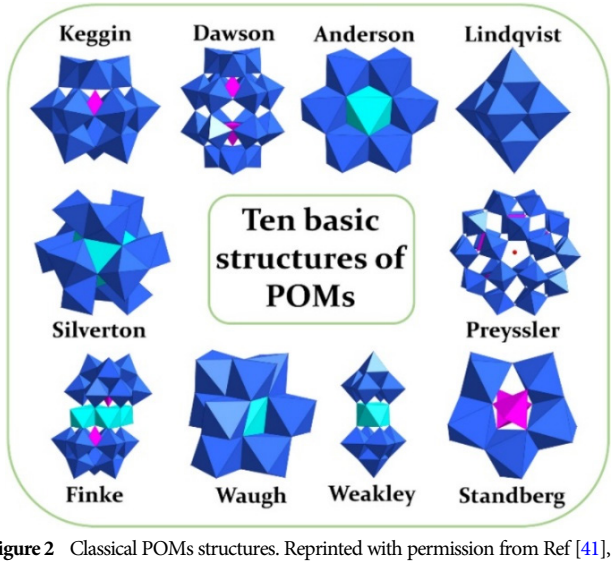

Figure 2 Classical POMs structures. Reprinted with permission from Ref [41], © Elsevier B.V. 2024.

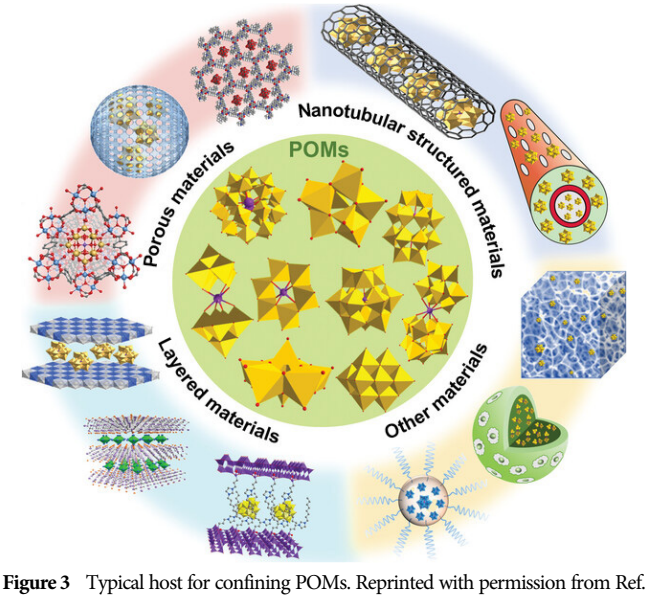

Figure 3 Typical host for confining POMs. Reprinted with permission from Ref. [55], © Wiley-VCH GmbH 2023.

components [66]. In recent years, continuous advances in synthetic methodologies have resulted in a broad and versatile toolkit, including ion-exchange reactions, oxidative polymerization, supramolecular-confinement-assisted pyrolysis, soft-template-directed growth, direct solid-state transformations, encapsulation strategies, sol–gel chemistry, magnesiothermic reduction, electrochemical etching, charge-mediated self-assembly, hot pressing in the solid phase, inkjet printing, interfacial engineering, and even single-molecule confinement techniques [25, 67–69]. These strategies not only expand the versatility of POM integration but also provide tailored conditions for immobilizing POMs on conductive substrates via electrostatic interactions, covalent linkages, supramolecular assembly, dip-coating, electrodeposition, electrophoretic deposition, drop-casting, ultrasound-assisted loading, hydrothermal or solvothermal crystallization, and sequential layer-by-layer deposition (Fig. 4) [70–72]. Importantly, the development of these methodologies represents not only a technical expansion in synthetic chemistry but also a shift toward accurate control of POM–substrate interfaces, which is crucial for optimizing catalytic activity and long-term stability in electrochemical applications.

POMs not only function as direct molecular catalysts but also represent a highly promising class of precursors for the construction of high-performance non-precious metal electrocatalytic materials, including transition metal carbides (TMCs), sulfides (TMS), phosphides (TMPs), and nitrides (TMNs) [73–77]. Their molecular-level accuracy and uniformity provide exceptional control over chemical composition and enable atomic-precision doping in the derived materials. The tunable nanostructures of POMs impart inherent self-templating capabilities, facilitating the synthesis of active phases with uniform dimensions, well-defined morphologies, and high dispersion, thereby effectively mitigating nanoparticle agglomeration [78]. Moreover, POMs themselves, along with carbon-thermal reduction processes, enable multidimensional *in situ* heteroatom doping (for example, with phosphorus or nitrogen), which modulates the electronic structure of the carbon matrix or metal active phases and optimizes the adsorption energetics of reaction intermediates[79]. Using POMs or POM-based frameworks as precursors also allows for the direct construction of heterojunction structures with well-defined interfaces, where synergistic interactions between components considerably enhance catalytic performance [56, 80]. Collectively, these unique advantages establish POMs as a powerful platform for the accurate design and controllable synthesis of high-performance electrocatalysts at the atomic level [81].

3 POM-based catalysts for HER

HER, serving as the cathodic half-reaction in water splitting, represents a critical step in sustainable clean hydrogen energy conversion [82]. In HER catalysis, the atomically defined metal centers of POMs provide a clear correlation between geometric configuration and hydrogen-binding energetics. Their tunable redox states allow accurate adjustment of the hydrogen adsorption free energy (ΔG_H), addressing the limitations of conventional heterogeneous catalysts, which often have ill-defined or reconstruction-prone active sites. In acidic media, HER proceeds through a proton–electron coupling process via a two-electron transfer mechanism, whereas in alkaline systems it also requires overcoming the activation barrier associated with water molecules [83, 84]. HER typically follows either the Volmer–Heyrovský or Volmer–Tafel pathway, both of which involve adsorption and subsequent conversion of hydrogen intermediates. As shown in Fig. 5, in acidic media, the reaction begins with proton–electron coupling to form adsorbed hydrogen (H^*, Volmer step), followed by electrochemical desorption or H^*–H^* recombination to generate molecular hydrogen. In alkaline systems, an additional water dissociation step is required, making the overall reaction intrinsically slower. For POM-based catalysts, the metal–oxygen framework provides abundant bridging and terminal oxygen sites that effectively stabilize H^* intermediates. High-valence metal centers promote rapid electron transfer, while the polyanionic structure facilitates proton accommodation and optimizes the ΔG_{H^*}. When coupled with conductive substrates, POMs further benefit from improved charge transport and tuned intermediate binding energies, resulting in accelerated HER kinetics [85]. Although HER has a low theoretical overpotential, its practical

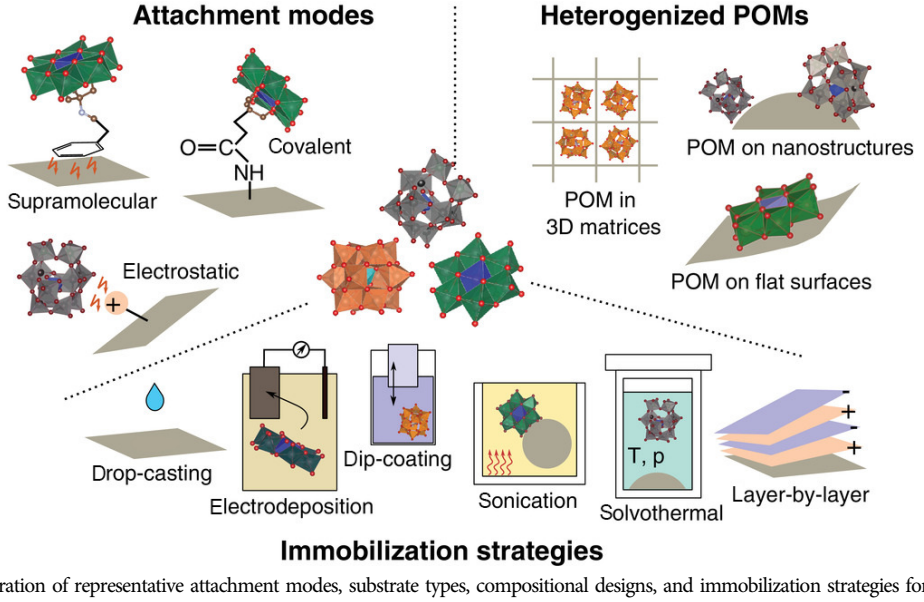

Figure 4 Schematic illustration of representative attachment modes, substrate types, compositional designs, and immobilization strategies for POM-based composites. Reprinted with permission from Ref. [70], © Cherevan A. S. et al. 2020.

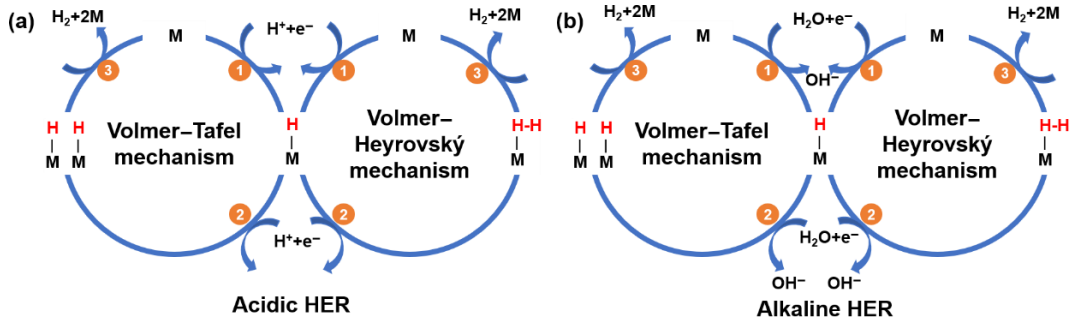

Figure 5 Schematic illustration of the HER pathways in acidic and alkaline media.

reaction rate is often limited by the adsorption behavior of intermediates, charge transport efficiency, and the electronic structure of the catalyst surface [86]. Therefore, the design of highly efficient HER catalysts to accelerate reaction kinetics and reduce energy consumption is of paramount importance for advancing the practical implementation of water electrolysis technologies [87–89].

In the field of HER electrocatalysts, Pt-based materials, such as Pt/C, are widely regarded as benchmark references owing to their nearly thermoneutral hydrogen adsorption free energy. However, the high cost and limited natural abundance of platinum severely restrict its large-scale application in sustainable hydrogen production [84, 85]. Therefore, developing non-noble-metal HER catalysts that are low-cost, highly active, and structurally robust has become a major research focus [90, 91]. The exploration of earth-abundant, non-precious metal catalysts with high catalytic efficiency and long-term durability has emerged as a key direction in the field [92, 93]. In recent years, POMs have demonstrated unique advantages for HER catalysis owing to their tunable structures, high redox activity, and multi-center electron transfer capabilities [15, 94]. Their rich charge distribution and multi-electron transfer properties enable effective electron transport and accurate regulation of reaction intermediates during HER processes [95]. The metal centers in POMs, such as Mo^{6+} and W^{6+}, provide synergistic pathways for proton adsorption and electron transfer, promoting the formation and dissociation of hydrogen intermediates and lowering reaction energy barriers [19, 96]. Sun et al. synthesized five structurally precise Keggin-type polyniobate analogues, including Na-$GeNb_{12}$, Cu-$GeNb_{12}$, GeV_2Nb_{12}, V_3Nb_{12}, and SiV_2Nb_{12}. By combining electrochemical measurements, *in situ* Raman spectroscopy, and density functional theory (DFT) calculations, they identified the bridging oxygen atoms in PONbs as the primary active sites for HER [97]. Compared with surface modification or counterion substitution, replacing Ge^{4+} or Si^{4+} with V^{5+} (e.g., in V_3Nb_{12}) considerably decreased the hydrogen adsorption free energy and enhanced electron conductivity, resulting in an HER overpotential as low as 121 mV and a turnover frequency of 9.51 h^{-1}. Additionally, the bridging and terminal oxygen sites in POM structures can be tuned to optimize the Gibbs free energy of hydrogen adsorption, further improving catalytic performance [98] (Table 1).

Table 1 POM-based and POM-derived Electrocatalysts for HER

Catalysts	Polyoxometalate	Tafel slope (mV·dec⁻¹)	η_{10}[a] (mV)	Electrolyte	Ref.
CoMoS@CN	$(NH_4)_6Mo_7O_{24}·4H_2O$	62/33	95/164	1 M KOH/0.5 M H_2SO_4	[5]
CoP/MoP@NC/CC	$[PMo_{12}O_{40}]^{3-}$	40	94	1.0 M KOH	[75]
C-MoP-0.1	$[PMo_{12}O_{40}]^{3-}$	56.9	82	1.0 M KOH	[109]
POM@ZnCoS/NF	$[PMo_{12}O_{40}]^{3-}$	53.5	170	1.0 M KOH	[110]
CNT-g-PSSCo/PW_{12}	$[PMo_{12}O_{40}]^{3-}$	25	31	0.5 M H_2SO_4	[135]
Pt_1-Mo_2C-C	$[PMo_{12}O_{40}]^{3-}$	64	155	1.0 M KOH	[154]
Pt-Cu/Mo_2C	$[PMo_{12}O_{40}]^{3-}$	28.2	12.9	0.5 M H_2SO_4	[155]
N@Mo_2C-3/CFP	$[Mo_6O_{19-n}(NAr)_n]^{2-}$	49/51	66/56	1 M KOH/0.5 M H_2SO_4	[156]
3D Mo_2C	$[PMo_{12}O_{40}]^{3-}$	73.9	110	1.0 M KOH	[159]
Ni/N-Mo_2C@C	$[NiMo_6O_{21}\{(CH_2O)_3CNH_3\}]^{3-}$	82	148	1.0 M KOH	[161]
P-W_2C@NC	$[PMo_{12}O_{40}]^{3-}$	53	89	0.5 M H_2SO_4	[164]
CoS_2-MoS_2	$(NH_4)_6[Co_2Mo_{10}O_{38}H_4]$	64/71	120/153	1 M KOH/0.5 M H_2SO_4	[177]
MoS_2/CoS_2@Ni_3S_2/Ni_3Se_2	$(C_3H_5N_2)_6[CoMo_{12}O_{40}]·10H_2O$	83	54	1 M KOH	[179]
Ni-Mo-S-rGO	$[GeMo_{12}O_{40}]^{4-}$	132.2	118	1 M KOH	[180]
h-MoN@BNCNT	$(NH_4)_6Mo_7O_{24}·4H_2O$	46/59	78/118	1 M KOH/0.5 M H_2SO_4	[185]
$NiMoO_4$@NiMoS@Ni_2P	$[Mo_7O_{24}]^{6-}$	65.7	72	1.0 M KOH	[187]
P–MoP@C	$[PMo_{12}O_{40}]^{3-}$	98/86	149/162	1 M KOH/0.5 M H_2SO_4	[199]
LPOM@EtPZn	$[V_6O_{19}]^{8-}$	115	20.4	1.0 M KOH	[207]
PtW/SNC	$[H_3PtW_6O_{24}]^{5-}$	41	29.4	1.0 M KOH	[208]

[a]Overpotential at the current density of 10 mA·cm⁻².

Although POMs show great potential in the HER field owing to their tunable molecular structures and remarkable multi-electron transfer capabilities, their use as standalone catalysts remains associated with significant challenges. The inherently poor electrical conductivity of most POMs limits efficient charge transport during electrocatalytic processes, thereby constraining current density and reaction kinetics [99]. The main limitation stems from their inherently low electrical conductivity, leading to substantial charge-transfer resistance and sluggish reaction kinetics [100]. Structural stability under electrochemical conditions, especially in extreme pH environments, is often compromised, with risks of decomposition or irreversible reduction [101]. As discrete molecular entities, POMs typically have small specific surface areas and limited accessibility of active sites, and inadequate immobilization on electrode surfaces can lead to detachment from substrates [102]. In terms of intrinsic catalytic activity, the HER performance of POMs generally remains lower than that of benchmark noble-metal catalysts, and their efficiency is strongly dependent on electrolyte pH, restricting broader applicability [103]. Finally, complex synthesis procedures and high production costs pose considerable constraints on their economic viability and scalability for large-scale implementation [104].

3.1 Effects of metal centers and extrinsic modulation on HER performance

The catalytic performance of POM-based materials in the HER is fundamentally determined by the type and arrangement of metal centers in their molecular frameworks. These metal centers, typically high-valence transition metals, act not only as electron reservoirs and redox-active sites but also regulate the adsorption of hydrogen intermediates and influence electron transfer kinetics [105]. Beyond the primary framework metals, introducing extrinsic atoms or partially substituting with transition metals such as Co, Ni, and Fe is an effective approach to modulate electronic structures and enhance catalytic activity [106]. DFT studies on representative α-Keggin-type mixed-metal polyoxoanions $[PW_{11}O_{39}ME]^{4-}$ (M = Nb, Ta; E = O, S, Se) show that introducing chalcogen terminal atoms at the M = Nb/Ta positions simultaneously fine-tunes the acceptor orbital energy levels of the cluster and adjusts the acidity of external oxygen sites. In alkaline media, the HER is kinetically limited by the Volmer step, in which water adsorption and dissociation require substantial energy owing to the lack of free protons. The structural features of POMs offer distinct advantages in overcoming this limitation. Terminal M=O groups and bridging μ_2-O sites serve as strong proton-accepting centers, facilitating water polarization and accelerating O–H bond cleavage. In addition, high-valence Mo or W centers increase the electrophilicity of adjacent oxygen atoms, lowering the activation barrier for hydroxide desorption and stabilizing intermediate hydrogen species. Substitution of transition metals (e.g., Co, Ni, or V) in POMs further enhances water activation by increasing local charge density and creating coordinatively unsaturated sites that efficiently couple with proton-coupled electron transfer (PCET) pathways. These synergistic structural and electronic features give POM-based clusters an intrinsic ability to accelerate alkaline water dissociation and overcome the slow Volmer kinetics typically observed in non-noble catalysts [107]. This dual modulation affects both proton adsorption and activation during the Volmer step, as well as the hydrogen–hydrogen coupling kinetics in the subsequent Heyrovsky or Tafel steps [108]. The Nb or Ta centers determine the acidity of external oxygen sites and establish the fundamental electronic baseline, while S or Se substitution increases the proton affinity of external acid sites and narrows the highest occupied molecular orbital (HOMO)–lowest unoccupied molecular orbital (LUMO) energy gap without changing the distribution of reduction centers. This synergistic effect enhances proton adsorption and charge transfer during the Volmer step. Tantalum centers, combined with S or Se terminal atoms, promote the formation of strong acid sites and accelerate proton activation, whereas Nb centers provide a balance between electron supply and moderate proton affinity. This offers an effective strategy for designing POM-based HER catalysts optimized for different pH values and electrolyte environments. For example, Bibi et al. recently reported a supramolecular hybrid material, Hybrid-1, constructed from Co-EDTA and a Ni-Anderson-type POM (Fig. 6(a)) [109]. Hybrid-1, prepared via hydrothermal synthesis, exhibits a well-developed mesoporous structure and large surface area, enabling low overpotentials of 80 mV for HER and 111 mV for OER at a current density of 10 $mA{\cdot}cm^{-2}$. The corresponding Tafel slopes are 45 and 48.8 mV dec^{-1}, respectively (Figs. 6(b) and 6(c)). These electrochemical properties surpass those of many noble-metal-based catalysts. The enhanced electrocatalytic performance arises from synergistic interactions between Co-EDTA and the Ni-Anderson POM, with sodium ions acting as interfacial bridges to facilitate efficient electron transfer. In another example, Gautam et al. constructed a POM-anchored zinc-cobalt sulfide nanowire (POM@ZnCoS NW) bifunctional catalyst on an Ni foam (NF) substrate via a hydrothermal method, achieving a substantial increase in electrochemically active surface area and active site density (Figs. 6(d)–6(f)) [110]. The heterointerface between POM and ZnCoS accelerates charge-transfer kinetics, while the hierarchical porous nanowire architecture promotes bubble release and mass transport. The integrated three-dimensional conductive network further enhances structural stability, achieving a HER Tafel slope of 53.5 $mV{\cdot}dec^{-1}$.

Recent studies have shown that extrinsic doping strategies, including heteroatom incorporation and partial metal-site substitution, can effectively regulate charge distribution, optimize the hydrogen adsorption free energy, and synergistically enhance the intrinsic activity of catalytic centers. Therefore, atomic-level engineering of metal centers and their coordination environments, combined with systematic analysis of the relationships between structure, electronic properties, and catalytic performance, provides a robust framework for the rational design of highly efficient and durable electrocatalysts for hydrogen production via water splitting.

3.2 Effect of POMs architectures and defect engineering on HER performance

Beyond elemental composition, the geometric configuration and defect structures of POMs play critical roles in determining their HER catalytic efficiency [111–113]. Classical structural types, including Keggin, Dawson, Anderson, and Lindqvist, provide diverse coordination environments, surface charge distributions, and active-site accessibility [114]. These structural parameters strongly influence proton diffusion pathways, electron migration, and interactions with substrates. In particular, lacunary POMs—defect-engineered species formed by removing specific metal–oxo units—have attracted considerable attention owing to their enhanced reactivity and their ability to coordinate additional metal atoms or molecules [115]. Furthermore, the dimensionality and structural compactness of POM frameworks considerably influence

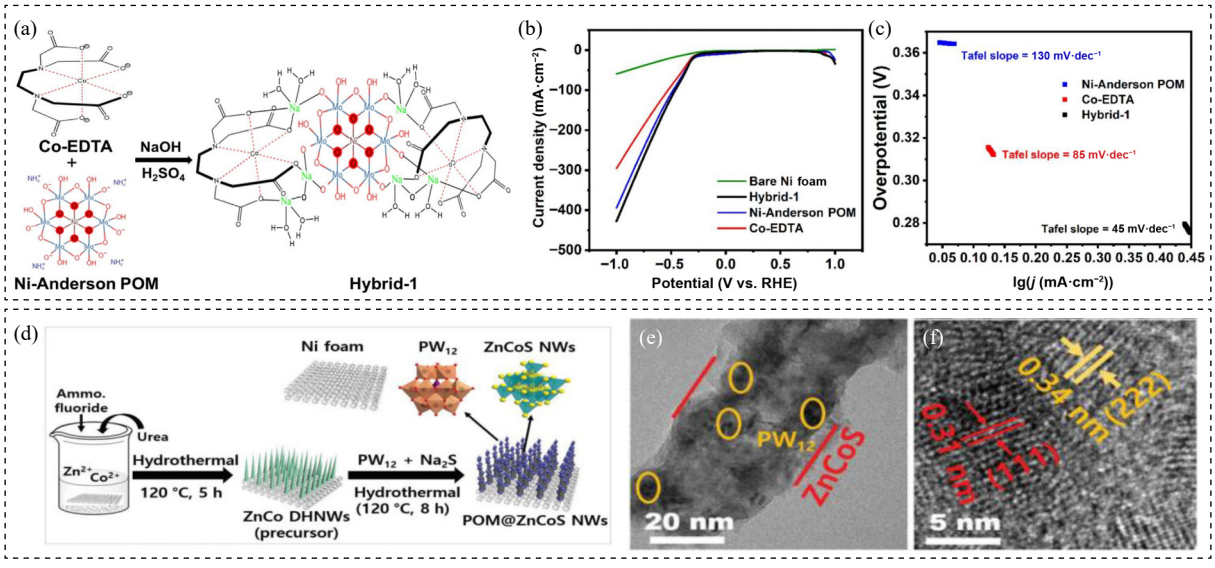

Figure 6 (a) Pictorial illustration of the synthesis of Hybrid-1. (b) Linear sweep voltammetry (LSV) measurements for HER. (c) Tafel plots. Adapted with permission from Ref. [109], © Elsevier Ltd. 2025. (d) Schematic illustration of the synthesis of POM@ZnCoS NWs (color code: WO_6 octahedron, brown; PO_4 tetrahedron, purple; W, black; O, red; ZnS_4/CoS_4 tetrahedron, green; S, yellow; Zn/Co, green). (e) Transmission electron microscopy (TEM) image of POM@ZnCoS NWs at different magnifications. (f) High-resolution TEM (HR-TEM) image of POM@ZnCoS NWs. Reprinted with permission from Ref. [110], © Wiley-VCH GmbH 2021.

electron density distribution and charge delocalization capabilities [116]. Wang et al. successfully synthesized four Keggin-type POM-based coordination polymers (POMCPs) containing different transition-metal centers (Ni, Co, Cd, and Zn) via a hydrothermal method, demonstrating the structural diversity and tunability of POMCPs [117]. Structural analysis showed that Ni-POMCP and Zn-POMCP form three-dimensional and two-dimensional frameworks, respectively, with POM anions embedded in cavities through hydrogen bonding and electrostatic interactions (Figs. 7(a)–7(e)). After optimizing pyrolysis temperatures, the derived materials exhibited excellent HER activity in acidic media. In particular, Ni-POMCP-700, Co-POMCP-700, and Cd-POMCP-800 achieved low overpotentials of 69, 64, and 96 mV at a current density of 10 $mA·cm^{-2}$, respectively, while maintaining long-term operational stability (Figs. 7(f)–7(i)).

Shen et al. developed a strategy using lacunary Keggin-type POMs to anchor ultra-low-loading platinum catalysts. Highly negatively charged trivacant $SiW_9O_{34}^{10-}$ clusters were immobilized on platinum nanoparticle surfaces to form Pt NPs@SiW_9/CNT composite electrocatalysts with a "proton pump" function [118]. The SiW_9 clusters not only stabilized the ultrafine Pt nanoparticles but also enhanced the connectivity of interfacial hydrogen-bonding

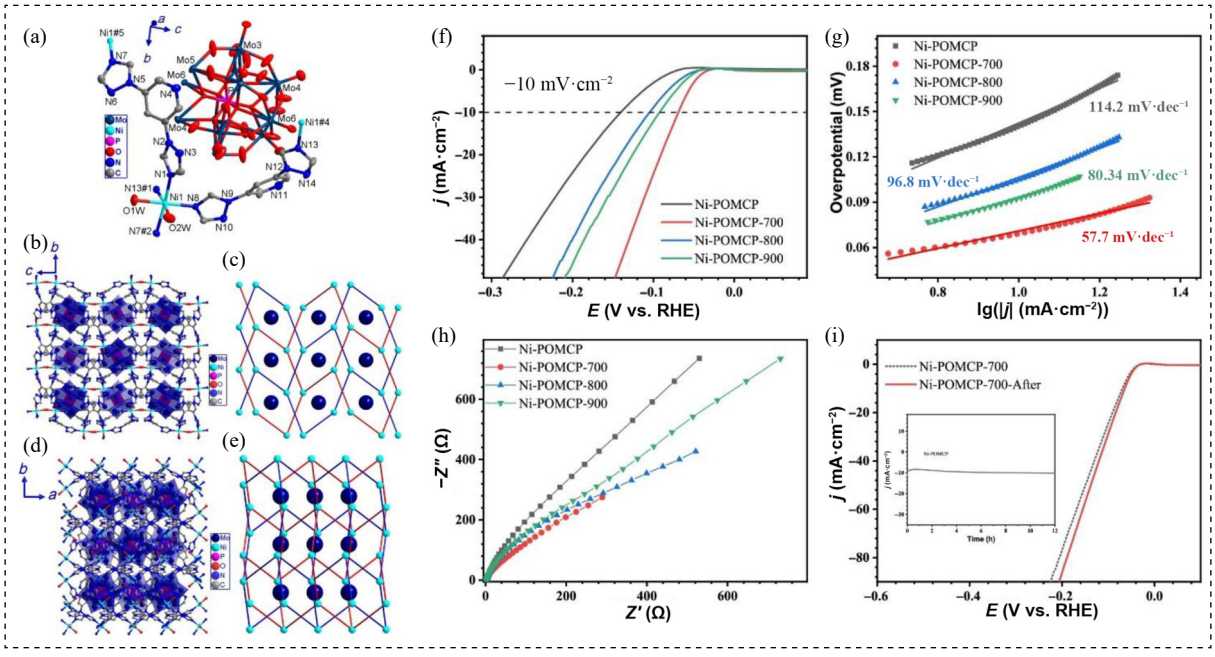

Figure 7 (a) Coordination environment (at 50% probability level) of the Ni(II) centers in Ni-POMCP. (b) and (d) Perspective view of the 3D host–guest supramolecular network in Ni-POMCP along the *a* and *c*-axis, respectively. (c) and (e) Schematic representation of the 2-fold interpenetrating 3D (2,4)-connected framework with a $(12^6)(12^3)$ topology in Ni-POMCP, illustrating the encapsulation of polyoxometalate units within the nanocages. (f) LSV curves, (g) Tafel slope, (h) EIS Nyquist diagram, and (i) LSV curves of Ni-POMCP-700 before and after the chronoamperometric experiment. Reprinted with permission from Ref. [117], © Elsevier B.V. 2025.

networks, facilitating PCET and creating short-path hydrogen spillover pathways. This synergistic effect considerably lowered the proton transport energy barrier under high current density conditions.

The studies discussed above demonstrate that the spatial coordination environments and surface charge distributions of POMs have a direct impact on proton transport efficiency, electron migration, and active-site accessibility. In particular, lacunary POMs, created through defect engineering, not only expose numerous unsaturated coordination sites and provide additional space to accommodate metal atoms after removing specific metal–oxo units, but also optimize the local electronic structure and enhance charge delocalization. These modifications effectively lower the hydrogen adsorption free energy, improve HER reaction kinetics, and enable tunable catalytic activity and stability.

3.3 Composite strategies of POMs with functional materials

Despite their intrinsic redox properties and multi-proton/electron transfer capabilities, the practical application of POMs in HER is limited by two major challenges: inherently low electrical conductivity and structural instability under reductive conditions [119, 120]. To overcome these limitations, composite strategies that integrate POMs with functional materials have been widely used to construct efficient electrocatalytic systems. By coupling POMs with conductive supports—such as NF, CNTs, graphene, or MOFs—synergistic interfaces are formed that facilitate rapid electron transfer, increase active-site exposure, and enhance structural stability [31, 57, 121, 122]. These composite architectures also stabilize POM molecules during prolonged electrolysis and create hierarchical pore structures that improve mass transport and catalytic kinetics [123, 124]. In particular, interfacial electronic coupling between POMs and the substrate can modulate charge distribution and intermediate adsorption, ultimately enhancing HER efficiency. Therefore, composite design with functional materials has emerged as a critical strategy for advancing POM-based HER catalysts toward practical applications [125].

The structural properties of NF make it an ideal support for POMs. With a porosity of 96%–98% and an exceptionally high specific surface area, NF allows uniform distribution of POMs across both external and internal surfaces, thereby enhancing catalytic activity [126, 127]. In addition, its high electrical conductivity promotes rapid electron transfer, improving the efficiency of electrochemical reactions [128]. During the synthesis of POM-based materials, NF not only serves as a support but can also actively participate in the reaction process. Its three-dimensional architecture and high porosity provide excellent mass transport and gas release capabilities during electrocatalysis, facilitating rapid hydrogen desorption and enhancing overall electrochemical performance. Furthermore, NF serves as an effective substrate for constructing bifunctional electrodes. For example, decorating Dexter–Silverton POM-based composites with TMPs or TMS produces electrodes that exhibit both HER and OER activity. Wei et al. reported POM-modified ZnCoS nanowires on NF (POMs@ZnCoS/NF), prepared via a two-step hydrothermal method, which showed notable HER activity [110]. Detailed characterization revealed that the enhanced performance arises from increased active site density, expanded electrochemically active surface area, and optimized electronic and chemical properties. In another study, Cui et al. synthesized self-supported nanoflower-like heterostructures via *in situ* growth of tri-vanadium-substituted Keggin-type POM $H_6PV_3Mo_9O_{40}$ and $Fe_{0.2}Ni_{0.8}Co_2O_4$ on NF through a hydrothermal reaction [129]. The resulting nanoflower-like structure considerably increased accessible surface area, enhanced interfacial reaction kinetics, and facilitated efficient gas evolution. As a result, the optimized electrode achieved a low overpotential of 93 mV at 10 mA·cm^{-2} with a Tafel slope of 52 mV·dec^{-1}, while maintaining stable current density over prolonged operation. DFT calculations indicated preferential adsorption of water molecules at Co sites on the POM–FNCO heterointerface, and Bader charge analysis confirmed substantial interfacial charge redistribution, which promoted adsorption and desorption of hydrogen intermediates and lowered reaction energy barriers.

Carbon-based materials are widely used as supports for anchoring POMs, owing to their superior conductivity, high surface area, and adjustable structural features [57, 130, 131]. By integrating POMs with highly conductive carbon materials—such as graphene, CNTs, mesoporous carbon, or N-doped carbon frameworks—the intrinsic limitations of POMs, including low electrical conductivity and limited stability under reductive conditions, can be effectively addressed [132]. POMs also improve the dispersion of carbon supports and help identify intrinsic catalytic sites, thereby influencing reaction mechanisms. For example, Liu et al. synthesized electrochemically reduced graphene oxide (rGO) decorated with cyclic 48-tungsto-8-phosphate $[H_7P_8W_{48}O_{184}]^{33-}$, referred to as P_8W_{48}/rGO [133]. In this composite electrode, P_8W_{48} clusters were uniformly anchored on the graphene sheets. The proton- and electron-rich nature of the POMs created a favorable local microenvironment, while the rGO framework enhanced the overall conductivity of the electrode. Wei et al. prepared $NiCo_2S_4$/PANI@POM/rGO composites by combining oxidative polymerization with hydrothermal synthesis, resulting in nanosheets in which $NiCo_2S_4$ and PANI@POM were uniformly anchored on rGO [134]. Under alkaline conditions, this material exhibited HER activity with an overpotential of 197 mV, attributed to its high surface area and mesoporous structure, which provided abundant active sites and facilitated rapid electron transport during the reaction. In another study, Sakthinathan et al. used a layer-by-layer self-assembly strategy to construct well-ordered POM/polypyrrole (PPy) nanostructures ($[SiW_{12}]$@PPy) by exploiting electrostatic interactions between the POM anion $[SiW_{12}O_{40}]^{4-}$ and the cationic conductive PPy [135]. This approach involved alternating immersion of the substrate into POM and PPy solutions at room temperature, with each cycle forming a uniform composite layer, ultimately producing a multi-layered, ordered nanoarchitecture (Fig. 8(a)). The synergistic combination of POMs' multi-electron redox properties and PPy's high conductivity considerably enhanced electron and proton transfer efficiency. In 0.5 M H_2SO_4, the electrode achieved an overpotential of 68 mV at a current density of 10 mA·cm^{-2}, with a Tafel slope of 52 mV·dec^{-1}, outperforming electrodes composed of either POM or PPy alone, and maintained stability over 1000 cyclic voltammetry (CV) cycles without noticeable degradation (Figs. 8(b) and 8(c)). This study demonstrates that layer-by-layer self-assembly allows uniform distribution of POMs and tight integration with conductive networks, enabling molecular-scale interfacial optimization to enhance HER activity and durability. CNTs, with their excellent conductivity, mechanical strength, thermal stability, high aspect ratio, and large surface area, also serve as effective supports. For example, Zhang et al. proposed a strategy to anchor Keggin-type phosphomolybdic acid, $H_3PMo_{12}O_{40}$ (PMA, PMo_{12}), onto CNT

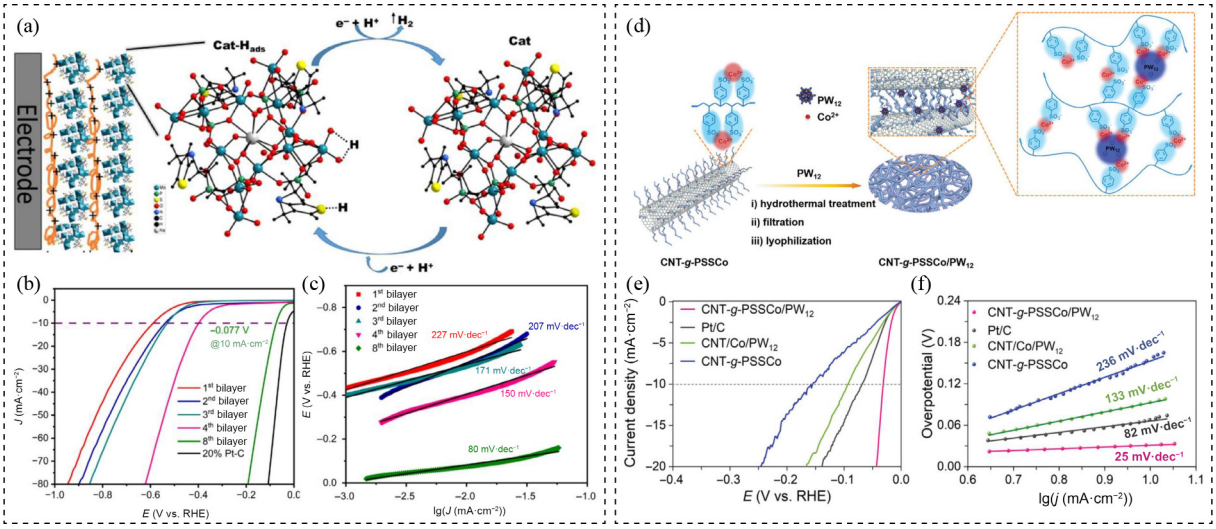

Figure 8 (a) Proposed electrocatalytic pathway of proton reduction at the PEI/[(TBA)Mo_{12}(AleThio)$_4$] bilayer-modified interface. (b) LVS profiles comparing the HER activity of the first to eighth bilayers in 0.5 M H_2SO_4 at 1 mV·s^{-1}. (c) Corresponding Tafel curves and slope values. Reprinted with permission from Ref. [135], © American Chemical Society 2023. (d) Schematic illustration of the preparation for CNT-*g*-PSSCo/PW_{12}. Electrocatalytic HER performance in 0.5 m H_2SO_4. (e) LSV curves and (f) Tafel plots of CNT-*g*-PSSCo/PW_{12}, CNT/Co/PW_{12}, CNT-*g*-PSSCo, and commercial Pt/C. Reprinted with permission from Ref. [136], © Wiley-VCH GmbH 2022.

surfaces to construct efficient HER catalysts [133]. The protons in POMs can form strong non-covalent interactions with the π-conjugated surfaces of CNTs, enabling stable binding without chemical modification. Using a simple impregnation method, well-dispersed POM@CNT composites were obtained, exhibiting excellent conductivity. In this system, the CNT framework stabilizes the molecular POM structure and promotes synergistic electron–proton transfer. Under acidic conditions, the catalyst required an overpotential of only 65 mV at 10 mA·cm^{-2}, with a Tafel slope of 48 mV·dec^{-1}. In another study, Liu et al. loaded Keggin-type phosphomolybdic acid onto porous CNTs (p-CNTs) to construct efficient HER electrocatalysts [57]. The CNTs were pretreated with nitric acid to introduce oxygen-containing functional groups, enhancing POM binding capacity. After ultrasound-assisted impregnation, POMs were uniformly anchored on the CNT surface. The resulting POM@p-CNT composites exhibited excellent electron transport, high electrochemically active surface area, and strong interfacial coupling, achieving a low overpotential of 86 mV at 10 mA·cm^{-2} in acidic conditions, along with good cycling stability. This study highlights the ability of carbon nanostructures to enhance the electrocatalytic performance of POMs through confinement and synergistic effects. Such composite systems improve electron transport pathways, enhance POM dispersion, and strengthen interfacial interactions, enabling more efficient charge transfer and better utilization of active sites during HER. Additionally, the porous or hierarchical structure of carbon supports facilitates reactant diffusion and increases exposure of catalytic sites, thereby improving overall HER performance. Lin et al. developed a self-supporting catalytic membrane with a three-dimensional nano-network structure (CNT-*g*-PSSCo/PW_{12}) through synergistic self-assembly mediated by electrostatic interactions between CNT backbones, cobalt–polystyrene sulfonate branches (CNT-*g*-PSSCo), and Keggin-type phosphotungstate PW_{12} nanodots (Fig. 8(d)) [136]. The Co^{2+} coordination centers served both as connection sites for the molecular brushes and as anchors for the negatively charged POM nanoclusters, while the CNT backbone provided highly conductive pathways for electron transport. This flexible membrane electrode exhibited an overpotential of only 31 mV at 10 mA·cm^{-2} in 0.5 M H_2SO_4, with a Tafel slope of 25 mV·dec^{-1}, and maintained stable performance after 1000 CV cycles, demonstrating excellent HER activity and long-term durability (Figs. 8(e) and 8(f)).

Yan et al. proposed a nanoscale "proton shuttle" strategy by encapsulating POMs inside single-walled CNTs (SWCNTs) while selectively depositing Pt nanoclusters on the exterior (Figs. 9(a) and 9(b)) [137]. The resulting Pt-POM catalyst exhibited a high proton conductivity of 3.54 × 10^{-3} S·m^{-1}, considerably higher than that of non-encapsulated POM-based catalysts. The Pt/POM@SWCNT electrode achieved an overpotential of 134 mV at 100 mA·cm^{-2}, substantially lower than commercial Pt/C electrodes, with a Tafel slope of 20.15 mV·dec^{-1}, indicating a Volmer–Heyrovsky-dominated mechanism in which proton transport accelerates the rate-determining step (Figs. 9(c)–9(e)). HER tests under varying pH conditions revealed that the overpotential difference between Pt/POM@SWCNT and Pt/SWCNT increased as proton concentration decreased, demonstrating that the proton shuttle mechanism effectively enhances HER activity across a wide pH range.

MOFs, with their highly tunable porous structures, provide an ideal platform for immobilizing POMs to form ordered hybrid systems with synergistic electrocatalytic properties [22, 121]. MOFs feature high specific surface areas, well-defined pore channels, and diverse coordination environments, which facilitate uniform POM dispersion and stabilize their structures under electrochemical conditions [138, 139]. The modular nature of MOF architectures allows accurate control over pore size, hydrophilicity, and active-site distribution, further optimizing HER reaction kinetics [140]. For example, Zhang et al. developed a POM-directed etching strategy to construct defective hollow MOF structures. Using Keggin-type PMo_{12} as an etchant, they transformed ZIF-8 MOFs encapsulating $SiW_{11}NiO_{35}$ clusters (WNi) from solid cubes into hierarchically defective hollow structures in aqueous solution at room temperature [141]. A recently developed class of MOFs, known as POMOFs, incorporates POMs as inorganic structural units rather than conventional metal ions, with frameworks constructed via transition-metal centers or bridging organic linkers [80]. These

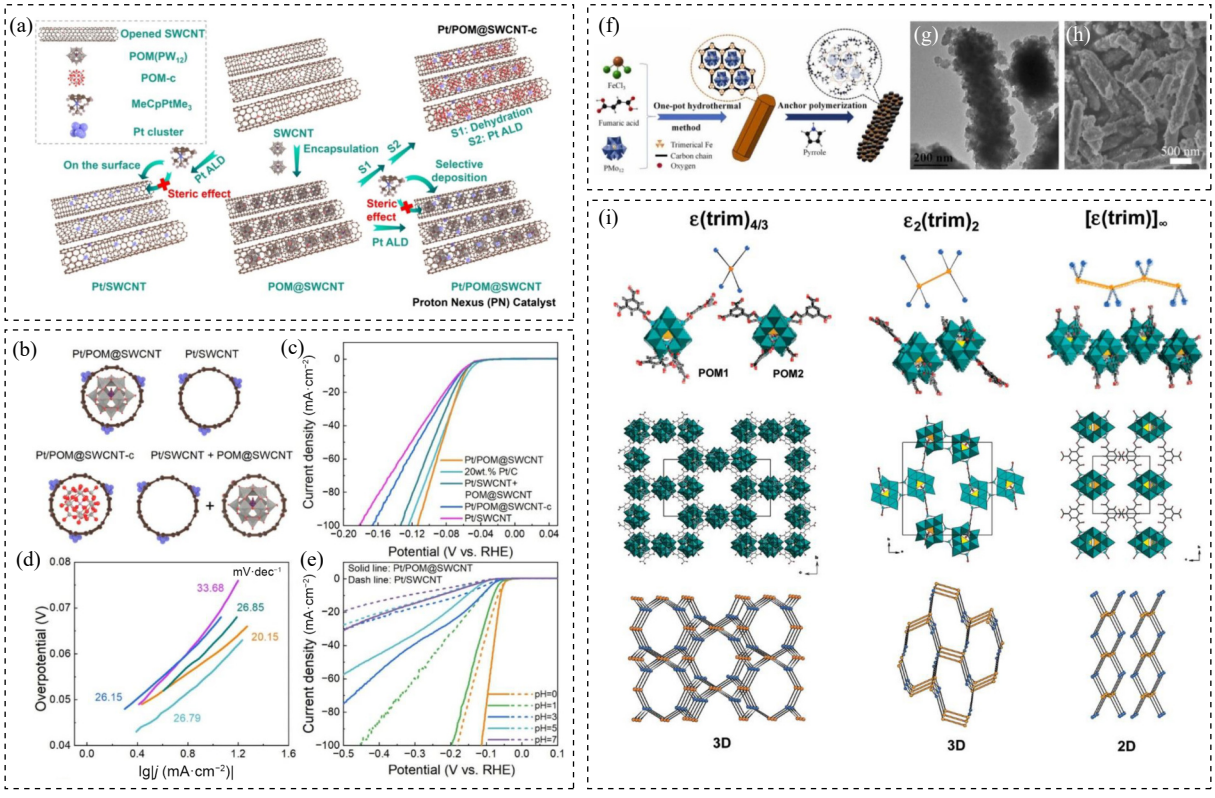

Figure 9 (a) Schematic illustration of the preparation of the corresponding catalysts. Pt was selectively deposited on the outside of SWCNT due to the steric effect. (b) Proposed structures for four catalysts with different modes. (c) LSV curves of all Pt-based catalysts in 0.5 M H_2SO_4 at a scan rate of 5 mV·s^{-1}. (d) Corresponding Tafel plots of all prepared electrocatalysts. (e) HER tests over the PN catalyst (Pt/POM@SWCNT) and pure Pt/SWCNT at different pH conditions. Reprinted with permission from Ref. [137], © American Chemical Society 2025. (f) Schematic process of synthesis, (g) TEM image, (h) SEM image of PMo_{12}-PPy@Fe-MOF. Reprinted with permission from Ref. [142], © Elsevier B.V. 2025. (i) POM building blocks of ε(trim)$_{4/3}$, ε$_2$(trim)$_2$, and [ε(trim)]$_\infty$, a view of their unit cell, and their schematic representation; black lines indicate connections between POMs and trim linkers, while orange lines symbolize condensation reactions between POMs. Reprinted with permission from Ref. [143], © American Chemical Society 2011.

materials exhibit enhanced proton and electron transfer, confined active-site environments, and superior durability. Hao et al. used a two-step "positioning–coating" approach to confine Keggin-type PMo_{12} in spindle-shaped Fe-MOF channels, mitigating dissolution and agglomeration issues. Subsequent oxidative polymerization of pyrrole formed a PPy coating, which enhanced conductivity through electrostatic interactions, including Mo–N bond formation (Figs. 9(f)–9(h)) [142]. Nohra et al. immobilized soluble ε-Keggin POMs in a three-dimensional porous framework to construct POMOFs, considerably improving electrode stability. The resulting material achieved an overpotential of 260 mV under acidic conditions, outperforming platinum electrodes (Fig. 9(i)) [143]. Its structure, $(TBA)_3[PMoV_8MoV_{14}O_{36}(OH)_4Zn_4][C_6H_3(COO)_3]_4 \cdot 3.6H_2O$, features a 3D open framework of molecular Keggin segments connected by organic linkers, with tetrabutylammonium counterions (TBA^+) residing in the channels, which stabilizes the POMs and enhances electrocatalytic activity in three-dimensional configurations.

The studies discussed above demonstrate that various conductive substrates, including NF, carbon-based materials, and MOFs, can be effectively combined with appropriate POM structures to create highly efficient and stable HER electrocatalysts. Through diverse synthesis strategies, strong interfacial interactions between POMs and the substrates enable the formation of composites with controlled morphologies. The synergistic effects between conductive matrices and POMs optimize the active sites, leading to considerably enhanced HER performance. Notably, these systems have shown remarkable electrocatalytic efficiency under acidic conditions.

3.4 POM-derived HER electrocatalysts

Beyond their intrinsic catalytic activity, POMs serve as structurally accurate precursors for designing a wide range of HER electrocatalysts with controllable metal composition, oxidation states, and active-site environments. During thermal or chemical transformation, the polynuclear metal–oxygen frameworks of POMs guide the formation of uniformly distributed metal clusters, heteroatom-doped matrices, and well-defined nanoalloy or heterostructure interfaces [144]. These molecularly pre-organized architectures offer advantages not achievable with conventional precursors, including predictable phase evolution, atomic-level dispersion, and tunable electronic structures optimized for hydrogen adsorption and water dissociation. Therefore, POM-derived systems have emerged as a versatile platform for the design of high-performance HER catalysts across diverse material classes.

3.4.1 Carbon-confined metal catalysts derived from POM precursors

Carbon-confined metal catalysts are highly suitable for HER because carbon matrices provide excellent conductivity, structural stability, and efficient charge transfer. POMs, as atomically accurate metal–oxygen clusters, serve as ideal precursors for constructing

carbon-confined metal electrocatalysts owing to their unique compositional and structural features [145]. Upon pyrolysis under inert or reductive atmospheres, the oxygen-rich frameworks of POMs can *in situ* generate TMCs, metal nanoparticles, or atomically dispersed metal species embedded in N-doped carbon matrices [16, 95, 146]. This self-templating transformation enables atomic-level homogeneous distribution of metal elements and heteroatoms while forming strong metal–support interactions, resulting in exceptional structural stability and enhanced electronic conductivity [147]. Thus, POM-derived catalysts exhibit uniform particle dispersion, abundant interfacial active sites, and superior charge-transfer kinetics [86]. Moreover, the synergistic integration of conductive carbon frameworks with metal active centers endows these catalysts with excellent HER activity and great potential for practical applications [148]. In 2012, Hu et al. first reported the HER performance of Mo_2C, showing that commercial Mo_2C is a promising candidate for HER under both acidic and alkaline conditions [145]. Benefiting from its high electrical conductivity, stability, melting point, and low cost, Mo_2C has been recognized as a highly promising HER electrocatalyst [149, 150]. The hybridization between Mo d-orbitals and C s/p-orbitals provides Mo_2C with an electronic structure similar to that of Pt, imparting Pt-like catalytic properties and enabling high HER activity [151]. However, the development of Mo_2C-based catalysts with HER performance comparable to Pt-based catalysts remains a formidable challenge [152]. To address this limitation, extensive efforts have been devoted to enhancing the catalytic activity of Mo_2C through nanostructure engineering, integration with conductive supports, and heteroatom doping to tune its electronic structure [153]. Ni et al. used a synergistic strategy combining ammonium hydroxide treatment with hydrothermal processing, which considerably increased the content of surface hydroxyl groups and pyridinic nitrogen, imparting superhydrophilic characteristics. Additionally, electron transfer effects reduced the oxidation state of Mo sites, achieving dual regulation of surface wettability and electronic states in Mo_2C [151]. Niu et al. developed a single-atom Pt-modified Mo_2C catalyst (Pt_1-Mo_2C-C) via a MOF-confinement carbonization approach, containing only 0.7 wt.% Pt [154]. This catalyst exhibited excellent HER performance in 1 M KOH, achieving an overpotential of 155 mV and a mass activity approximately seven times higher than commercial 20 wt.% Pt/C. The enhanced electronic coupling between single-atom Pt and Mo_2C facilitated water dissociation and optimized hydrogen adsorption energy, resulting in considerably improved catalytic efficiency. Jia et al. proposed a POMOF-derived strategy to construct porous Mo_2C octahedra decorated with Pt–Cu nanocrystals (Pt–Cu/Mo_2C) [155]. Using NENU-5 as a precursor, high-temperature carbonization followed by galvanic replacement with H_2PtCl_6 enabled uniform deposition of Pt–Cu bimetallic nanoparticles on Mo_2C supports. The resulting Pt–Cu/Mo_2C catalyst exhibited outstanding HER activity in acidic electrolyte, achieving an ultra-low overpotential of just 12.9 mV at 10 mA·cm^{-2}, along with excellent cycling stability. Huang et al. developed a novel atomic-level nitrogen-doping strategy to accurately tune the electronic structure of Mo_2C [156]. Using organic imine-derived POM nanoclusters containing intrinsic Mo–N bonds as precursors, the number of imine ligands was carefully controlled to regulate nitrogen incorporation into the Mo_2C lattice, producing a series of N@Mo_2C–*n* catalysts. The optimized N@Mo_2C–3 catalyst delivered exceptional HER activity and stability in both acidic and alkaline electrolytes. Combined experimental characterizations and DFT calculations confirmed that N doping effectively modulated the Mo d-band electronic structure and reduced the Mo–H bond strength, thereby considerably improving HER kinetics. This work highlights the unique advantages of POM precursors for atomic-scale engineering and provides valuable guidance for the rational design of high-efficiency energy conversion catalysts. Yue et al. reported the fabrication of stable Pt single-atom sites in Mo_2C nanodomains using Zn–Mo POM clusters ($ZnMo_6$) as precursors via a "vacancy-substitution" strategy, forming Mo(C)–Pt–N three-dimensional coordination environments (Figs. 10(a) and 10(b)) [157]. Leveraging the well-defined molecular structure of POMs and the volatile nature of Zn, controlled atomic vacancies were generated during pyrolysis, which effectively anchored Pt single atoms and prevented their agglomeration (Figs. 10(c) and 10(d)). The Pt atoms were firmly embedded in Mo_2C lattice vacancies and coordinated with surrounding C, Mo, and axial N atoms, tuning the Pt charge state and d-band center. As a result, the resulting PtSA@Mo_2C@NC catalyst exhibited ultra-low overpotentials and superior mass activity in both acidic and alkaline electrolytes, outperforming commercial Pt/C and a range of reference catalysts (Figs. 10(e) and 10(f)). This study clearly demonstrates the unique advantages of POMs in enabling single-atom confinement and multidimensional chemical environment regulation, providing new strategies for the rational design of highly efficient HER catalysts. Zhao et al. developed a multifunctional carbon-based electrocatalyst (PMA@ZIF-67–C–AT) by integrating POMs with the ZIF-67 framework [158]. In this approach, Keggin-type phosphomolybdic acid was encapsulated in the pores of ZIF-67 and subsequently subjected to high-temperature carbonization and acid treatment, yielding a catalyst with abundant defects and a capsule-like porous architecture. The resulting material exhibited remarkable HER activity in both neutral phosphate buffer and natural seawater, requiring only 570 mV overpotential to achieve 10 mA·cm^{-2} in seawater electrolysis. Yang et al. further encapsulated PMA into a ZIF-8 framework, followed by high-temperature carbonization to produce a nitrogen-doped Mo_2C electrocatalyst with a coral-like porous architecture, denoted as 3D Mo_2C (Figs. 10(g)–10(i)) [159]. By tuning the molar ratio of POMs to Zn in the precursor, accurate control over the exposure of Mo_2C (101) and (002) facets was achieved. The optimized 3D Mo_2C (1:1) catalyst exhibited excellent HER performance in 1 M KOH, with an overpotential of 110 mV at 10 mA·cm^{-2} and a Tafel slope of 73.9 mV·dec^{-1} (Figs. 10(j)–10(l)).

Liao et al. developed a self-supporting porous conductive carbon aerogel derived from POM hydrogels, successfully constructing a composite electrocatalyst with Pt-doped Mo_2C active sites (Pt@Mo_2C) [160]. By electrostatically assembling PVA/chitosan hydrogels with POMs, followed by carbonization and electrodeposition, Pt single atoms, clusters, and nanoparticles were uniformly distributed on the Mo_2C support while preserving a three-dimensional continuous porous conductive network (Figs. 11(a) and 11(b)). The optimized Pt@Mo_2C/CFP catalyst demonstrated excellent alkaline HER activity and stability, despite an ultra-low Pt loading of only 0.03 mg·cm^{-2}. Combined experimental and theoretical analyses showed that the Pt/Mo_2C heterostructure facilitated synergistic interactions between Pt–H and Mo–OH bonds, accelerating water dissociation and considerably improving alkaline HER kinetics (Figs. 11(c) and 11(d)). Li et al. used a mono-trihydroxymethyl-functionalized Anderson-type POM as a precursor, which was composited with chitosan and subjected to

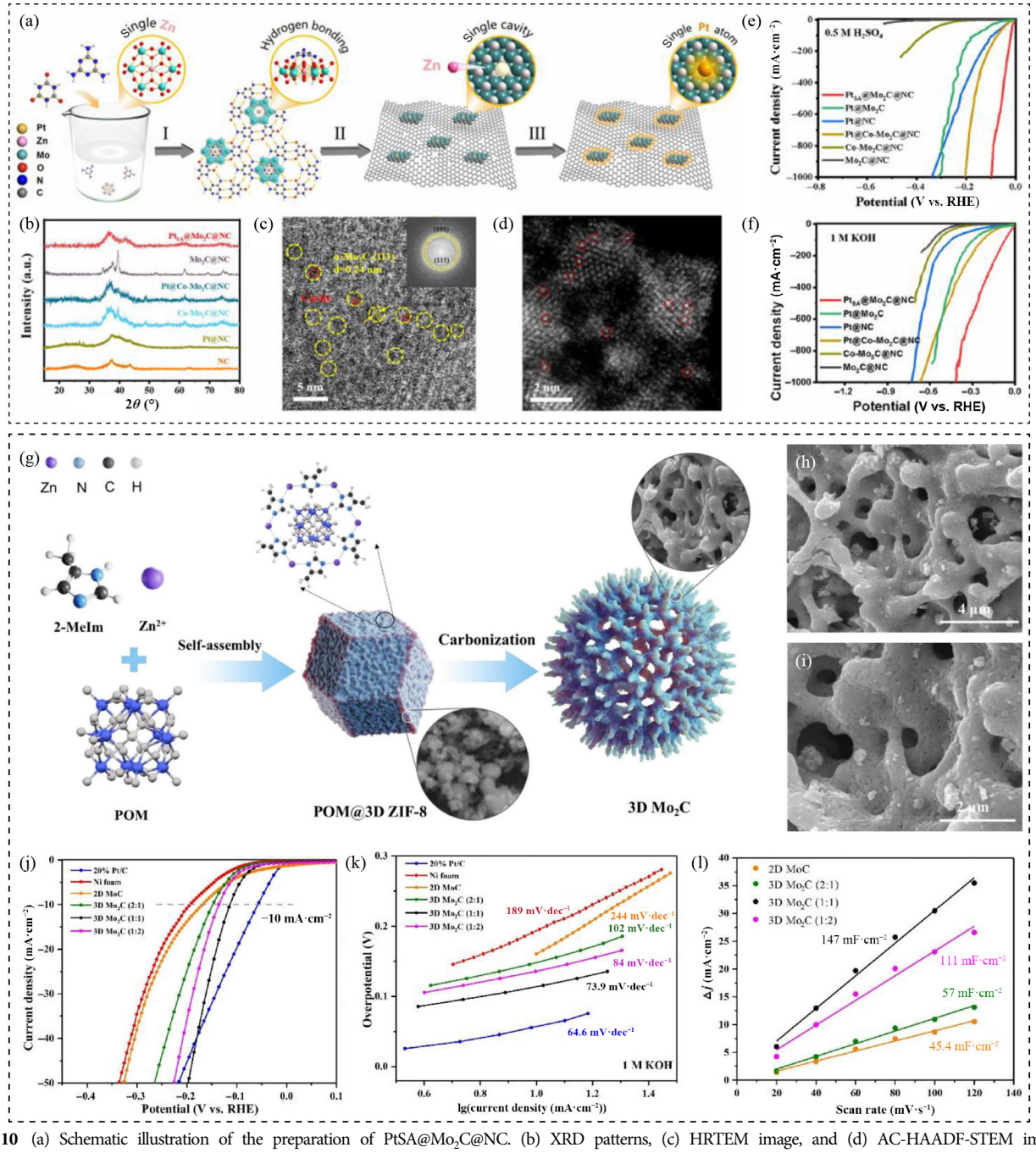

Figure 10 (a) Schematic illustration of the preparation of PtSA@Mo_2C@NC. (b) XRD patterns, (c) HRTEM image, and (d) AC-HAADF-STEM image of PtSA@Mo_2C@NC. (e) Polarization curves of the HER in 0.5 M H_2SO_4 and (f) 1.0 M KOH solution of PtSA@Mo_2C@NC and compared catalysts. Reprinted with permission from Ref. [157], © Royal Society of Chemistry 2024. (g) Synthesis procedure of porous 3D Mo_2C electrocatalyst. (h) and (i) SEM images of 3D Mo_2C (1:1) electrocatalyst at various magnifications. (j) Polarization curves and (k) Tafel plots of 2D MoC, 3D Mo_2C_x (x = 2:1, 1:1, 1:2), Ni foam and 20% Pt/C. (l) Estimated C_{dl} and relative ECSA. Reprinted with permission from Ref. [159], © Elsevier B.V. 2022.

high-temperature carbonization to produce Ni, N-codoped Mo_2C nanoparticles (Ni/N-Mo_2C@C) (Fig. 11(e)) [161]. By leveraging the accurate metal stoichiometry at the molecular level (Mo:Ni ≈ 6:1) provided by POMs, this strategy enabled the uniform incorporation of heteroatoms, effectively circumventing the inhomogeneity commonly observed in conventional post-synthetic doping methods. The resulting Ni/N-Mo_2C@C catalyst exhibited outstanding HER activity under alkaline conditions, requiring only 148 mV overpotential to achieve 10 mA·cm^{-2}, surpassing both undoped samples and control catalysts prepared from physically mixed precursors, while also demonstrating excellent cycling stability (Figs. 11(f) and 11(g)). This work underscores the unique advantages of Anderson-type POMs in constructing precisely doped electrocatalysts and offers a promising approach for the rational design of high-performance HER catalysts. Yang et al. further reported the synthesis of a six-pointed star-shaped porous nitrogen-doped Co/MoC Mott–Schottky heterostructure catalyst (Co/MoC@NC) by introducing phosphomolybdic acid into Zn/Co ZIF-L precursors, followed by high-temperature carbonization [162]. In this design, POMs acted as the Mo source, while the

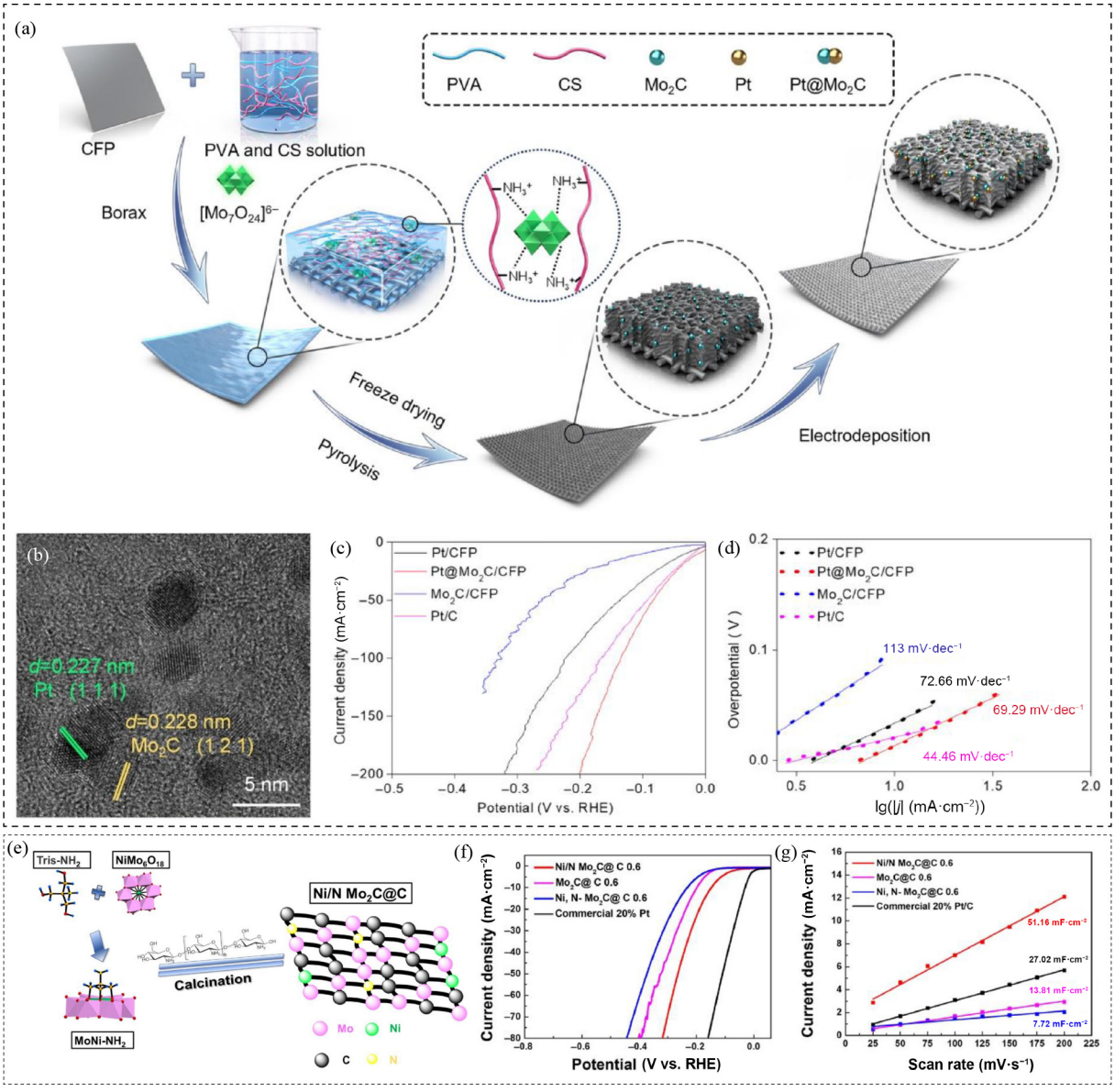

Figure 11 (a) Illustration of the synthesis process for Pt@Mo_2C/CFP carbon aerogel electrocatalyst. (b) HRTEM image of Pt@Mo_2C/CFP. (c) LSV curves in 1.0 M KOH. (d) Tafel slopes of the different electrocatalysts. Reprinted with permission from Ref. [160], © Youke Publishing Co., Ltd. 2025. (e) The synthetic procedure of Ni/N Mo_2C@C nanocomposite. (f) LSV curves of Ni/N Mo_2C@C 0.6, Mo_2C@C 0.6, Ni, N-Mo_2C@C 0.6, and commercial 20% Pt/C in alkaline condition (1 M KOH). (g) C_{dl} values evaluated by CV measurements under different scan rates. Reprinted with permission from Ref. [161], © Hydrogen Energy Publications LLC. 2022.

carbonization process promoted the formation of Mott–Schottky interfaces between Co and MoC, thereby enhancing electron transfer efficiency and optimizing water dissociation kinetics. DFT calculations and COMSOL simulations further demonstrated that the "tip effect" of the six-pointed star morphology generated localized regions of high charge density, enriching H^+ ions and accelerating alkaline HER processes. Therefore, Co/MoC@NC exhibited excellent HER performance in 1 M KOH electrolyte. To date, various advanced strategies have been used to construct MoC_x materials with well-defined architectures, including ultrathin porous nanosheets and self-supporting structures with surface defects. These tailored structures not only provide high specific surface areas and abundant active sites but also hold considerable promise for industrial-scale HER applications.

Tungsten carbide (WC_x) exhibits Pt-like catalytic behavior toward hydrogen evolution owing to its d-band structure, which closely resembles that of Pt. The incorporation of transition metals such as Co, Ni, or Fe can further tune the d-band structure of the parent material, optimizing hydrogen adsorption energies and thereby enhancing HER performance [163]. Yan et al. synthesized a P/N codoped W_2C@NC catalyst via a POM-confinement pyrolysis strategy (Fig. 12(a)) [164]. N-doped carbon encapsulation and phosphorus modification enabled uniform dispersion of W_2C nanoparticles, resulting in an exchange current density comparable to that of Pt/C and demonstrating Pt-like catalytic activity in acidic, alkaline, and neutral electrolytes (Figs. 12(b)–12(e)). To reduce the high cost and scarcity of Pt, developing efficient, stable, and high-activity alternatives is crucial. Notably, the surface electronic structures of WC and MoC resemble that of Pt(111), owing to the hybridization of C 2s/2p orbitals with the broadened d-orbitals of W or Mo. However, during high-temperature synthesis, Pt tends to migrate and agglomerate into particles or clusters, leading to

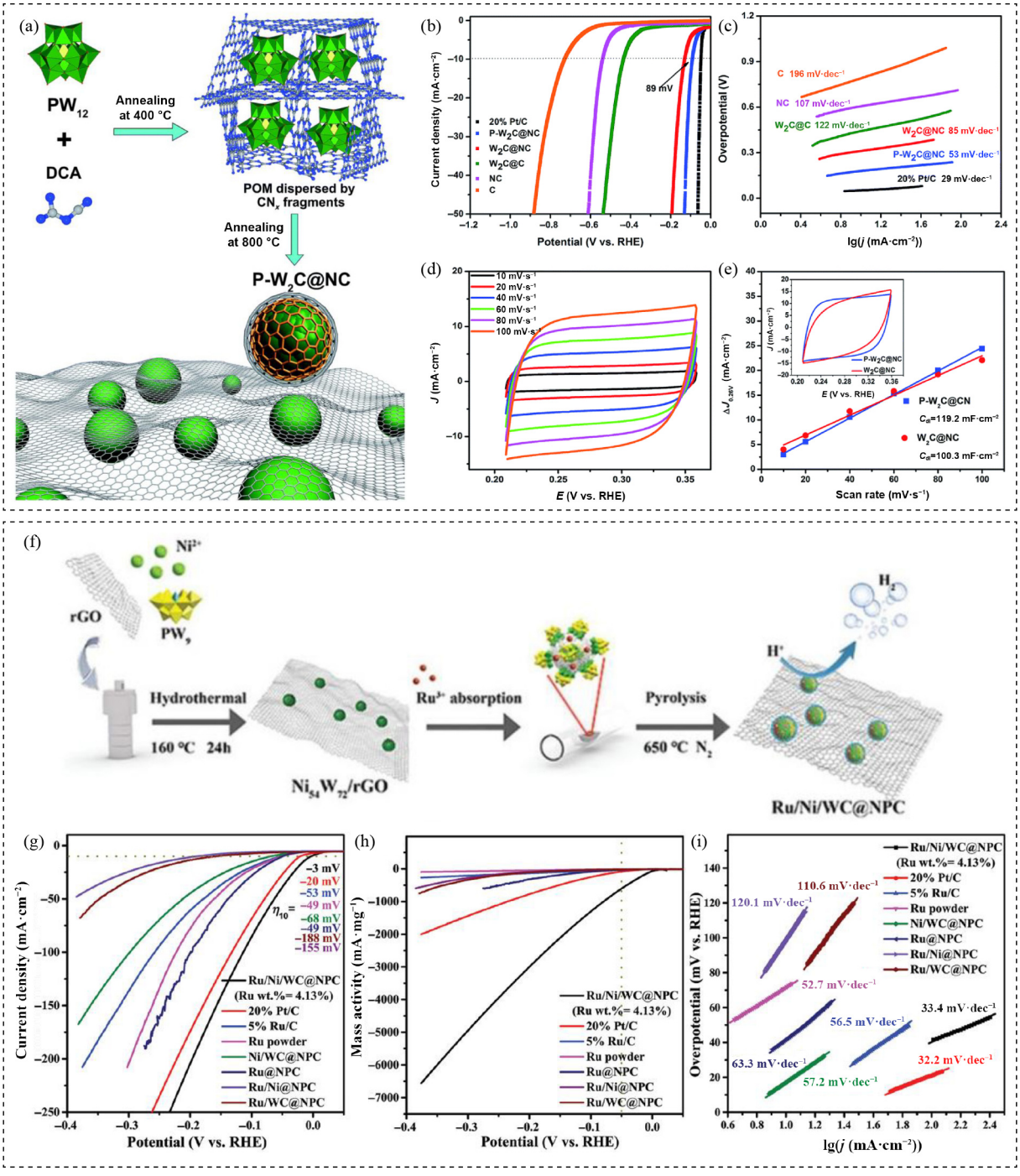

Figure 12 (a) Schematic representation of the synthesis and structural features of P-W_2C@NC. (b) Polarization curves, (c) Tafel plots of 20% Pt/C, P-W_2C@NC, W_2C@NC, W_2C@C, N-doped carbon (NC), and pure graphene. (d) Cyclic voltammograms of P-W_2C@NC. (e) Plot of the current density difference between anodic and cathodic sweeps vs. scan rate at 0.26 V. Reprinted with permission from Ref. [164], © Royal Society of Chemistry 2017. (f) Illustration of the preparation procedure for Ru/Ni/WC@NPC electrocatalysts and evaluation of their HER performance in 1 M KOH at room temperature. (g) Possesses curves of Ru/Ni/WC@NPC, 20% Pt/C, Ru powder, 5% Ru/C, Ni/WC@NPC, Ru@NPC, Ru/Ni@NPC, and Ru/WC@NPC electrocatalysts. (h) The related mass activities of the previous electrocatalysts in (g). (i) Tafel plots gained from the polarization curves in (g). Reprinted with permission from Ref. [166], © Wiley-VCH GmbH 2022.

electronic structures and catalytic behaviors that differ from those of metallic Pt. To address this, Ma et al. used a POM precursor containing Pt centers (PtW_6O_{24}) to confine atomically dispersed Pt in the WC_x lattice ($Pt_{doped}@WC_x$) [165]. The 5d electronic configuration of Pt in this catalyst closely resembled that of metallic Pt(111), with a Gibbs free energy of −0.36 eV, nearly identical to that of Pt(111) (−0.37 eV). Under alkaline HER conditions, the WC support lowered the energy barrier for water dissociation to 0.15 eV, while the Pt sites directly adsorbed H^*, thereby avoiding the additional 0.47 eV energy penalty associated with H^* migration from W sites in conventional Pt catalysts. Therefore, the $Pt_{doped}@WC_x$ catalyst achieved an impressive mass activity of 49.5 $A{\cdot}mg^{-1}$ at an overpotential of 150 mV, approximately 40 times higher than that of commercial Pt/C.

Salah et al. used a Ni-substituted tungsten-based POM/rGO composite ($Ni_{54}W_{72}$/rGO) as a precursor, and by introducing $RuCl_3$ and hexachlorocyclotriphosphazene ($N_3Cl_6P_3$) followed by high-temperature pyrolysis, they successfully constructed a multi-interfaced Ru/Ni/WC composite catalyst (Ru/Ni/WC@NPC) anchored in an N, P codoped carbon shell (Fig. 12(f)) [166]. Leveraging the pre-existing Ni–W submolecular interfaces and abundant surface oxygen atoms in the POM precursor, Ru species were effectively dispersed and immobilized, resulting in a composite featuring multiple Ru/Ni, Ni/WC, and Ru/WC interfaces. Therefore, Ru/Ni/WC@NPC exhibited excellent activity and durability toward alkaline HER (Figs. 12(g)–12(i)). Yue et al. further developed an innovative *in situ* "from atomic bonding to heterointerface" strategy to synthesize a composite catalyst, Co_2P/WC@NC/CNTs, enriched with Co_2P/WC heterointerfaces [167]. Using a sandwich-type Keggin-defect POM, $K_{10}[Co_4(H_2O)_2(PW_9O_{34})_2]$, as the molecular precursor, the intrinsic Co–W quasi-interface guided the atomic-level formation of Co_2P/WC heterojunctions during high-temperature carbonization and phosphidation. Confinement in ZIF-8 suppressed nanoparticle aggregation, while CNTs enhanced both conductivity and surface area. The resulting catalyst exhibited robust HER activity and stability across multiple media, achieving 10 mA·cm^{-2} at overpotentials of 171, 198, 525, and 483 mV in 0.5 M H_2SO_4, 1.0 M KOH, 1.0 M PBS, and seawater, respectively. DFT calculations further revealed that the Co_2P/WC heterointerface effectively optimized hydrogen adsorption free energy, thereby accelerating the reaction kinetics along the Volmer–Heyrovsky pathway. This work underscores the unique advantages of POMs as molecular precursors for the accurate construction of multicomponent heterostructured electrocatalysts, providing valuable insights for designing high-performance, pH-universal POM-based HER catalysts. Leveraging POMs as molecular pre-assembly platforms for heterostructure engineering, Yao et al. accurately tuned the Ni/W atomic ratio in Ni-substituted POM precursors to synthesize a series of N-doped carbon-encapsulated Ni/WC heterostructure catalysts ($Ni_{xx}W_{yy}$@C) [168]. Among these, $Ni_{44}W_{99}$@C, derived from a Ni:W = 4:9 precursor, exhibited uniformly distributed Ni/WC interfaces and the highest intrinsic HER activity, requiring only 38 mV overpotential to reach 10 mA·cm^{-2} in 0.5 M H_2SO_4, with a Tafel slope of 43 mV·dec^{-1} and an exchange current density of 0.90 mA·cm^{-2}, approaching the performance of commercial 20% Pt/C. X-ray photoelectron spectroscopy (XPS) and electrochemical analyses revealed that the homogeneous heterointerfaces facilitated electron transfer from WC to Ni, thereby optimizing hydrogen adsorption free energy and considerably accelerating the reaction kinetics. Moreover, this catalyst demonstrated excellent activity and durability across a wide pH range, showing no noticeable degradation after 10,000 cycles. This study not only highlights the unique advantage of POMs in atomic-level tuning of bimetallic ratios but also provides valuable guidance for the rational design of efficient, interface-engineered catalysts. Tungsten-based POM-derived materials can further modulate electrocatalytic properties through diverse synthesis strategies, enabling the fabrication of MoC_x/WC_x-based composites with optimized HER performance. Using non-noble-metal POM precursors, a variety of heteroatom-doped carbon frameworks hosting WC_x nanostructures can be obtained. Notably, heteroatom doping effectively tunes the d-band electronic structure of WC_x, optimizes hydrogen adsorption free energy, and thus offers a promising pathway for the rational design and controllable synthesis of high-performance, low-cost, non-noble-metal electrocatalysts.

Overall, carbon-confined metal catalytic systems derived from POM precursors demonstrate unique advantages in structural stabilization, conductivity enhancement, and heterointerface engineering. The self-templated conversion of POMs ensures atomic-level metal dispersion within conductive carbon matrices, thereby optimizing hydrogen adsorption and accelerating HER kinetics. These findings underscore the pivotal role of POM-based carbon-confinement strategies in the development of highly active, durable, and cost-effective electrocatalysts.

3.4.2 *Heteroatom-regulated sulfide hybrid catalysts*

Sulfide derivatives have attracted considerable attention owing to their compatibility with alkaline HER kinetics. Recently, sulfide materials derived from POM-based precursors have emerged as promising HER electrocatalysts owing to their tunable electronic structures, excellent conductivity, and abundant edge-active sites [169]. Through accurately controlled sulfidation processes, transition-metal-containing POMs can be converted into uniformly dispersed metal chalcogenides, while simultaneously forming heteroatom-enriched architectures from residual elements such as W, Mo, or V. These heterostructures often adopt nanosheet-like or porous morphologies, which favor exposure of catalytic sites and facilitate efficient charge transport [146, 170, 171]. Moreover, the intrinsic electronic heterogeneity imparted by POMs effectively regulates hydrogen adsorption free energy and enhances interfacial charge-transfer efficiency [153]. Owing to their structural anisotropy and compositional complexity, these materials exhibit superior HER kinetics across a wide pH range [172]. Molybdenum disulfide (MoS_2), a two-dimensional transition metal dichalcogenide with a graphene-like layered structure, is a representative Pt alternative for energy conversion and storage, owing to its atomic hydrogen adsorption free energy being comparable to that of platinum-group metals [173–175]. However, crystalline MoS_2 electrodes suffer from low electrical conductivity, synthetic complexity, limited stability in acidic media, solubility issues, and scalability challenges [176]. To address these limitations, Wu et al. used a POM-based precursor (Co_2Mo_{10}) to rationally design and hydrothermally synthesize novel bimetallic sulfide nanocomposites (CoS_2-MoS_2) (Fig. 13(a)) [177]. The resulting CoS_2-MoS_2 featured large-scale, uniformly distributed "flower-like" architectures composed of interlaced nanosheets, generating abundant mesopores and ensuring intimate contact with the electrolyte, thereby exposing a higher density of catalytically active sites (Fig. 13(b)). Compared to pristine MoS_2, the CoS_2-MoS_2 nanocomposite exhibited considerably enhanced HER performance, requiring overpotentials of only 120 and 153 mV to achieve a current density of 10 mA·cm^{-2} in 1.0 M KOH and 0.5 M H_2SO_4, respectively, while maintaining excellent chemical stability and long-term durability (Figs. 13(c)–13(h)). Similarly, Wang et al. used Keplerate-type POM nanospheres as molecular precursors to synthesize transition-metal-doped MoS_2 on carbon cloth (M-MoS_2/CC) via a one-step hydrothermal sulfidation process (Fig. 13(i)) [178]. The unique spherical and porous structure of the Keplerate POMs, coupled with their atomically homogeneous metal distribution, enabled uniform sulfur penetration during sulfidation and effectively suppressed phase segregation (Fig. 13(j)). Fe doping further increased the interlayer spacing of MoS_2, generated abundant sulfur vacancies, and tuned the electronic structure, thereby exposing more active sites, optimizing hydrogen adsorption, and enhancing charge transfer. Therefore, the resulting

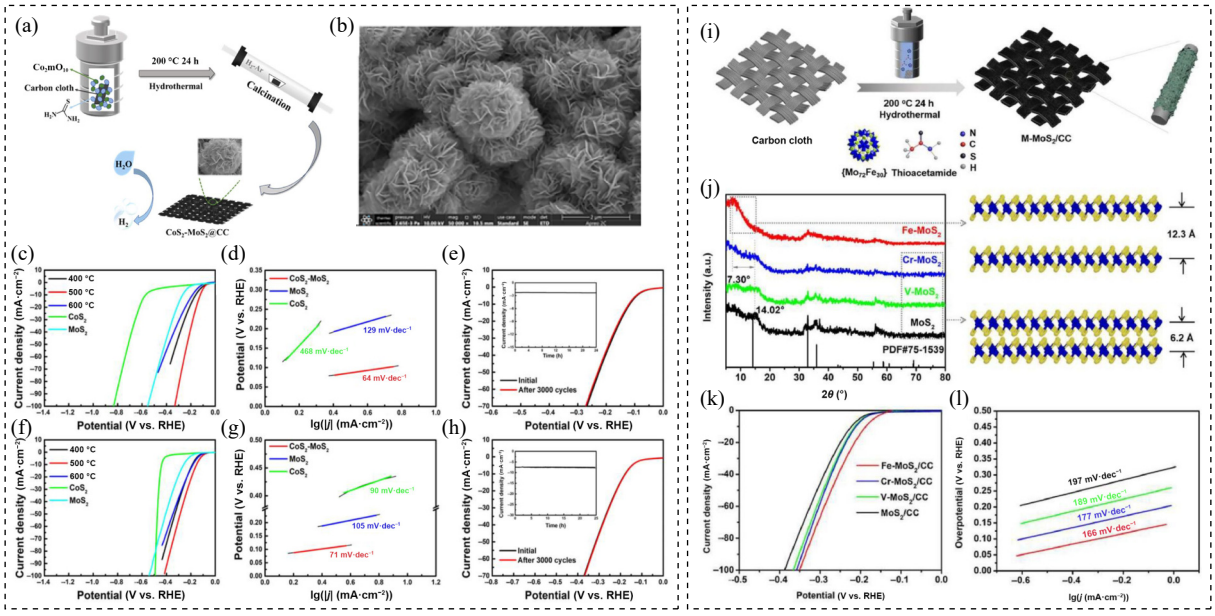

Figure 13 (a) Synthetic route and (b) SEM image of CoS_2-MoS_2. (c)–(e) HER performance of the catalyst in 1 M KOH. (d)–(f) HER performance of the catalyst in 0.5 M H_2SO_4. Reprinted with permission from Ref. [177], © American Chemical Society 2023. (i) Illustration of the preparation of M-MoS_2/CC. (j) XRD patterns of $MMoS_2$/CC. At the right, the structural models of MoS_2 with different interlayer spacings. (k) LSV curves and (l) Tafel plots of M-MoS_2/CC in 0.5 M H_2SO_4. Reprinted with permission from Ref. [178], © Published by Elsevier B.V. on behalf of Chinese Chemical Society and Institute of Materia Medica, Chinese Academy of Medical Sciences 2024.

catalyst demonstrated outstanding HER activity in both acidic and alkaline media (Figs. 13(k) and 13(l)). This work provides valuable insights for the rational design of POM-derived HER electrocatalysts with broad pH applicability and high operational stability.

Yu et al. prepared a POM-derived multi-metal chalcogenide composite, $MoS_2/CoS_2@Ni_3S_2/Ni_3Se_2$, via a two-step hydrothermal sulfidation–selenization procedure (Figs. 14(a) and 14(b)) [179]. The heterometallic polyoxometalate $(C_3H_5N_2)_6CoMo_{12}O_{40}{\cdot}10H_2O$ served as a uniform Co–Mo precursor, while the NF simultaneously supplied the Ni source and served as a conductive scaffold (Figs. 14(c) and 14(d)). As molecular precursors, POMs enabled accurate control over composition and structure during thermal processing, facilitating the formation of a tri-metal synergistic chalcogenide architecture. The resulting material exhibited a layered morphology, with the NF surface densely covered by Ni_3S_2 and monolayer 2H-phase MoS_2 nanosheets uniformly grown atop Ni_3Se_2 regions. The combination of Ni-derived conductivity and MoS_2–CoS_2 synergy led to considerably enhanced HER performance, achieving a current density of 10 $mA{\cdot}cm^{-2}$ at an overpotential of 54 mV in 1.0 M KOH—approaching the activity of commercial Pt catalysts.

Wang et al. constructed a Mo_7-based POM superlattice coordinated with triazine (CTA) and Co^{2+} (Mo_7-Co-CTA) via a hydrothermal method, which was subsequently converted by sulfidation into a C_3N_4-encapsulated $CoMoS_{3.13}$ nanocomposite catalyst CoMoS@CN (Fig. 14(e)) [5]. The long-range ordered arrangement of POM units effectively suppressed aggregation of the metal centers, achieving molecular-level pre-isolation of Mo and Co sites. This approach minimized the migration and clustering of active components during thermal treatment, overcoming the self-aggregation and random distribution issues common in conventional POM precursors, and thereby enabling highly dispersed active centers. Following high-temperature sulfidation, the superlattice precursor was converted into $CoMoS_{3.13}$ nanoparticles embedded within a C_3N_4 matrix, resulting in a composite with a high specific surface area of 33.59 $m^2{\cdot}g^{-1}$, abundant porosity, and a hydrophilic surface (Figs. 14(f)–14(h)). The CoMoS@CN catalyst exhibited excellent HER performance, achieving a current density of 10 $mA{\cdot}cm^{-2}$ at overpotentials of 164 mV in acidic media and 95 mV in alkaline media, with Tafel slopes of 33.02 and 62.05 $mV{\cdot}dec^{-1}$, respectively. The C_3N_4 shell not only enhanced electronic conductivity and chemical stability but also supplied abundant interfacial active sites. Hou et al. used a POMCP, $(trz)_3Ni_2[H_3GeMo_{12}O_{40}]$, as a molecularly homogeneous precursor and obtained a Ni_3S_2/MoS_2/rGO ternary composite catalyst via a one-step hydrothermal sulfidation route [180]. Similarly, Singh et al. used a one-step hydrothermal method followed by annealing to induce an *in situ* reaction between Mo-containing POM precursors and NF, resulting in Ni_3S_2-MoS_2 heterostructured nanosheet arrays uniformly anchored on the NF surface. The molecular-level Mo source provided by the POM ensured uniform nucleation and growth of MoS_2 during sulfidation, while the concurrently formed Ni_3S_2 on NF established intimate coupling with MoS_2. This synergistic interface facilitated abundant defect formation and efficient electronic pathways. Therefore, the Ni_3S_2–MoS_2 heterostructures exhibited outstanding HER performance in alkaline media, achieving a current density of 10 $mA{\cdot}cm^{-2}$ at only 88 mV overpotential, with a Tafel slope of 52 $mV{\cdot}dec^{-1}$, while maintaining structural and catalytic stability during long-term cycling. The electronic interaction between Ni_3S_2 and MoS_2 optimized the hydrogen adsorption free energy, simultaneously enhancing conductivity and the utilization of active sites.

POM-derived, heteroatom-regulated chalcogenide hybrids have demonstrated high efficacy for HER catalysis. The incorporation of multiple transition metals allows accurate electronic tuning, defect engineering, and the formation of hierarchical heterostructures. Representative systems—such as $MoS_2/CoS_2@Ni_3S_2/Ni_3Se_2$, CoMoS@CN, and Ni_3S_2–MoS_2 heterostructures—exhibit low overpotentials, rapid reaction kinetics, and excellent stability across

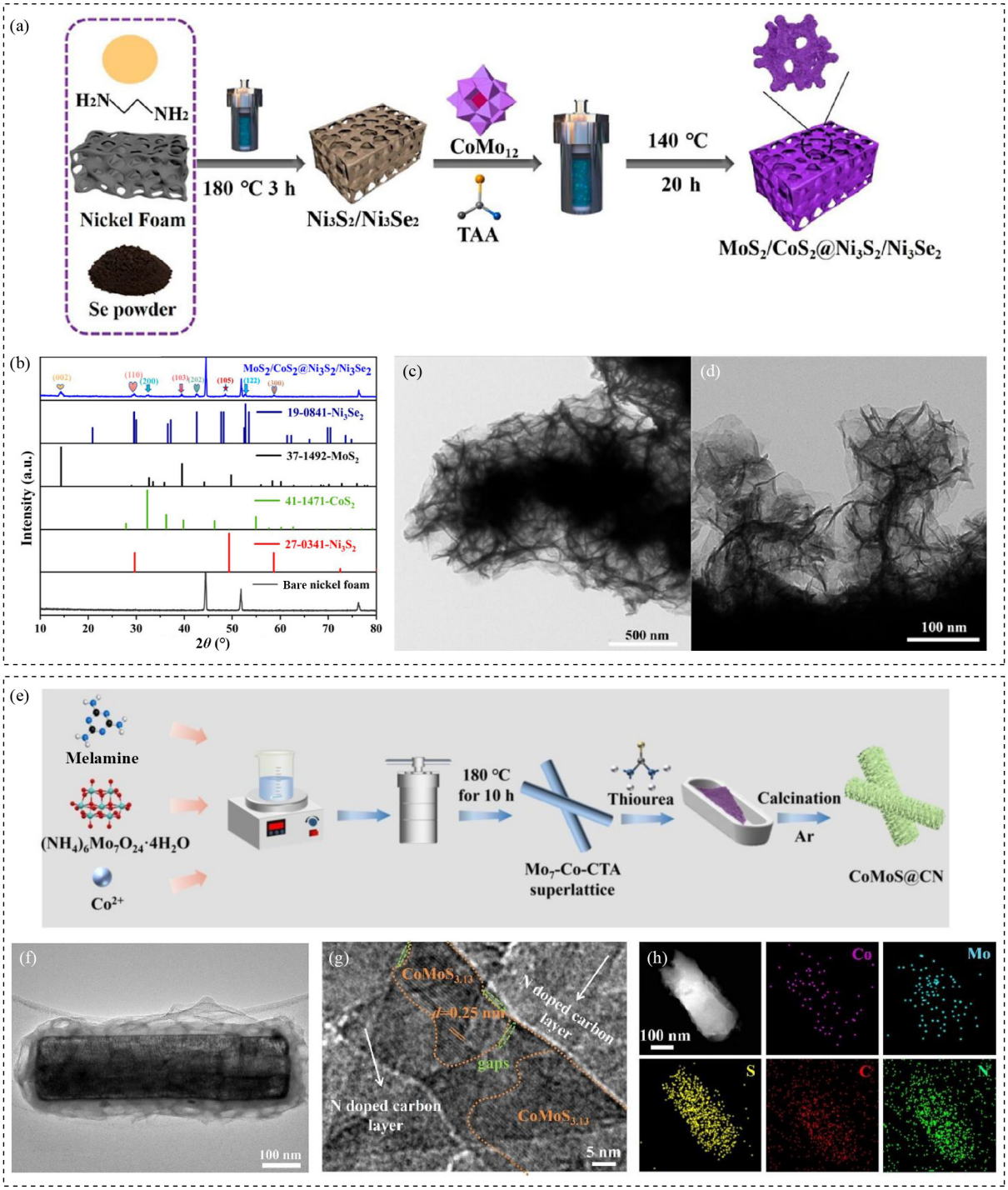

Figure 14 (a) Formative strategy of $MoS_2/CoS_2@Ni_3S_2/Ni_3Se_2$. (b) PXRD patterns of $MoS_2/CoS_2@Ni_3S_2/Ni_3Se_2$. (c) and (d) TEM images of the $MoS_2/CoS_2@Ni_3S_2/Ni_3Se_2$ composite. Reprinted with permission from Ref. [179], © American Chemical Society 2024. (e) Illustration of the synthetic process of Mo_7-Co-CTA-derived CoMoS@CN. (f) TEM image, (g) HRTEM image and (h) TEM EDX mapping images of Co, Mo, S, C, and N in CoMoS@CN-500. Reprinted with permission from Ref. [5], © Elsevier Inc. 2024.

a wide pH range. These studies underscore that POMs act as uniform metal sources while facilitating heteroatom enrichment and structural anisotropy, providing a versatile strategy for designing high-performance HER electrocatalysts.

3.4.3 POM-derived nitrogen-activated metal cluster catalysts

Nitrogen-activated catalysts, such as TMNs, benefit from optimized d-band states, enhanced conductivity, and moderate hydrogen-binding energies. TMNs are typically formed by incorporating nitrogen atoms into the interstitial sites of metal precursors. Thermal conversion of POMs under ammonia or nitrogen-rich atmospheres offers an effective strategy to synthesize nitrogen-activated metal clusters, including TMNs and nitrogen-doped metal composites [181]. In this process, nitrogen acts not only as a structural dopant but also modulates the electronic configuration of the metal centers, promoting charge delocalization and enhancing

intrinsic catalytic activity. POM-derived materials such as Mo_2N, VN, and Co_3N generally exhibit excellent conductivity, chemical stability, and moderate hydrogen adsorption energies, making them representative high-performance HER catalysts [182–184]. Additionally, the *in situ*-generated carbon matrix during pyrolysis provides confinement for the metal clusters, preventing aggregation and improving structural stability [152]. For instance, Miao et al. reported a composite catalyst in which hexagonal MoN (h-MoN) nanoparticles were encapsulated in boron- and nitrogen-codoped CNTs (BNCNTs), forming h-MoN@BNCNT (Fig. 15(a)) [185]. Using $(NH_4)_6Mo_7O_{24}$ as the Mo source, h-MoN nanoparticles were generated *in situ* in BNCNTs via post-synthetic ammonolysis, effectively preventing particle aggregation and preserving structural integrity in complex electrolytes (Figs. 15(b)–15(e)). The h-MoN@BNCNT catalyst delivered a current density of 10 $mA{\cdot}cm^{-2}$ at an overpotential of only 78 mV in 0.5 M H_2SO_4, with a Tafel slope of 46 $mV{\cdot}dec^{-1}$, outperforming most reported Mo-based catalysts and doped carbon materials (Fig. 15(f)). DFT calculations further revealed that the hydrogen adsorption free energy at the h-MoN (001) surface interfaced with BN or N-doped carbon was near thermoneutral, considerably optimizing hydrogen adsorption and desorption kinetics. This work provides valuable guidance for the rational design of POM-derived MXene/carbon composites for efficient and stable HER catalysis under complex conditions.

Wen et al. used a one-step ammonia nitridation strategy to *in situ* load Pt nanoclusters onto the surface of Mo_2N nanosheets, constructing a Pt/Mo_2N heterostructure with high-density interfacial contact (Fig. 15(g)) [186]. Mo_2N was derived from a POM precursor through simultaneous thermal decomposition and ammonia treatment, achieving both structural nitridation and uniform dispersion of metal clusters. This approach preserved the molecular-level uniformity of Mo from the POM while introducing excellent conductivity and nitrogen-activated sites via nitridation. The resulting Pt/Mo_2N catalyst exhibited HER activity in acidic media comparable to commercial Pt/C, achieving 10 $mA{\cdot}cm^{-2}$ at an overpotential of only 22 mV, with a Tafel slope of 20 $mV{\cdot}dec^{-1}$, while maintaining stability during prolonged cycling (Figs. 15(h)–15(j)). DFT calculations further indicate that electronic redistribution at the Pt–Mo_2N interface effectively lowers the free energy of hydrogen intermediates, considerably accelerating proton–electron coupled transfer. Huang et al. developed a highly efficient HER catalyst, Al- and O-codoped Mo_2N quantum dots anchored on N-doped rGO (AlO@Mo_2N-NrGO), via atomic-level interface engineering (Fig. 16(a)) [187]. Using an Anderson-type POM ($AlMo_6$) as the precursor, this strategy enabled uniform dispersion of Mo_2N quantum dots and *in situ* Al/O doping. Al doping effectively suppressed Mo_2N aggregation (Figs. 16(b) and 16(c)), while surface reconstruction produced Al–OH hydrates, considerably enhancing hydrophilicity and catalytic activity. The AlO@Mo_2N-NrGO catalyst exhibited outstanding HER performance in 1.0 M KOH, achieving an overpotential of 82 mV and maintaining stable operation at a high current density of 400 $mA{\cdot}cm^{-2}$ for 300 h (Figs. 16(d) and 16(e)). DFT calculations further confirmed that Al–OH adsorption optimized the hydrogen adsorption free energy and lowered the energy barriers for water dissociation and hydrogen desorption.

Thus, exploiting the atomic-level uniformity of POMs enables the design of high-activity, compositionally tunable TMN catalytic systems. Nitrogen incorporation modulates the metal d-band and electronic structure, imparting Pt-like catalytic properties to TMNs. By engineering heterointerfaces and establishing clear structure–activity relationships, the hydrogen adsorption free energy can be optimized, considerably enhancing both HER activity and long-term stability.

3.4.4 *Phosphorus-doped nanoalloy and composite catalysts*

Phosphorus doping in nanoalloy catalysts plays a crucial role in tailoring metal–phosphorus coordination, modulating the electronic states of active metal centers, and optimizing hydrogen adsorption thermodynamics. This P-induced electronic modulation also promotes interfacial water dissociation, accelerating the Volmer step and enabling high HER activity in alkaline environments [188, 189]. Recently, POM-derived phosphorus-containing HER catalysts have attracted considerable attention owing to their strong metal–phosphorus interactions and favorable electronic structures, which endow them with excellent catalytic potential [92, 169, 190]. Phosphidation of metal-rich POMs enables the formation of various TMPs, such as CoP and MoP, characterized by high specific surface areas and nanoscale crystalline structures [146, 191]. The incorporation of phosphorus induces electronic redistribution at the catalyst–electrolyte interface, thereby reducing reaction energy barriers [192]. Using POMs as precursors enables atomic-level metal dispersion and accurate stoichiometric control, allowing the fabrication of structurally well-defined, stable TMP composites or core–shell architectures [193, 194]. However, previously reported MoP materials often suffer from large particle sizes, which limit catalytic performance. Reducing particle size is therefore a key strategy for enhancing activity because the "small-size effect" exposes more active atoms. For instance, phosphomolybdic acid $H_3PMo_{12}O_{40}$, a Keggin-type molybdenum oxide cluster of ~ 1 nm, is an ideal molybdenum precursor [195]. Conductive supports, such as CNTs and graphene, can anchor POMs through covalent or intermolecular interactions, further preventing aggregation [196]. Moreover, MOF-derived phosphides enable molecular-level dispersion of POMs, effectively suppressing MoP particle aggregation and yielding highly active MoP with rapid electron and energy transfer [197]. Liu et al. adopted a POMs@MOFs confined-conversion strategy, using Keggin-type PMo_{12} encapsulated within UiO-66 as the precursor. Through a three-step process involving carbonization, template etching, and phosphidation, they fabricated an ultrastructurally hydrophilic HER electrocatalyst composed of molybdenum phosphide quantum dots embedded in a porous carbon matrix (MoP-QDs@PC) (Figs. 17(a)–17(d)) [77]. The MoP quantum dots were *in situ* integrated into the porous carbon scaffold, and the resulting catalyst exhibited excellent HER performance in both acidic and alkaline media, delivering overpotentials of 118.8 and 98.8 mV at 10 $mA{\cdot}cm^{-2}$, respectively, and outperforming commercial Pt/C at high current densities. The molecular-level dispersion of the POM precursor, together with the confinement effect of the MOF, effectively inhibited MoP sintering, while the P/O codoped carbon matrix formed during phosphidation enhanced electrical conductivity and imparted superhydrophilicity, thereby facilitating mass transport at the three-phase interface.

Zhao et al. reported the synthesis of a MoP/MoNiP@NPC electrocatalyst using a Ni–POM complex, $[Ni(2,2'\text{-bipy})_3][Mo_6O_{19}]$, as the precursor. With NaH_2PO_2 as the phosphorus source, high-temperature phosphidation enabled the accurate conversion of the POM into bimetallic phosphides (Fig. 17(e)) [198]. Highly dispersed MoP and MoNiP nanoparticles were embedded in an

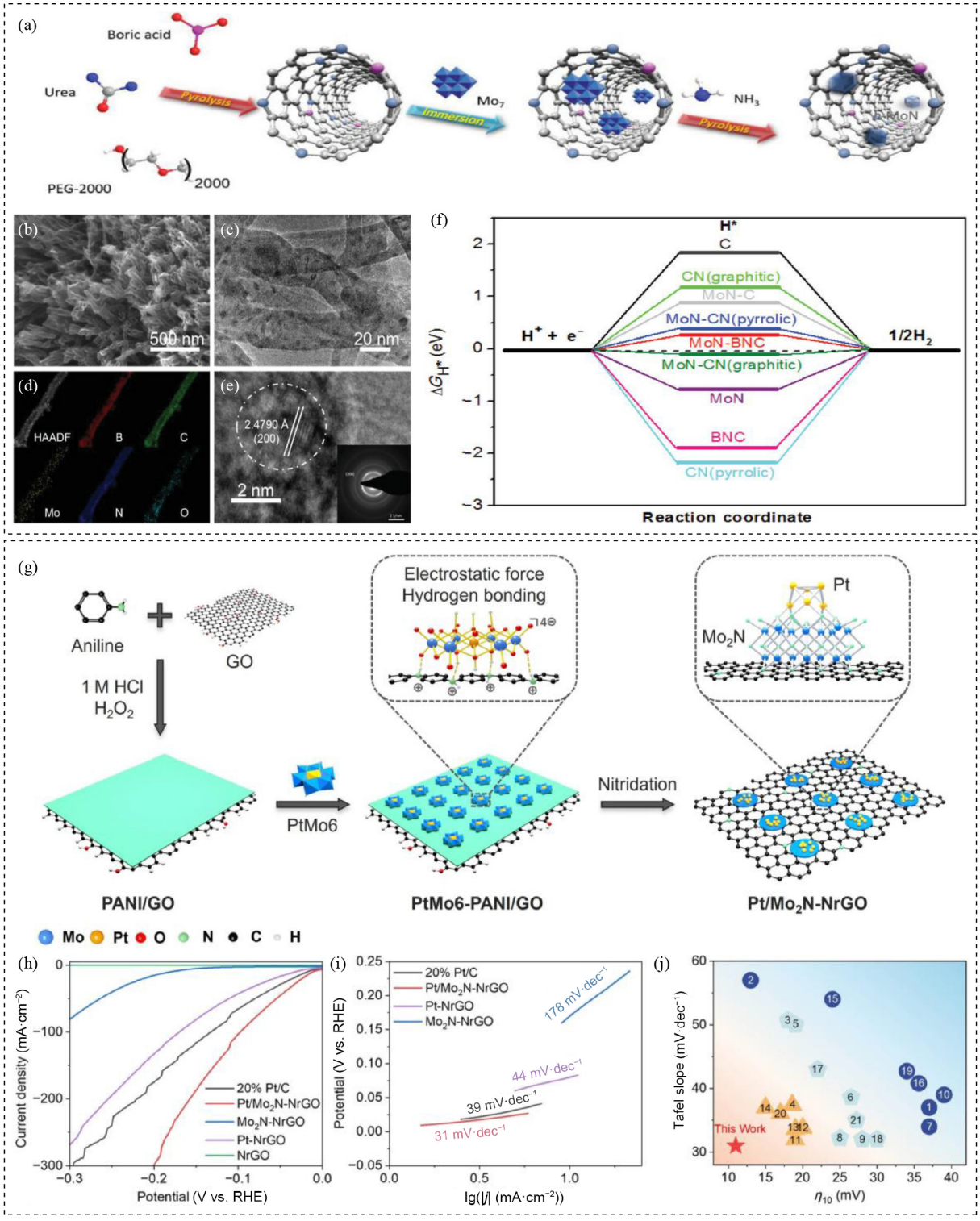

Figure 15 (a) Schematic illustration for the fabrication process, (b) SEM image, (c) TEM image, (d) corresponding elemental mapping of C, N, and Mo, and (e) HRTEM image (inset: SAED pattern) of h-MoN@BNCNT. (f) DFT-calculated free energy for H* adsorption on various surfaces. Reprinted with permission from Ref. [185], © WILEY-VCH Verlag GmbH & Co. KGaA, Weinheim 2018. (g) Schematic illustration of synthetic route to the Pt/Mo_2N-NrGO electrocatalyst. (h) LSV curves and (i) Tafel slope diagrams of 20% Pt/C, Pt/Mo_2N-NrGO, Pt-NrGO, and Mo_2N-NrGO. (j) Comparison of merits concerning Tafel slop. Reprinted with permission from Ref. [186], © Zhou, W. B. et al. 2025.

N,P codoped carbon matrix, forming a three-dimensional honeycomb-like porous structure (Figs. 17(f)–17(i)). The catalyst achieved low overpotentials of 50.4 and 72.6 mV at 10 mA·cm^{-2} under alkaline and acidic conditions, respectively (Figs. 17(j)–17(m)). The N,P codoped carbon substrate effectively modulated the electronic density and suppressed particle aggregation, while the strong coupling at the MoP/MoNiP interface promoted charge transfer and optimized intermediate adsorption and desorption.

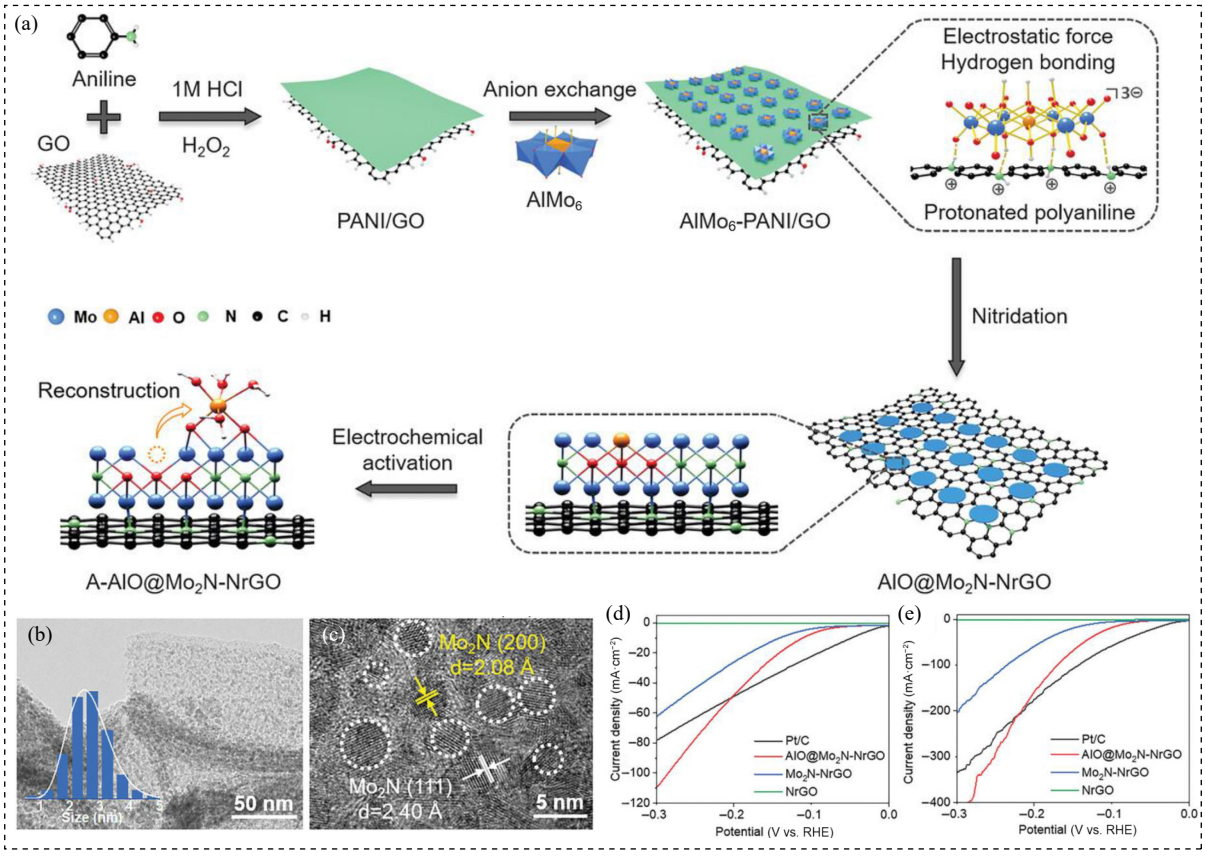

Figure 16 (a) Schematic illustration of the synthesis of AlO@Mo_2N-NrGO quantum dots. (b) TEM image (inset: particle size distribution). (c) HRTEM image. Polarization curves of Pt/C, AlO@Mo_2N-NrGO, Mo_2N-NrGO, and NrGO (d) without and (e) with *iR* compensation. Reprinted with permission from Ref. [187], © Huang, Y. C. et al. 2022.

DFT calculations revealed that the negatively charged P sites acted as the optimal active centers, with Gibbs free energies close to thermoneutral, enabling rapid Volmer–Heyrovsky kinetics. In addition, Tang et al. developed a solvent-free, solid-state hot-pressing method to rapidly fabricate POMs-ZIF precursors on carbon cloth, which were subsequently phosphidated to yield N-doped carbon-encapsulated bimetallic phosphide composites (CoP/MoP@NC/CC) [75]. This method enabled uniform and robust loading of the precursors onto the conductive substrate, preventing detachment of active materials during electrocatalysis. The resulting CoP/MoP@NC/CC catalyst exhibited outstanding bifunctional performance. In 1 M KOH, it achieved 10 mA·cm^{-2} for HER at an overpotential of 94 mV, with a Tafel slope of 40 mV·dec^{-1}. Its enhanced activity and stability at high current densities were attributed to the synergistic interaction between CoP and MoP, the *in situ* formation of oxide/hydroxide layers on the phosphide surface, and the protective N-doped carbon coating, enabling HER to proceed at 1000 mA·cm^{-2} with an overpotential of 475 mV. When assembled in a full water electrolysis cell, the system required only 1.71 V to drive 50 mA·cm^{-2}, outperforming noble-metal benchmarks such as 20% Pt/C. In a related study, Ma et al. embedded Keggin-type POMs into a ZIF-67 framework as a precursor and, via two-step oxidation–phosphidation on NF, successfully constructed a crystalline/amorphous coupled CoP/a-CoMoP electrocatalyst [78]. Mo doping and the abundant crystalline–amorphous interfaces effectively tuned the electronic structure, increased the density of catalytic sites, and promoted interfacial electron transfer, thereby enhancing both OER and HER kinetics. Li et al. used a soft-templating strategy using POMs, gallic acid, and ammonium polyphosphate as precursors, followed by one-step phosphidation and high-temperature calcination to prepare mesoporous phosphorus-doped molybdenum phosphide (P-MoP@C) (Fig. 18(a)) [199]. The triphenol groups in gallic acid formed strong hydrogen-bond interactions with block copolymers, guiding self-assembly into a highly ordered mesoporous framework that increased active-site exposure and facilitated electron transfer and electrolyte diffusion (Figs. 18(b) and 18(c)). The combination of the mesoporous architecture, carbon layer protection, and P-doping-induced electronic optimization endowed the catalyst with excellent HER performance. At 10 mA·cm^{-2}, the overpotentials were 162 mV in 0.5 M H_2SO_4 and 149 mV in 1.0 M KOH, with Tafel slopes of 86 and 98 mV·dec^{-1}, respectively (Figs. 18(d)–18(g)), while maintaining good cycling stability and long-term durability.

Phosphorus-doped nanoalloys and POM-derived composite materials have emerged as highly efficient HER catalysts owing to strong metal–phosphorus interactions and tunable electronic structures. Rich-metal POMs can be atomically dispersed and transformed into CoP, MoP, or bimetallic phosphides, forming nanoparticles or core–shell architectures with high surface area, hierarchical porosity, and excellent structural stability. Common strategies—including POM@MOF confinement, Ni–POM transformation, and POM–ZIF phosphidation—effectively suppress sintering, optimize electronic structure, and expose abundant active sites. N/P-doped carbon frameworks and crystalline–amorphous interfaces further enhance interfacial synergistic effects, yielding low overpotentials, high current

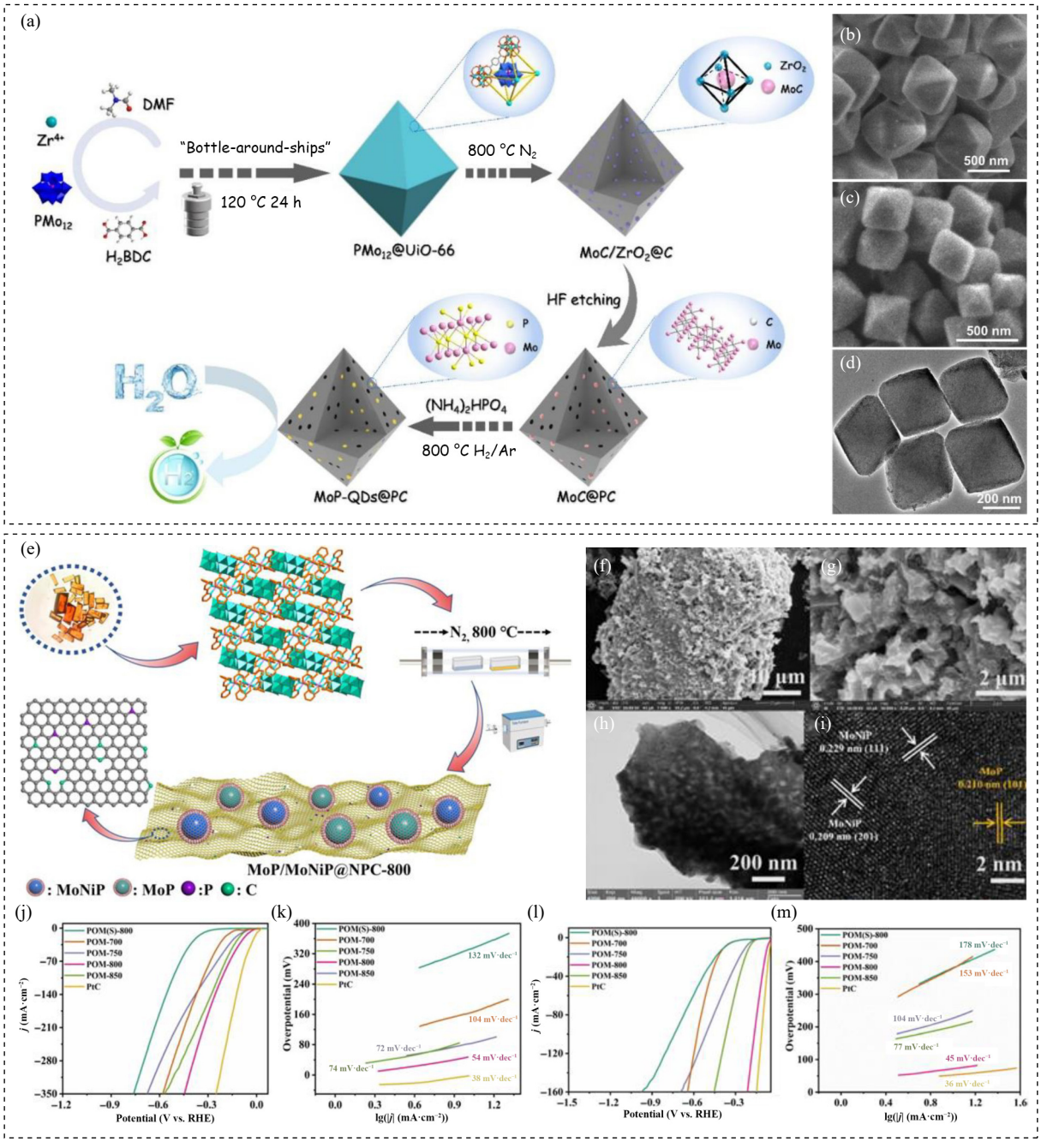

Figure 17 (a) Schematic illustration of synthetic process of MoP-QDs@PC electrocatalyst via MOF-assisted *in-situ* confined conversion strategy. (b) SEM image of PMo_{12}@UiO-66. (c) SEM and (d) TEM images of MoP-QDs@PC. Reprinted with permission from Ref. [77], © Elsevier B.V. 2022. (e) The fabrication of the MoP/MoNiP@NPC-800 catalyst by pyrolysis. (f) and (g) SEM images of MoP/MoNiP@NPC-800 at different magnifications. (h) TEM and (i) HRTEM images of MoP/MoNiP@NPC-800. (j) Polarization curves and (k) Tafel slopes calculated from the LSV of five POM-derived catalysts and Pt/C in 1 M KOH. (l) Polarization curves and (m) Tafel slopes calculated from the LSV of five POM-derived catalysts and Pt/C in 0.5 M H_2SO_4. Reprinted with permission from Ref. [198], © Royal Society of Chemistry 2024.

densities, and long-term HER stability in both acidic and alkaline media. The molecular-level uniformity and compositional tunability afforded by POM precursors provide a versatile platform for the rational design of highly active, cost-effective TMP-based HER electrocatalysts.

3.4.5 POM-derived composite systems beyond conventional classifications

The structural accuracy of POM precursors also enables the design of unconventional HER catalysts, where atomic-level metal distribution and heteroatom incorporation can be accurately controlled. Beyond traditional carbides, nitrides, and chalcogenides, recent studies have shown that POMs serve as versatile precursors for constructing novel HER-active materials, including metal oxynitride complexes, SACs, and bimetallic heterostructures [200–203]. These systems benefit from the accurate metal–oxygen connectivity and rich heteroatom composition intrinsic to POMs, allowing atomic-level dispersion, electronic structure tuning, and

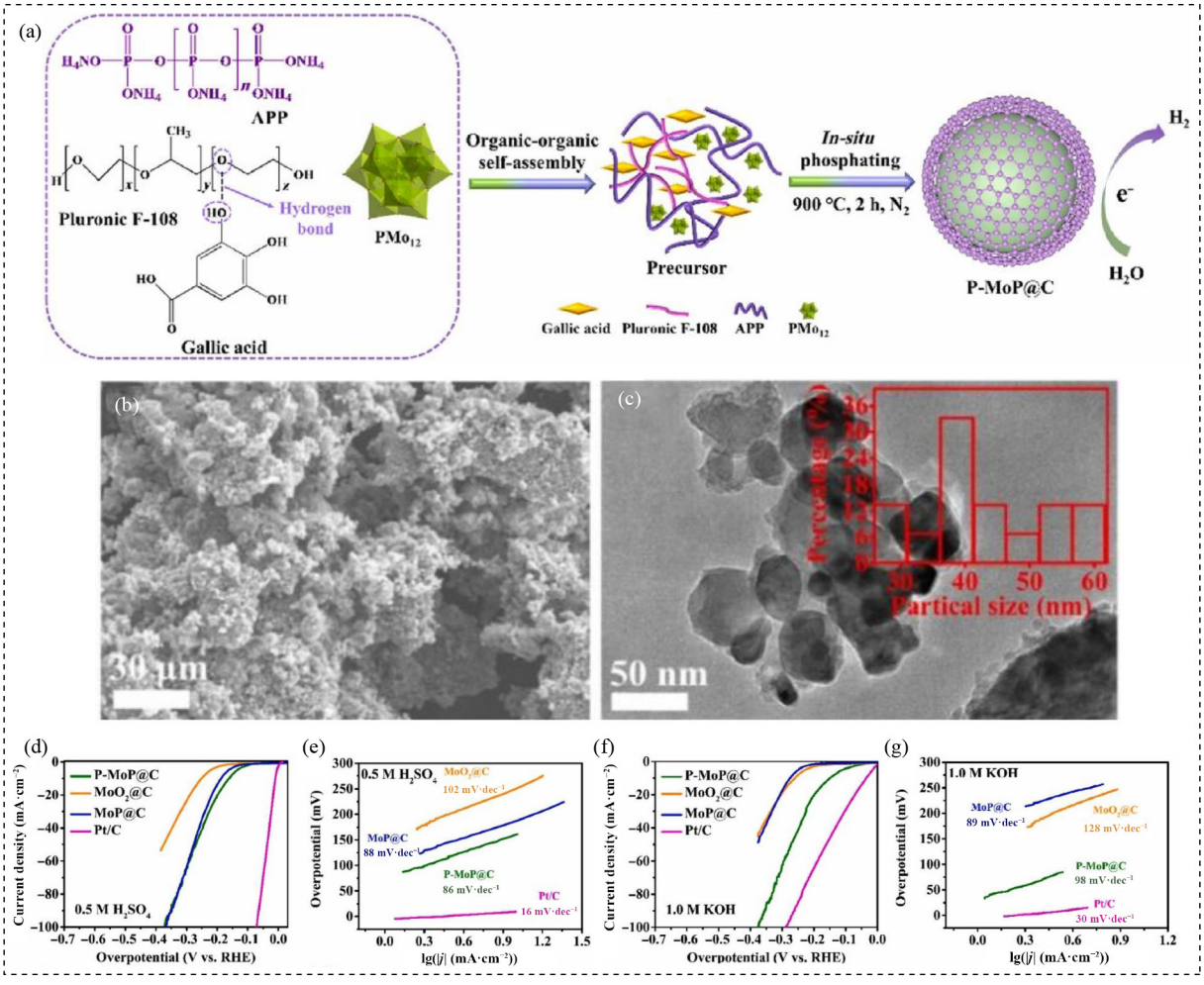

Figure 18 (a) The schematic diagram of the synthesis, (b) SEM image, and (c) TEM image of P-MoP@C. In 0.5 M H_2SO_4, (d) LSV curves and (e) Tafel slope plots of P-MoP@C, MoO_2@C, MoP@C, and Pt/C. In 1.0 M KOH, (f) LSV curves and (g) Tafel slope plots of P-MoP@C, MoO_2@C, MoP@C, and Pt/C. Reprinted with permission from Ref. [199], © Hydrogen Energy Publications LLC 2024.

defect engineering [14]. Ma et al. reported a strategy based on POM reconstruction and directional immobilization induced by metal–organic coordination units to enhance HER performance (Fig. 19(a)) [204]. Crystalline MOFs constructed with bis-pyrazole–bis-amide ligands induced *in situ* POM reconstruction and directional fixation, effectively controlling the spatial distribution of active sites. The resulting complexes containing discrete $[AlMo_6(OH)_7O_{17}]^{2-}$ anions exhibited exceptional electrocatalytic activity, achieving a remarkably low overpotential of 17 mV at 10 mA·cm^{-2} in 1 M KOH, while maintaining excellent stability and low overpotential in simulated seawater. Wei et al. used DFT calculations to study the effect of single transition metal doping on surface HER efficiency, proposing a Lindqvist-type POM cluster $[VW_5O_{19}]^{3-}$, where transition metals were anchored on the V-POM surface to enhance activity [205]. DFT calculations identified the three-vacancy site (3H-site), located at the center of the O_{12}–O_{14}–O_{17} triangle, as the optimal anchoring position. Upon metal doping, stable configurations formed, and for the Volmer step, V@V-POM exhibited ΔG_{H^*} = 0.03 eV, lower than Pt(111) (0.09 eV), representing a theoretical optimum. Along the Volmer–Tafel pathway, V@V-POM achieved ΔG_{H^*} = 0 eV with a reaction barrier lower than that of Pt. Moreover, the lowest Bader charge of Au@V-POM was 0.99 eV, indicating minimal electron transfer and facilitating efficient H* desorption. The d-band center of V@V-POM (ε_d = 0.382 eV) lies near the Fermi level, optimizing H* binding energy. Incorporation of POMs into covalent organic frameworks (COFs) provides another effective strategy to enhance HER electrocatalysis. Beyond their performance in alkaline HER systems, POM-based single-atom catalysts are particularly relevant for proton exchange membrane (PEM) electrolyzers, which require operation under strongly acidic conditions. Lacunary and Anderson-type POM frameworks offer well-defined O-donor coordination pockets that stabilize isolated metal atoms (e.g., Pt_1, Ir_1, Co_1) via robust M–O bonding, preventing atom migration and dissolution in corrosive environments. Additionally, the strong electron-withdrawing properties of Mo/W–O clusters modulate the oxidation state and d-band center of the anchored atoms, improving ΔG_H and accelerating PCET. Recent studies have shown that POM-anchored Pt single atoms retain high mass activity and structural integrity in acidic PEM-relevant electrolytes, highlighting the potential of POM-supported SACs as low-loading, durable acidic-HER electrocatalysts [206]. Recently, Sohail et al. immobilized a Lindqvist-type POM onto COFs containing metal–porphyrin and ethylenediamine units (Et@PZn), forming the LPOM@EtPZn hybrid system [207]. This POM–COF hybrid leveraged molecular confinement and interfacial synergistic effects, substantially reducing the HER overpotential in alkaline media, with the Tafel slope decreasing from 161 mV·dec^{-1} for the pristine

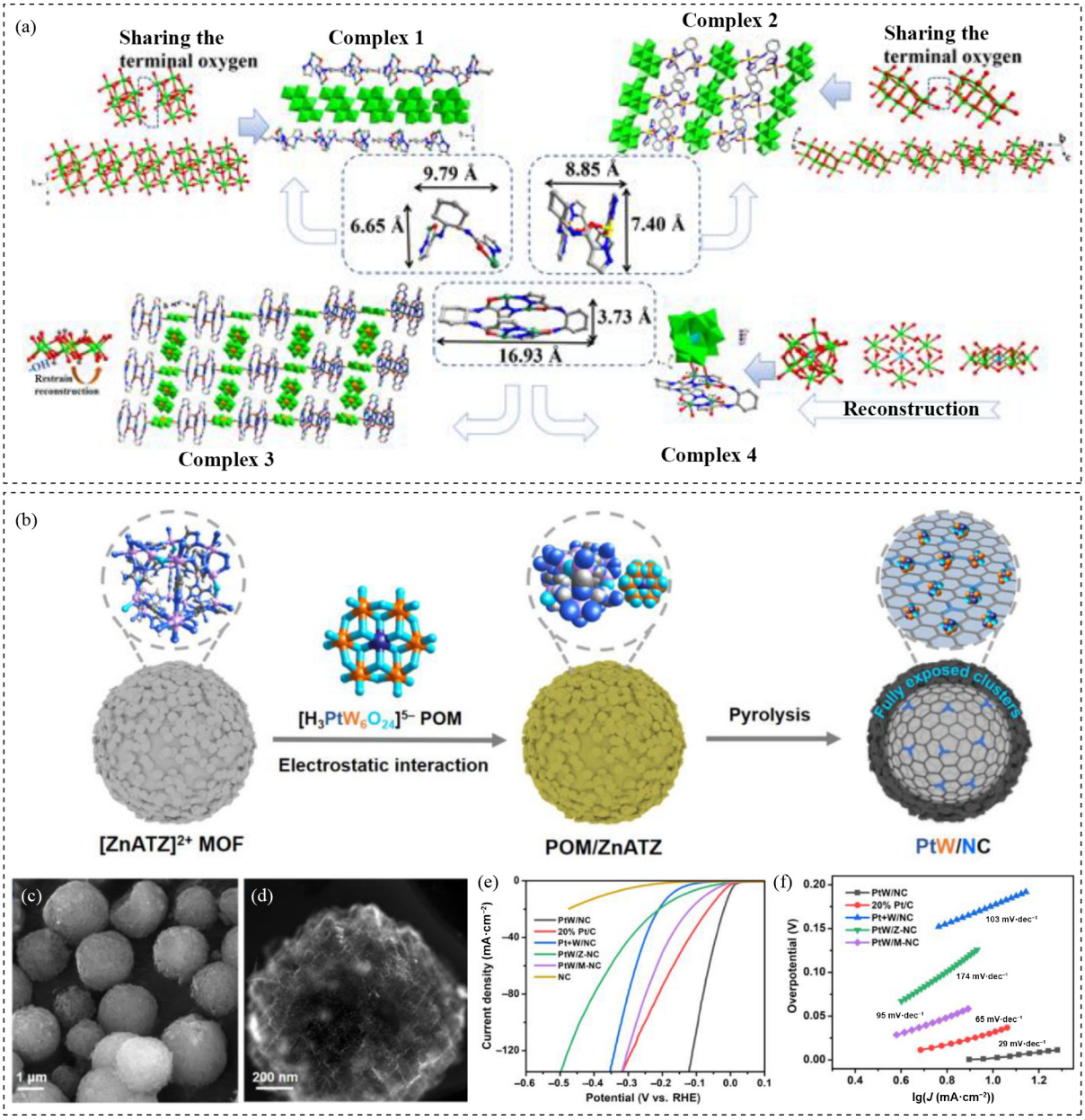

Figure 19 (a) Schematic diagram of the reconstruction of polymolybdate induced by metal–organic coordination units. Reprinted with permission from Ref. [204], © Royal Society of Chemistry 2024. (b) Schematic illustration of the fabrication of PtW/NC. (c) SEM image of the as-prepared POM/ZnATZ. (d) HAADF-STEM image of PtW/NC with a spherical morphology. (e) Polarization curves for PtW/NC, control samples, and commercial Pt/C in 1.0 M KOH with a scan rate of 10 mV·s^{-1}. (f) Tafel plots for different catalysts. Reprinted with permission from Ref. [208], © American Chemical Society 2024.

COF to 115 mV·dec^{-1}—surpassing even commercial 20% Pt/C. Electrochemical impedance spectroscopy (EIS) and electrochemically active surface area (ECSA) measurements further confirmed enhanced charge transfer and efficient utilization of active sites in the hybrid material.

Chen et al. reported the synthesis of fully exposed sub-nanometer PtW bimetallic clusters on nitrogen-doped carbon via an electrostatic interaction strategy (Fig. 19(b)) [208]. Negatively charged $[H_3PtW_6O_{24}]^{5-}$ POMs were electrostatically anchored onto the positively charged MOF $[ZnATZ]^{2+}$, enabling uniform dispersion of PtW clusters on the NC surface and preventing aggregation or embedding of metal species during high-temperature pyrolysis (Figs. 19(c) and 19(d)). In 1 M KOH, the catalyst achieved 100 mA·cm^{-2} at an overpotential of 95 mV, with a Tafel slope of 29 mV·dec^{-1} and remarkable long-term stability, exhibiting a Pt mass activity approximately 34 times higher than that of commercial Pt/C (Figs. 19(e) and 19(f)). DFT calculations indicated that W incorporation into the PtW clusters optimized H_2O adsorption and dissociation barriers and reduced H adsorption free energy, considerably enhancing HER activity.

Li et al. synthesized a novel two-dimensional MoCu-POMOF material via a hydrothermal method, which was subsequently subjected to acid etching and high-temperature carbonization to yield a MoO_2/MoOC heterostructure with high specific surface area and abundant active sites [209]. Ultra-low loading of Pt nanoparticles (Pt NPs) was electrodeposited onto this support to construct the Pt@MoO_2/MoOC composite electrocatalyst. In 0.5 M H_2SO_4, the catalyst achieved 10 mA·cm^{-2} at an overpotential of

98.99 mV, with a Tafel slope of 81.4 mV·dec^{-1}, while maintaining excellent stability. The synergy between Pt NPs and the MoO_2/MoOC support tuned the electronic structure, lowered the hydrogen adsorption free energy, and accelerated HER kinetics. In a related study, Wen et al. used PMo_{12} as both Mo and P sources, together with Co salts, to synthesize a three-dimensional hierarchical nanoflower array of P-doped $CoMoO_4$ on NF (P-$CoMoO_4$@Ni-1) via a one-step hydrothermal and calcination process [210]. By leveraging the high solubility and structural-directing ability of POMs, uniform self-supporting arrays with high surface area were fabricated, exposing abundant active sites and facilitating electron transfer and gas bubble release. In alkaline electrolytes, P-$CoMoO_4$@Ni-1 exhibited excellent HER activity with low charge-transfer resistance. In another approach, Yan et al. considerably enhanced hydrogen migration kinetics in Pt-based single-atom catalysts by constructing a multi-shell H-buffer chain [211]. Using a dual-confinement strategy, individual Pt atoms were anchored onto tetra-coordinated oxygen sites of Keggin-type POMs and further confined in sub-nanometer porous carbon, yielding a Pt_1@POMs@PC composite structure.

Beyond intrinsic activity, the durability of POM-derived HER catalysts is critically influenced by structural reconstruction during prolonged cycling. In both alkaline and acidic media, POM-derived carbides, nitrides, and phosphides often undergo surface oxidation, Mo/W leaching, and transformation into hydroxide or oxyhydroxide phases, while isolated POM fragments may experience dissolution–redeposition that dynamically alters surface composition. These reconstructed layers can generate new active motifs (e.g., M–OH or MOOH), yet excessive metal loss can compromise the metal–oxygen framework and accelerate degradation. Recent operando Raman and X-ray absorption spectroscopy (XAS) studies reveal that vacancy-rich domains and atomically anchored metal centers help stabilize H-intermediate binding, suppress uncontrolled reconstruction, and prevent agglomeration under high current densities. These findings show that controlling the interplay between the initial structure and reconstruction pathways is essential for designing durable POM-derived electrocatalysts.

4 POM-based catalysts for OER

The OER during water electrolysis is a critical step in overall water splitting. Its mechanism involves a four-electron–proton transfer, leading to high overpotentials and relatively slow reaction kinetics [212]. Because the OER occurs at the anode and proceeds much more slowly than the HER, developing efficient catalysts is essential to reduce energy consumption and improve overall performance [212, 213]. Currently, iridium (Ir) and ruthenium (Ru) oxides (e.g., IrO_2 and RuO_2) are regarded as state-of-the-art electrocatalysts for OER systems [214]. However, their high cost, limited stability, and solubility issues hinder widespread practical application. Therefore, research has increasingly focused on developing efficient, cost-effective, and stable non-precious metal catalysts [8, 215].

POMs are molecular inorganic nanoanion clusters characterized by spatial network structures that form through high degrees of polymerization [216]. These structures are constructed from high-valence transition metal centers (primarily Mo^{VI} and W^{VI}) coordinated with oxygen ligands in the presence of specific heteroatoms. The high oxidation states of these metals facilitate the selective incorporation of desired cations near OER active sites, enhancing overall catalytic activity [217]. Additionally, their unique anionic frameworks allow modulation of electronic configurations, optimizing metal–metal interactions and further improving catalytic efficiency (Table 2). For instance, Sood et al. synthesized $(C_5H_7N_2)_6[NiW_{12}O_{44}]$—designated PS-78—using Keggin-type POM clusters as the substrate, achieving a low overpotential of 347 mV and stable operation for 96 h at 10 mA·cm^{-2} [218]. However, POMs functioning as OER catalysts exhibit several inherent limitations. First, POMs generally exhibit poor electronic conductivity; most POM assemblies behave as insulators, and their weak electron transport severely limits electrocatalytic performance [219]. Second, their structural stability is often suboptimal: under electrocatalytic conditions, POM-based catalysts frequently undergo structural degradation, particularly during prolonged exposure to corrosive media, mechanical stirring, or alkaline environments, leading to considerable declines in catalytic activity. Third, the catalytic sites in conventional POM clusters typically display limited intrinsic activity; the metal centers often exhibit low efficiency due to saturated coordination environments, and the absence of distinct oxidation or reduction reactive sites hinders robust and synergistic catalysis [110]. Finally, the high solubility of many POMs in reaction media compromises their recyclability. Therefore, researchers are actively exploring strategies to improve both the structural integrity and catalytic performance of POMs [220].

Table 2 POM-based and POM-derived electrocatalysts for OER

Catalysts	Polyoxometalate	Tafel slope (mV·dec^{-1})	η_{10}[a] (mV)	Electrolyte	Ref.
Co_9S_8@$H_3PMo_{12}O_{40}$	$H_3PMo_{12}O_{40}$	68	320	1.0 M KOH	[8]
Fe-S-NiMoO$_4$/MoO$_3$@NF	$(NH_4)_3[FeMo_6O_{24}H_6]\cdot 7H_2O$	41	212	1.0 M KOH	[217]
NiCo-POM/Ni	$Co_{6.8}Ni_{1.2}W_{12}O_{42}(OH)_4(H_2O)_8$	126	360	0.1 M KOH	[219]
POM@ZnCoS/NF	$H_3PMo_{12}O_{40}$	67.7	200	0.5 M H_2SO_4	[110]
Fe_2Ni_2@MWCNT_N6	$Na_{14}[(FeOH_2)_2Ni_2(As_2W_{15}O_{56})_2]\cdot 55H_2O$	45	580	0.1 M KOH	[220]
Mo_1-CoOOH@CP	$PMo_{12}O_{40}\cdot xH_2O$	66	274	1.0 M KOH	[224]
PBA@POM	$H_3PMo_{12}O_{40}$	235	440	1.0 M KOH	[232]
3-CoFeW	$[\{FeCo_3(OH)_3PO_4\}_4(SiW_9O_{34})_4]^{28-}$	36	192	1.0 M KOH	[241]
$Co_5Mo_{10}S_x$/CC	Co_2Mo_{10}/Co_5Mo_{10}	57.8	153	1.0 M KOH	[234]
MWCNT_N8_Co4	$[Co_4(H_2O)_2(PW_9O_{34})_2]^{10-}$	55	400	0.1 M KOH	[242]
O-CoMoS	$(NH_4)_4[Co^{2+}Mo_6O_{24}H_6]\cdot 6H_2O$	45	272	1.0 M KOH	[235]

[a]Overpotential at the current density of 10 mA·cm^{-2}.

The OER typically proceeds via a four-step proton–electron transfer pathway, in which surface-bound OH^*, O^*, and OOH^* intermediates are sequentially formed prior to O_2 release, as shown in Fig. 20. In alkaline electrolytes, the reaction is initiated by the deprotonation of OH^- to form M–OH, whereas in acidic systems it begins with H_2O adsorption. Subsequent oxidation to M–O and M–OOH constitutes the core of the adsorbate evolution mechanism, with the O–O bond formation step generally governing the overall reaction rate. In certain transition-metal systems, lattice oxygen oxidation (LOM) can also contribute, providing alternative O–O coupling pathways, though often at the expense of structural stability.

Mechanistically, the OER generally follows the anion exchange membrane (AEM), involving sequential formation of M–OH, M–O, and M–OOH^* intermediates prior to O_2 release. In certain transition-metal systems, LOM can also participate, providing alternative O–O coupling pathways, though often at the cost of structural stability. For POM-based catalysts, the presence of high-valence Mo^{6+}/W^{6+} centers and delocalized metal–oxygen frameworks offers efficient electron-transfer channels that stabilize key intermediates at each proton–electron transfer step. Specifically, W–O–M and Mo–O–M bridges facilitate rapid electron flow toward adsorbed O^* and OOH^* species, lowering the activation barrier for O–O bond formation. Additionally, the strong terminal M=O groups can serve as nucleophilic centers that assist intra-cluster O–O coupling, accelerating the rate-determining step. These structural features help explain why certain POM architectures, particularly those with highly conjugated metal–oxygen backbones, exhibit enhanced OER activity despite their inherently limited conductivity.

4.1 Doping strategy

POMs offer considerable advantages in the OER owing to their highly tunable structural characteristics, exceptional redox activity, and robust stability [221]. Through accurate molecular-level structural design, the catalytic performance of POMs can be finely tuned. Incorporation of additional metal ions (e.g., Ni and Co) into POM frameworks considerably enhances catalytic efficiency by overcoming the intrinsic limitations of metal-site activity in conventional POM clusters [222], opening new avenues for the development of high-performance electrocatalysts. For instance, Zheng et al. used an "*in situ* isomorphic substitution" strategy in which Co atoms in the well-defined Co-phosphorus POM anion $[(Co_4(OH)_3PO_4)_4(SiW_9O_{34})_4]^{32-}$ were replaced by iron atoms during synthesis. Subsequent introduction of Ba^{2+} ions via ion exchange yielded a water-insoluble multiphasic catalyst that preserved the POM anion structure. In 0.5 M H_2SO_4 and without *iR* compensation, this catalyst required an overpotential of only 385 mV to reach 10 $mA{\cdot}cm^{-2}$—66 mV lower than for the Ba-based material without Fe substitution and 8 mV lower than for commercial IrO_2. Notably, the catalytic performance exhibited a "volcano" trend with respect to Fe content; an optimal level of Fe doping effectively modulated the adsorption energies of reaction intermediates, thereby enhancing catalytic efficiency. Moreover, after 2000 CV cycles, the structure and activity of the Fe-doped catalyst in acidic media remained virtually unchanged. These results indicate that Fe incorporation not only improves catalytic performance but also considerably enhances durability by mitigating issues related to POM dissolution and deactivation in acidic environments [223]. In an alkaline medium, Song et al. (2017) successfully synthesized a NiCo-POM catalyst (Figs. 21(a)–21(g)) via a straightforward one-step hydrothermal reaction using $(PW_{12}O_{40})^{3-}$, Co nitrate, and porous Ni, while maintaining the overall POM framework. In 0.1 M KOH, the catalyst achieved an overpotential of 360 mV at 10 $mA{\cdot}cm^{-2}$ and a Faradaic efficiency of up to 96%. Furthermore, the NiCo-POM/Ni electrode exhibited excellent long-term stability; during continuous operation over 10 h, the current initially decreased but eventually recovered and stabilized at approximately 85% of its original value. SEM and powder XRD analyses confirmed the preservation of the catalyst's morphology and crystal structure [219]. Overall, the integration of metal elements not only enhances the catalytic performance of POMs but also improves their stability under highly alkaline conditions, highlighting their potential for practical applications.

Inorganic element doping is widely recognized as a key strategy to enhance the OER performance of POMs [220]. This approach not only optimizes the electronic and surface properties of POM materials but also allows accurate control over dopant type and ratio [18,94], reinforcing the mechanical strength and chemical stability of the POM framework and ensuring superior catalytic activity even under highly alkaline conditions. Gao et al. used an *in situ* encapsulation method to incorporate cobalt, nitrogen, and carbon into the Keggin-type $H_3PW_{12}O_{40}$, yielding the CNCP-6 catalyst. Remarkably, CNCP-6 achieved a low overpotential of 241 mV at 10 $mA{\cdot}cm^{-2}$, outperforming commercial IrO_2, which required 307 mV. Moreover, constant-current electrolysis over 24 h showed that CNCP-6 maintained excellent stability with negligible performance loss. This enhanced performance is primarily attributed to the "egg-shell" structure formed during codoping. The hollow nanoframework provides a high specific surface area, and the *in situ* encapsulation of Co, N, and C ensures uniform, dense distribution of active components, further improving the catalyst's

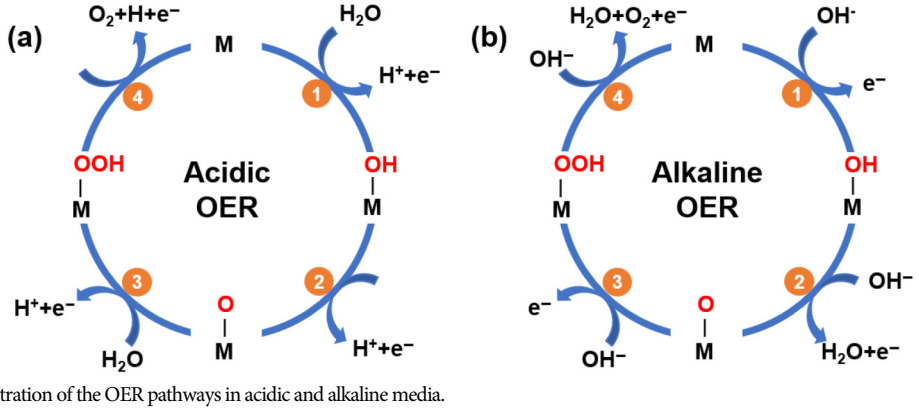

Figure 20 Schematic illustration of the OER pathways in acidic and alkaline media.

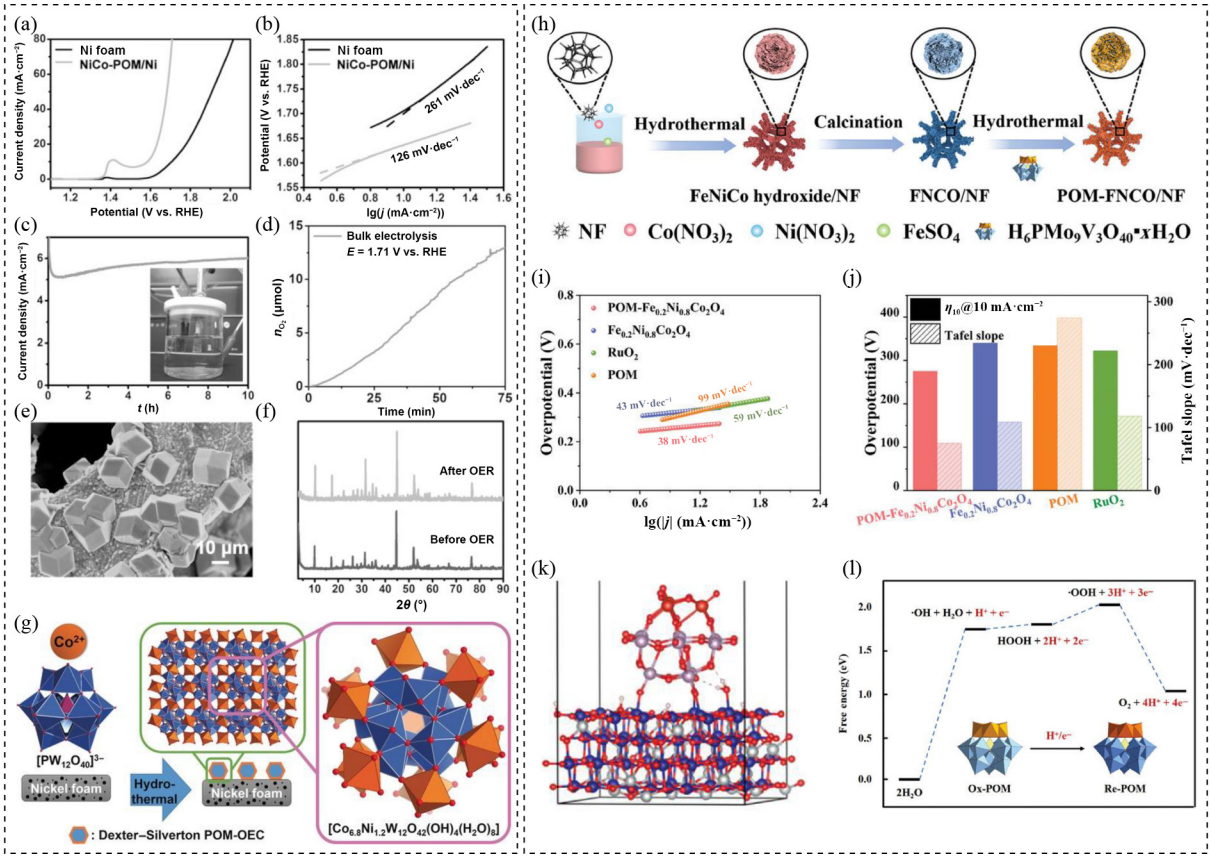

Figure 21 (a) LSV of Ni foam and the NiCo-POM/Ni electrode in 0.1 M KOH (scan rate = 5 mV· s^{-1}). (b) Tafel plots of Ni foam and the NiCo-POM/Ni electrode. (c) Variation of current density during OER at E = 1.67 V vs. RHE. (d) Oxygen evolution quantification during electrochemical OER (E = 1.71 V vs. RHE). (e) SEM image of NiCo-POM/Ni electrode after 10 h OER. (f) Powder XRD data of NiCo-POM/Ni electrode before and after 10 h OER. (g) Deposition of Dexter–Silverton polyoxometalate microcrystals on nickel foam electrodes. Reprinted with permission from Ref. [219], © Wiley-VCH Verlag GmbH & Co. KGaA, Weinheim 2017. (h) Composite diagram of POM-FNCO/NF. (i) Tafel slopes. (j) Contrast of overpotentials at 10 mA·cm^{-2}. (k) The adsorption configuration of H_2O on the POM-FNCO. (l) Thermodynamic characteristics of overall water splitting catalyzed by POMs. Reprinted with permission from Ref. [129], © Wiley-VCH GmbH 2024.

stability [79].

Recent studies on heteroatom-doped POMs demonstrate that strategic tuning of metal composition, incorporation of organic ligands, or hybridization with other materials can considerably enhance OER catalytic performance [16]. These materials combine intrinsic advantages such as cost-effectiveness and environmental sustainability with innovative design opportunities, providing a promising route for developing efficient and durable non-precious metal OER catalysts.

4.2 POM-based composite electrode

High-performance composite materials based on POMs clusters, single atoms, and their hybrids have demonstrated exceptional chemical advantages in hydrogen production through water electrolysis [31, 32, 224]. The unique properties of POMs—such as their high negative charge and robust structural stability—make them promising candidates for heterogeneous catalysis. POMs can form composite systems with other metals through electrostatic interactions, inducing synergistic effects that enhance OER efficiency [56, 225]. Moreover, their remarkable reducibility and stability allow them to function as both reducing agents and stabilizers, effectively modifying and preserving metallic nanostructures. Their strong affinity for exogenous metal ions further enables performance optimization through controlled stoichiometry. Therefore, as fundamental building blocks for heterogeneous architectures, POMs offer extensive potential for the design of high-performance materials, owing to their structural diversity, tunability, exceptional physicochemical properties, and versatile synthetic strategies.

Transition metal oxides have long attracted considerable research attention owing to their abundance, low cost, and excellent electrocatalytic performance [226, 227]. Alloying enables accurate tuning of the metal electronic structure, optimizing the adsorption energies of key OER intermediates (e.g., $^{*}OOH^{-}$) and thereby enhancing catalytic activity [228, 229]. Moreover, doping with various metal elements not only modifies the electronic properties of the alloy but also increases the number of active sites, improves conductivity, and enhances mass transfer, ultimately influencing the adsorption behavior of OER intermediates [230]. In addition, POM-based materials, with their exceptional redox properties and tunable structures, are frequently used to further regulate and improve the performance of transition metal oxides in OER applications [231, 232]. In 2022, Yang et al. synthesized a POM–$ZnFe_2O_4$ heterostructure via a simple ion-exchange approach, achieving an ultra-low overpotential of 340 mV at 50 mA·cm^{-2}. The porous POM–$ZnFe_2O_4$ nanoplates form a unique heterostructure that considerably enhances wettability, ECSA, and OER kinetics. Additionally, Mo incorporation modulates the electronic environment of Zn and Fe, facilitating the formation of OER intermediates and substantially improving overall catalytic

performance [233]. In 2024, Zhou et al. combined a Keggin-type POM ($H_6PMo_9V_3O_{40}{\cdot}xH_2O$) with iron-doped Co–Ni oxide ($Fe_{0.2}Ni_{0.8}Co_2O_4$) to develop a sub-nanometer heterogeneous catalyst, designated POM-FNCO/NF (Figs. 21(h)–21(l)), featuring multiple active sites. This catalyst exhibited enhanced OER activity, reaching an overpotential of only 259 mV, compared to 317.6 mV for commercial RuO_2. The enhanced activity is primarily attributed to the heterogeneous interface formed between the POM and FNCO, which facilitates rapid electron transfer and lowers the reaction energy barrier. Additionally, the incorporation of the POM increases the catalyst's surface roughness and optimizes electron distribution, improving both its geometric and electronic properties. DFT calculations, supported by experimental evidence, indicate that the synergistic interaction between the POM and FNCO is critical for the observed activity enhancement. Considerable electron transfer across the POM–catalyst interface further promotes effective water molecule binding, ultimately leading to superior catalytic efficiency [129].

In recent years, there has been increasing interest in Earth-abundant TMS as cost-effective alternatives to conventional OER catalysts [234, 235]. Owing to their low cost, environmental friendliness, low electronegativity, and excellent electrocatalytic performance, TMS have emerged as promising candidates for sustainable energy applications [236, 237]. Furthermore, various morphologies—including nanowires, nanosheets, and nanotubes—can be synthesized directly on conductive substrates, enhancing catalytic activity. These *in situ*-grown nanostructures provide high specific surface areas and abundant active sites while substantially improving electron transport and ionic conductivity, offering multifaceted structural advantages [238, 239]. For example, Shit et al. developed an NF-supported CoS_x/Ni_3S_2 heterostructured electrocatalyst (CoS_x/Ni_3S_2@NF), achieving 20 $mA{\cdot}cm^{-2}$ for the OER at a low overpotential of 280 mV, comparable to commercial RuO_2 [240]. However, the broader application of TMS remains limited by poor conductivity and long-term stability. In contrast, POMs—with their unique structural configuration, exceptional electron and proton transfer and storage capabilities, robust thermal and structural stability, and adaptable lattice oxygen—offer a promising strategy to further enhance the electrocatalytic performance of TMSs. Based on these insights, Wei et al. synthesized a composite material, POM–ZnCoS nanowires, on a three-dimensional porous Ni substrate via a facile hydrothermal method. Incorporation of POMs enhanced heterojunction conductivity and reduced electron-transfer resistance, enabling an overpotential of 240 mV at 20 $mA{\cdot}cm^{-2}$ and considerably improving overall electrocatalytic performance. The POM@ZnCoS/NF catalyst also exhibited a Tafel slope of 67.7 $mV{\cdot}dec^{-1}$, lower than that of RuO_2 (~ 70 $mV{\cdot}dec^{-1}$). During a 20-h stability test at 1.5 V, the catalyst maintained a constant current without noticeable decay, demonstrating excellent long-term stability as well as superior durability and reliability compared to commercial RuO_2. The study demonstrated that POM not only provided additional electroactive sites but also promoted the OER. Compared with pure ZnCoS, POM@ZnCoS exhibited a considerably higher ECSA, with an electroactive site density of 2.012×10^{18} $atoms{\cdot}cm^{-2}$, compared to 0.983×10^{18} $atoms{\cdot}cm^{-2}$ for ZnCoS. This substantial increase in active sites enhances catalytic efficiency, while POM incorporation further modulates the electronic environment of ZnCoS, lowering the energy barrier for O_2 and H_2 evolution [110].

In summary, incorporating POMs considerably improves the performance of transition metal catalysts by enabling multiple mechanisms that enhance the efficiency and practicality of electrocatalytic water-splitting reactions. These advancements offer valuable theoretical insights and practical guidance for the development of novel catalysts for large-scale hydrogen production.

To develop high-performance systems for multi-acid-based composite electrodes with hierarchical regulation, the dispersion and immobilization of multi-acid clusters have been considerably improved by integrating layered or porous materials and using composite intercalation and spatial confinement strategies [241]. This approach effectively addresses the inherent challenges of multi-metal–oxygen cluster materials, such as low conductivity, high water solubility, and limited long-term electrocatalytic stability. LDHs are particularly effective carriers for POMs [242], and their electronic structures can be further tuned via physicochemical methods such as ionic doping and defect engineering to enhance electrocatalytic performance [243]. In this context, Liu et al. synthesized a tungsten-doped (W^{6+}) NiFe-LDH catalyst via a simple one-step hydrothermal method. The modified catalyst exhibited abundant accessible active sites and improved electrical conductivity, achieving 10 $mA{\cdot}cm^{-2}$ for the OER at an overpotential of ~ 200 mV with a Tafel slope of 67 $mV{\cdot}dec^{-1}$ in 0.1 M KOH, considerably outperforming both conventional doped metal oxides and pristine NiFe LDH. DFT calculations reveal that W doping alters the adsorption energy of $^*OH$ from −1.79 eV to approximately −1.30 eV, indicating that the introduction of tungsten ions weakens the binding between $^*OH$ and active sites and considerably lowers the adsorption energy barrier for this intermediate. This effect is primarily attributed to the strong hydroxide-binding capability of W, which enhances water adsorption and promotes the generation of OH^- [244]. Similarly, Mo-based POMs exhibit comparable advantages. Wang et al. used a wet-etching strategy to integrate PMo_{12} into the layered structure of NiFe LDH, producing a NiFe LDH-PMo_{12} composite (Fig. 22). This approach substantially improved the surface morphology of NiFe LDH by reducing its thickness to ~ 2.6 nm. At an overpotential of 350 mV, the composite achieved a turnover frequency of up to 2.03 s^{-1}, roughly double that of pristine NiFe LDH. Furthermore, a continuous electrolysis test was performed in a self-constructed AEM electrolytic cell at 400 $mA{\cdot}cm^{-2}$ for 90 h. During this period, the electrocatalytic performance remained stable, demonstrating both high activity and durability. The study revealed that POM incorporation induced lattice disorder in NiFe LDH and promoted the formation of a higher proportion of the α-$Ni(OH)_2$ phase, widely recognized as the principal active site for OER. Additionally, POMs introduced moderate oxygen and metal vacancies, subtly tuning the local coordination and electronic environment of Fe and Ni ions, thereby enhancing catalytic activity. This strategy enables alloy engineering to optimize stability and acid–alkali tolerance, producing a composite that combines the functional strengths of both POMs and LDHs [245]. Therefore, the approach increases the number of active sites, enhances catalytic activity, and achieves a synergistic improvement in overall performance.

MOFs are porous materials assembled from inorganic metal ions or clusters and organic ligands, forming three-dimensional architectures with extended crystallinity [246–248]. MOFs have attracted considerable attention owing to their intrinsic attributes, including high specific surface area, low density, substantial porosity, and tunable architectures [249, 250]. Their abundant

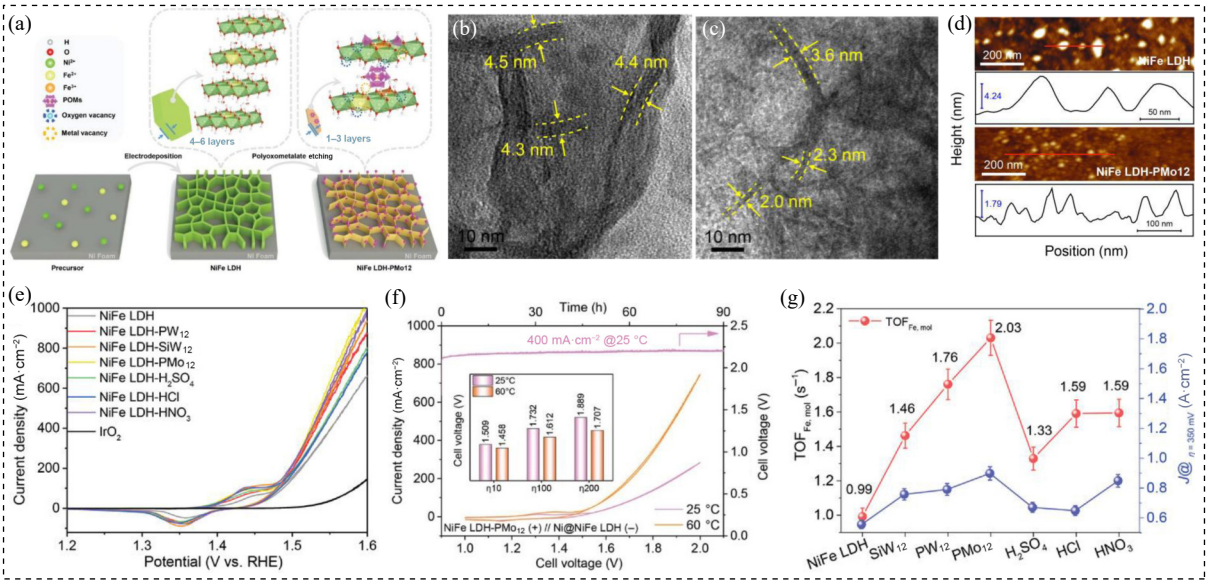

Figure 22 (a) Schematic illustration of the synthesis of NiFe LDH-POM. HR-TEM images of (b) NiFe LDH-PMo_{12} and (c) NiFe LDH. (d) AFM images with corresponding height profiles for NiFe LDH and NiFe LDH-PMo_{12}. (e) Comparison of the CV curves of the NiFe LDH-X with NiFe LDH and IrO_2 in 1 M KOH at a scan rate of 5 mV·s^{-1} (NiFe LDH-X are abbreviated as X, X = PW_{12}, SiW_{12}, PMo_{12}, H_2SO_4, HCl, and HNO_3). (f) Polarization curves of overall water splitting measurement in an electrolysis cell filled with 1 M KOH at 25 and 60 °C with a scan rate of 5 mV·s^{-1}, and the stability test in AEM cells for 90 h. (g) $TOF_{Fe,mol}$ in the NiFe LDH-X and corresponding current densities at the overpotential of 350 mV. Reprinted with permission from Ref. [245], © Wiley-VCH GmbH 2022.

metal active sites, ability to serve as templates for synthesizing other materials, and high chemical compositional tunability have further motivated research into their potential as OER catalysts [251]. However, MOFs often suffer from poor conductivity, limited stability, and low mass permeability, which can block the metal centers coordinated by organic ligands and hinder their effectiveness in water-splitting applications [251, 252]. In contrast, POMs exhibit high crystallinity and thermal stability, allowing their encapsulation within MOF pores and thereby enhancing framework stability under high current density conditions [253]. The integration of POMs and MOFs generates a synergistic effect: The high surface area and selective adsorption properties of POMs, combined with the porous MOF structure, confer superior electrocatalytic performance to the composite [254]. This synergy not only increases catalytic activity but also improves reactant diffusion and accessibility, optimizing overall electrochemical reaction efficiency. Additionally, the unique structure and excellent electrical conductivity of POMs facilitate efficient electron transfer, further enhancing the electrocatalytic capabilities of MOFs.

POMOFs, a subclass of MOFs incorporating channel-confined POM clusters, can generally be classified into two categories. The first involves encapsulating POM species in MOF channels, where the ordered pore architecture not only stabilizes the POM units but also enhances catalytic activity, structural integrity, and functional versatility. This encapsulation strategy effectively combines the advantages of both POMs and MOFs [56]. In 2020, Cristina Freire et al. used a "guest–host" approach to embed POMs in ZIF-67 pores. In this process, dissolved POM molecules were mixed with zinc salts and organic ligands such as 2-methylimidazole; as ZIF-67 crystals formed, the POM molecules became integrated into the framework, yielding POM@ZIF-67 nanocomposites. These nanocomposites exhibited considerably enhanced OER electrocatalytic activity, particularly at high POM loadings, such as $SiW_{11}Co$[h]@ZIF-67 and SiW_9Co_3[h]@ZIF-67, where the current density at 1.75 V versus RHE was approximately three to four times higher than that of pristine ZIF-67. These findings demonstrate that the introduction of POMs effectively improves OER catalytic efficiency. Moreover, ECSA calculations revealed that increasing POM loading led to a reduction in the effective active area, likely because POM clusters occupied the pores of ZIF-67 and potentially hindered access to surface active sites within the defect-rich open framework [255]. Based on this concept, Li et al. successfully synthesized PW_6Mo_6/ZIF-67@NF by self-assembling PW_6Mo_6 with ZIF-67 on the surface of NF. Their study showed that POM incorporation not only increased the ECSA of ZIF-67 but also improved its electrical conductivity. The resulting composite, PW_6Mo_6/ZIF-67@NF (Figs. 23(a)–23(f)), exhibited outstanding OER activity, achieving 10 mA·cm^{-2} at an overpotential of 201 mV, considerably lower than the 329 mV required for pristine ZIF-67@NF. This improvement is attributed to the synergistic interaction between POM and ZIF-67, which exposes Co active sites and strengthens interactions with hydroxyl species in the electrolyte, thereby promoting more efficient catalytic reactions. Additionally, the incorporation of PW_6Mo_6 partially corrodes the ZIF-67 framework, inducing a controlled collapse that creates a more open structure and enhances hydroxyl ion accessibility. At the same time, the ZIF-67 framework suppresses PW_6Mo_6 dissolution in the electrolyte, improving the overall stability of the composite. After prolonged current testing, the OER activity showed negligible degradation, demonstrating excellent durability [256]. Encapsulating POMs in MOF pores synergistically combines the advantages of both materials: POMs act as efficient catalysts for OER and redox reactions, while their active sites are protected in the MOF, reducing aggregation or dissolution. Simultaneously, the MOF's inherent porous architecture facilitates the diffusion of reactants and products, further enhancing catalytic efficiency. However, this assembly strategy requires that the size of the POMs be compatible with the pore dimensions of the MOFs. If the MOF windows are too small, POMs may be excluded, whereas excessively large windows can allow POMs to escape, resulting in uneven dispersion. Moreover, the encapsulation process requires accurate control of reaction conditions—including temperature,

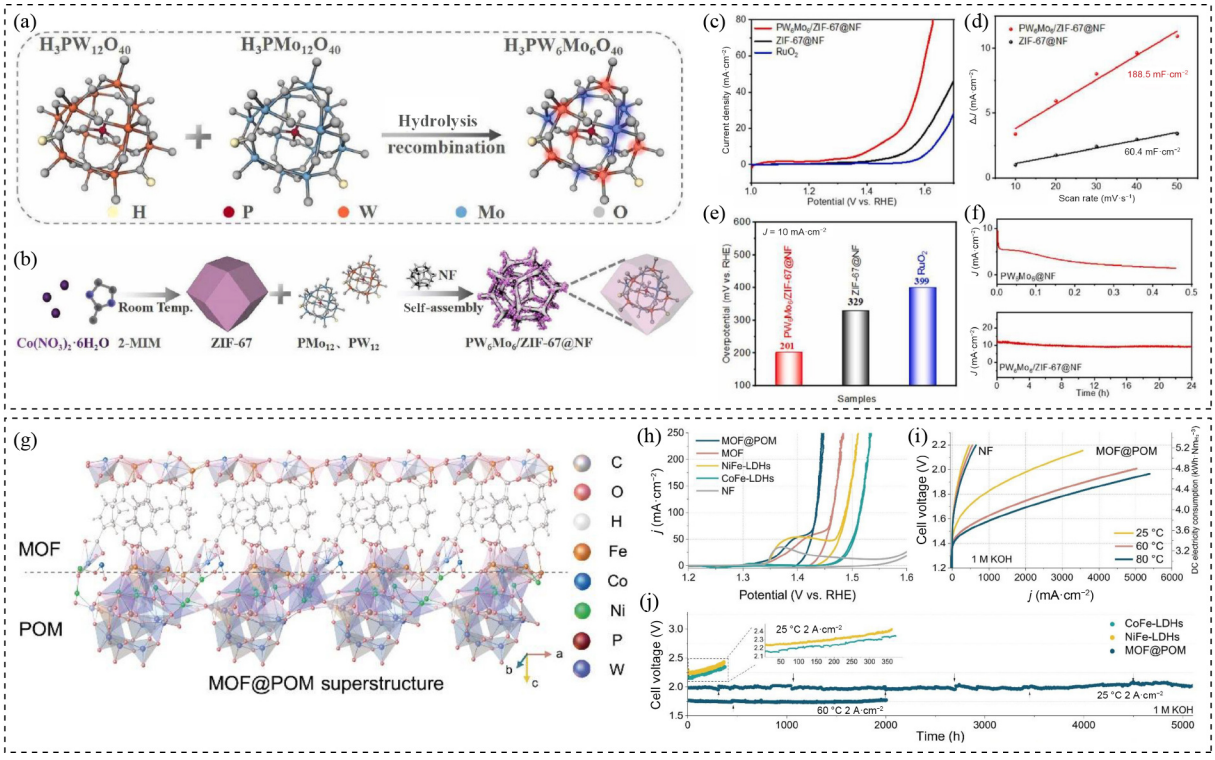

Figure 23 (a) The synthesis of PW_6Mo_6. (b) The synthesis of PW_6Mo_6/ZIF-67@NF. (c) LSV curves (85% *iR* compensation) with a scan rate of 5 mV·s^{-1}. (d) Tafel slopes of PW_6Mo_6/ZIF-67@NF, ZIF-67@NF, and RuO_2. (e) Comparison of overpotential. (f) Chronoamperometric response at a constant potential of 1.43 V vs. RHE of PW_6Mo_6@NF and PW_6Mo_6/ZIF-67@NF. Reprinted with permission from Ref. [256], © Hydrogen Energy Publications LLC. 2023. (g) Mercury-visualized structure model of the MOF@POM superstructure. (h) CV curves of MOF, MOF@POM, and the reference samples. (i) Polarization curves of the AEMWE cell using MOF@POM as the anode. (Electrode area: 5 cm ×5 cm; membrane: Versogen A40). Reprinted with permission from Ref. [257], © Yue, K. H. et al., some rights reserved; exclusive licensee American Association for the Advancement of Science 2025. No claim to original U.S. Government Works.

pH, and solvent choice—to ensure uniform distribution and maintain the structural integrity of the POMs. It is also important to note that encapsulation may occupy some of the MOF's active sites, potentially affecting the intrinsic catalytic performance of the framework.

The second assembly method uses POMs as cluster nodes in the MOF, directly integrating them into the construction of the entire framework [253]. This approach produces a porous, multilevel cluster material that synergistically integrates the advantages of both POMs and MOFs. Compared with conventional strategies that encapsulate POMs within MOF pores (Figs. 23(g)–23(j)), this approach offers several notable advantages: 1. Enhanced structural stability: POMs form robust covalent or coordination bonds through organic ligands or metal ions, reinforcing the overall MOF framework. These synergistic interactions improve durability under harsh conditions, including high temperature, high pressure, and strong acidic or alkaline environments. 2. Increased catalytic activity: Direct incorporation of POMs as structural nodes within the MOF exposes their active sites more effectively, thereby considerably enhancing catalytic performance. 3. Prevention of POM loss: When incorporated as nodes within the MOF framework, POMs form robust chemical bonds that mitigate the risk of leaching commonly associated with conventional encapsulation strategies. 4. Improved catalytic selectivity: Integration of POMs into the MOF framework enables the combination of multiple functionalities, which can result in enhanced catalytic selectivity. Yan et al. successfully constructed MOF@POM suprastructures through the self-assembly of POMs and MOFs, using Ni–O bridges as the connecting linkages. During the self-coordination-driven formation of CoFe-MOFs, the PW_9 polymetallic clusters from the POMs interact with Ni sites in the MOF, and the resulting Ni–O bonds strengthen the overall structural integrity. The MOF@POM suprastructure offers several distinct advantages: 1. High stability: During alkaline water oxidation, MOF@POM exhibits exceptional durability. Compared with conventional Co–iron oxyhydroxides (CoFe-LDHs) and NiFe-LDHs, it maintains a prolonged operational lifetime of up to 5000 h under high-voltage conditions, substantially reducing the dissolution of metal active sites. 2. Superior catalytic activity: In water-splitting reactions, MOF@POMs achieve an overpotential as low as 178 mV. At a current density of 10 mA·cm^{-2}, their performance surpasses that of pristine MOFs as well as traditional catalysts such as CoFe-LDHs and NiFe-LDHs. 3. Enhanced conductivity: Incorporation of POMs into the MOF framework improves electrical conductivity by providing more efficient electron-transfer pathways, thereby further enhancing catalytic efficiency. 4. Exceptional durability: Under practical operating conditions, the catalyst remains stable for over 5140 h at a current density of 2 A·cm^{-2} at room temperature, demonstrating its feasibility for large-scale applications. 5. Structural superiority: The unique architecture formed through the self-assembly of MOFs and POMs not only reinforces structural stability but also optimizes the dispersion of metal active sites. Collectively, these properties highlight the remarkable potential of MOF@POM composites as highly efficient and durable catalysts for advanced water-splitting technologies. *In situ* electrochemical spectroscopy and theoretical investigations indicate that synergistic interactions among metal atoms facilitate the formation of rapid electron-transport channels,

thereby enabling efficient electrical conductivity between the catalytic sites containing iron and Co and those comprising Ni and tungsten in the POM [257]. This process stabilizes the metallic centers and inhibits their dissolution. These findings demonstrate that directly incorporating POMs as cluster-based nodes within MOFs substantially enhances both catalytic activity and durability in water electrolysis systems, offering a promising strategy for developing robust and efficient catalysts for large-scale green hydrogen production.

In POM composite materials, POMs enhance the electronic structure through electron transfer with the metal support, increasing the density of active sites and fine-tuning the adsorption energies of reaction intermediates. Simultaneously, the compositing process induces the formation of oxygen and metal vacancies, which facilitate intermediate desorption and accelerate electron migration. However, existing experimental studies have not directly verified the accurate synergistic mechanisms in these composites, highlighting the need for comprehensive investigations into the coordination interactions that govern their behavior. This gap underscores the importance of moving beyond speculative material design toward mechanism-driven, accuracy studies. Future research should prioritize advanced characterization techniques, such as *in situ* Raman/infrared spectroscopy coupled with electrochemistry and in situ XPS/XAS, to monitor dynamic atomic and electronic changes at catalytic interfaces and elucidate the fundamental nature of synergistic catalysis. Moreover, current studies primarily report short-term testing (≤ 100 h); validating long-term performance over periods exceeding 500 h is essential for advancing these materials toward industrial-scale applications.

4.3 POM derivatives

POMs serve as excellent precursors for the development of high-performance OER catalysts owing to their distinctive structural features, including tunable metal valence states, diverse coordination environments, outstanding redox properties, and the capability for molecular- and atomic-level design control [258]. Comprised of high-valence transition metals such as Mo, W, V, Nb, and Ta interconnected by oxygen bridges, these compounds provide a variety of metal sites that serve as active centers for OER catalysis. Their structural versatility—from mononuclear and polynuclear arrangements to chain-like and cluster-like architectures—enables accurate molecular-level design to enhance catalytic performance. During pyrolysis, the release of oxygen atoms from POMs facilitates the formation of porous or hollow structures, increasing the specific surface area and improving electrolyte permeation and reactant diffusion [144, 259]. Additionally, heteroatoms (e.g., P, S, and N) intrinsic to the POM framework can be directly incorporated into the derived materials during thermal treatment, thereby enhancing electronic conductivity and further improving OER activity by mitigating the intrinsic limitations of POMs [260].

Conventional TMS encounter difficulties in achieving accurate compositional control [261]. Using POMs as precursors provides a controlled chemical environment that promotes accurate regulation of metal ratios during synthesis, thereby facilitating optimal catalytic activity. Moreover, POM precursors enable the formation of high-surface-area disulfide nanosheet structures, which offer abundant active sites and enhance electrocatalytic performance [262]. Building on this principle, Sun used an Anderson-type POM, $(NH_4)_4[CoMo_6O_{24}H_6]\cdot 6H_2O$, as a Co and Mo source. Through a high-temperature hydrothermal sulfidation process, vertically aligned heterogeneous nanosheets composed of Co disulfide and MoS_2 with oxygen-containing features (denoted O-CoMoS) were synthesized. These O-CoMoS nanosheets retain the intrinsic properties of their components and benefit from heterointerface synergism, achieving an overpotential of 272 mV at 10 $mA\cdot cm^{-2}$. This performance surpasses that of O-NiMoS (286 mV) and O-FeMoS (301 mV), highlighting the superior OER activity of the material. Furthermore, a Tafel slope of 45 $mV\cdot dec^{-1}$ reflects enhanced reaction kinetics. The presence of sulfur vacancies and disordered structures in O-CoMoS generates abundant active edge sites, increasing the ECSA and contributing considerably to the improved efficiency in both HER and OER [235]. Tang et al. proposed a novel methodology combining Anderson-type POMs with laser ablation techniques to rapidly synthesize an FeMoOS composite featuring hierarchical porosity and multicomponent architecture for OER applications. At a current density of 50 $mA\cdot cm^{-2}$, the catalyst exhibited a low overpotential of 240 mV, a Tafel slope of 79 $mV\cdot dec^{-1}$, and excellent durability over 80 h. The laser-induced synthesis not only dramatically reduced reaction time but also enabled accurate control over defect formation. Additionally, this approach allows for the direct fabrication of working electrodes on conductive metal substrates, ensuring strong adhesion and uniform material distribution. Furthermore, post-reaction physical characterization showed that the formation of NiO/NiOOH species, along with dissolved Mo- and S-containing components, increased the density of active sites and optimized the adsorption of oxygenated intermediates, collectively enhancing electron transfer and OER performance. Notably, the use of POM-based precursors effectively controls the ratio and distribution of metals, promoting the formation of uniformly dispersed active sites among transition metals during sulfidation [263]. Liu et al. used $(NH_4)_6[Co_2Mo_{10}H_4O_{38}]\cdot 7H_2O$ as a precursor and successfully replaced the native cations with Co^{2+} via ion exchange to synthesize Co_5Mo_{10}. Subsequent hydrothermal sulfidation on carbon cloth produced a heterogeneous $Co_5Mo_{10}S_x$/CC structure (Figs. 24(a)–24(d)), which demonstrated outstanding performance, achieving an overpotential of only 153 mV at 10 mA cm^{-2} in 1 M KOH, along with a Tafel slope of 57.84 mV dec^{-1}, considerably surpassing comparable materials. This strategy enables accurate atomic-level tuning of the Co and Mo ratio and distribution, where the dense and controlled arrangement of Co–Mo active sites enhances intrinsic catalytic activity. Additionally, the intimate integration of CoS_2 and MoS_2 generates abundant CoMoS active centers, which further improve catalytic performance via synergistic effects [234]. Overall, this POM-based molecular approach, combining rational structural design, effective active-site regulation, enhanced conductivity, and optimized synthesis conditions, provides a powerful strategy for developing high-efficiency electrocatalysts for water splitting.

TMCs possess high electronic conductivity, metallic characteristics, and chemical stability, making them highly attractive in the field of electrocatalysis [264]. In particular, molybdenum carbide has emerged as an affordable and relatively high-performance catalyst for the HER [265]. However, its application in the OER is limited by poor controllability and thermal instability during high-temperature synthesis, which often leads to severe aggregation, high overpotentials, and steep Tafel slopes [266]. To overcome these challenges, the incorporation of bimetallic elements into TMCs has been proposed as an effective strategy to manipulate the electronic structure and expose additional active sites [266, 267]. However, bimetallic carbide

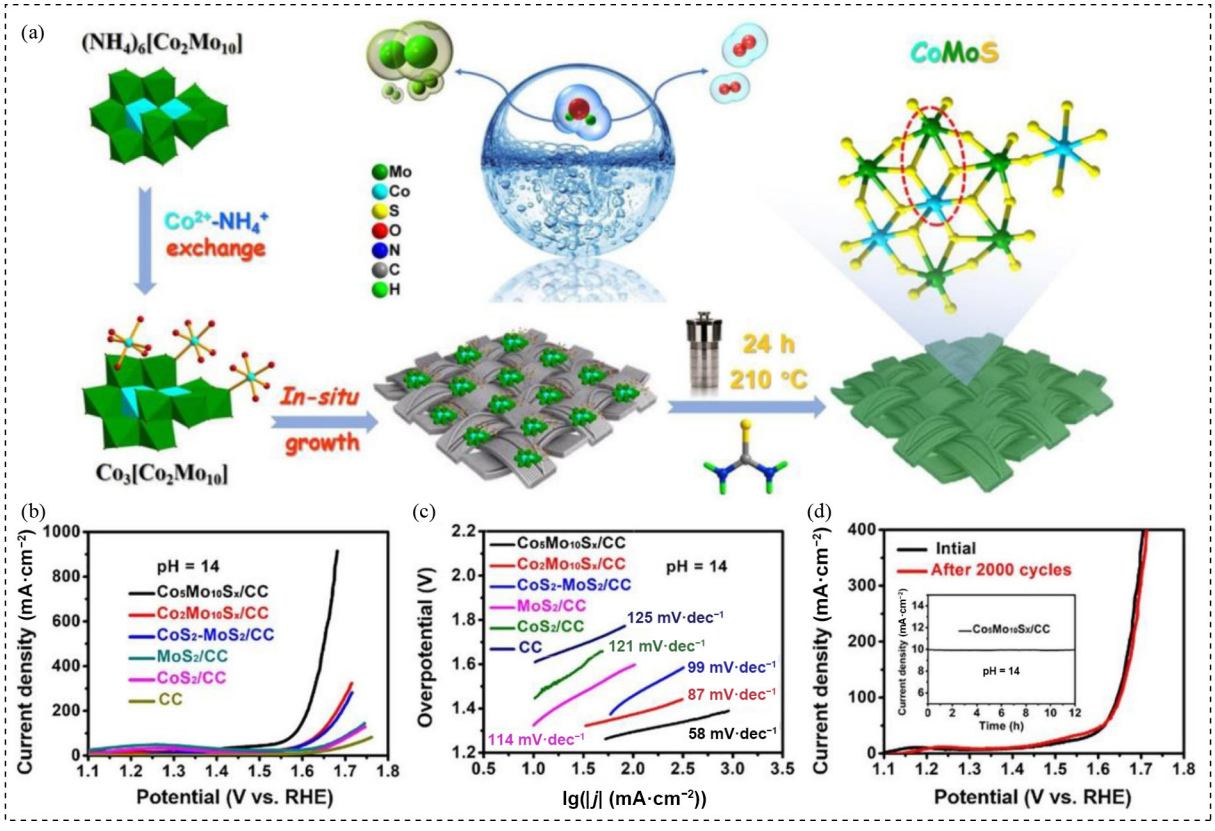

Figure 24 (a) Schematic illustration for the formation of CoMoS nanosheets on carbon cloth, $Co_5Mo_{10}S_x$/CC, through POMs molecular approach. (b) OER polarization curves of different electrodes and electrode materials in 1.0 M KOH and (c) the corresponding Tafel plot obtained from (b). (d) The OER durability of $Co_5Mo_{10}S_x$/CC in 1.0 M KOH: polarization curves; the inset is the time dependence of catalytic currents. Reprinted with permission from Ref. [234], © Elsevier B.V. 2020.

synthesis under high-temperature conditions frequently induces phase separation, making the preparation of phase-pure TMCs via mild synthetic routes particularly challenging. By exploiting the tunable structural characteristics of POMs to encapsulate transition metal ions in their frameworks, metal agglomeration during synthesis can be effectively suppressed, thereby improving phase purity and enhancing the structural integrity of the resulting materials [216]. Furthermore, the excellent aqueous solubility of POMs enables their uniform mixing with various materials, such as graphene oxide, to form stable precursor solutions. This homogeneity promotes intimate interfacial contact among the constituent components, ultimately enhancing the electrochemical performance of the resulting composites. Based on this strategy, Lan et al. used a PMo_{12} framework to incorporate Co ions, followed by the introduction of pyrrole monomers. Subsequent *in situ* polymerization of PPy on the surface of GO encapsulated the PMo_{12} particles, and further thermal treatment produced $Co_6Mo_6C_2$ encapsulated in nitrogen-doped porous carbon, uniformly anchored on rGO (Figs. 25(a)–25(i)). In alkaline media, this composite exhibited excellent OER activity, achieving a low overpotential of 260 mV at a current density of 10 mA·cm^{-2} while maintaining robust stability. During heat treatment, the nanoscale architecture of the POM precursor promoted the formation of finely dispersed, highly active carbide species, thereby enhancing

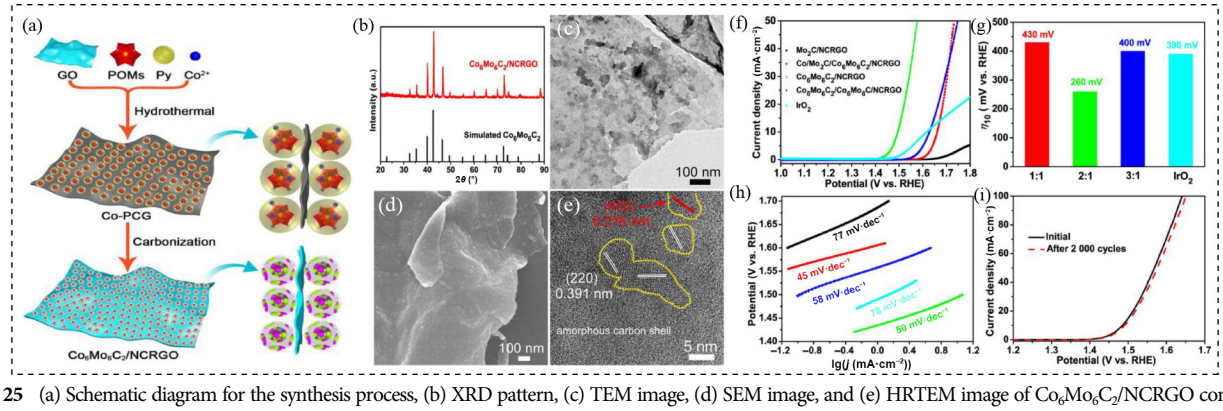

Figure 25 (a) Schematic diagram for the synthesis process, (b) XRD pattern, (c) TEM image, (d) SEM image, and (e) HRTEM image of $Co_6Mo_6C_2$/NCRGO composite. (f) LSV curves of Mo_2C/NCRGO, Co/Mo_2C/$Co_6Mo_6C_2$/NCRGO, $Co_6Mo_6C_2$/NCRGO, $Co_6Mo_6C_2$/Co_6Mo_6C/NCRGO, and commercial IrO_2. (g) Table for the comparison of η_{10} for corresponding samples. (h) Tafel plots for corresponding samples. (i) Cycle stability of $Co_6Mo_6C_2$/NCRGO composite before and after 2000 CV cycles. Reprinted with permission from Ref. [268], © American Chemical Society 2017.

electrocatalytic performance. Moreover, nitrogen incorporation generated multiple nitrogen configurations, including pyridinic, pyrrolic, and graphitic N, with pyridinic N presumed to be the most catalytically active, further boosting electrocatalytic activity. These nitrogen sites also effectively promote the oxygen reduction reaction [268]. In summary, POMs can considerably improve the electronic structure and distribution of active sites in electrocatalysts during synthesis, and their synergistic interaction with metal carbides substantially enhances overall catalytic performance.

MOFs and COFs exhibit high porosity, large surface areas, and flexible chemical compositions, often serving as important precursors for metal sources [269]. However, their formation of high-performance bimetallic catalyst materials is hindered by the limitations of metal coordination [270]. In contrast, POMs offer a wide variety of chemical states and can be anchored in MOF pores under different reaction conditions through accurate modulation of their surface properties and structural configurations. This approach enables the construction of heterogeneous architectures that integrate POMs with metal-based catalysts, such as Co-based systems. Li et al. incorporated appropriately sized PMo_{12}-based POMs into ZIF-67 and, by controlling the sulfidation temperature, successfully synthesized heterogeneous Co_9S_8@MoS_2 catalysts (Figs. 26(a)–26(g)). The resulting Co_9S_8@MoS_2 catalysts achieved a current density of 10 mA·cm^{-2} at an overpotential of 320 mV, where strong Co–Mo electronic interactions facilitated efficient electron transfer. This heterostructure effectively fine-tuned the electronic configuration of the metal centers, leading to enhanced OER activity [271]. Similarly, Ni et al. encapsulated Anderson-type POMs $[(NH_4)_4[NiH_6Mo_6O_{24}]$, abbreviated as $NiMo_6$, within the pores of an iron-based MOF (MIL-100) and subsequently converted the precursor into the target Fe,Mo-NiS/Ni_9S_8/NF catalyst via an *in situ* sulfidation process (Figs. 26(h)–26(m)). This product not only possesses abundant interfacial features that supply a high density of active sites and promote intimate contact between the catalyst and the electrolyte, but also exhibits a needle-like, multi-interface heterogeneous architecture. Such a structure effectively exposes additional active sites, while contact angle measurements confirm its exceptional hydrophilicity, which lowers proton transport barriers during electrochemical reactions and accelerates OER kinetics. As a result, the catalyst demonstrates outstanding OER performance, achieving an ultra-low overpotential of only 47 mV at a current density of 10 mA·cm^{-2} under alkaline conditions. These synthetic strategies fully exploit the high structural tunability of MOFs to support POMs, thereby improving their stability during high-temperature sulfidation processes [272]. Furthermore, the distinctive architecture readily forms binary metal-doped heterojunctions with abundant active sites, enhancing catalyst–electrolyte interfacial contact and ultimately increasing the overall reaction rate.

POM derivatives exhibit notable advantages as OER catalysts. These advantages primarily stem from their Pt-like electronic structures formed after high-temperature inorganic transformation,

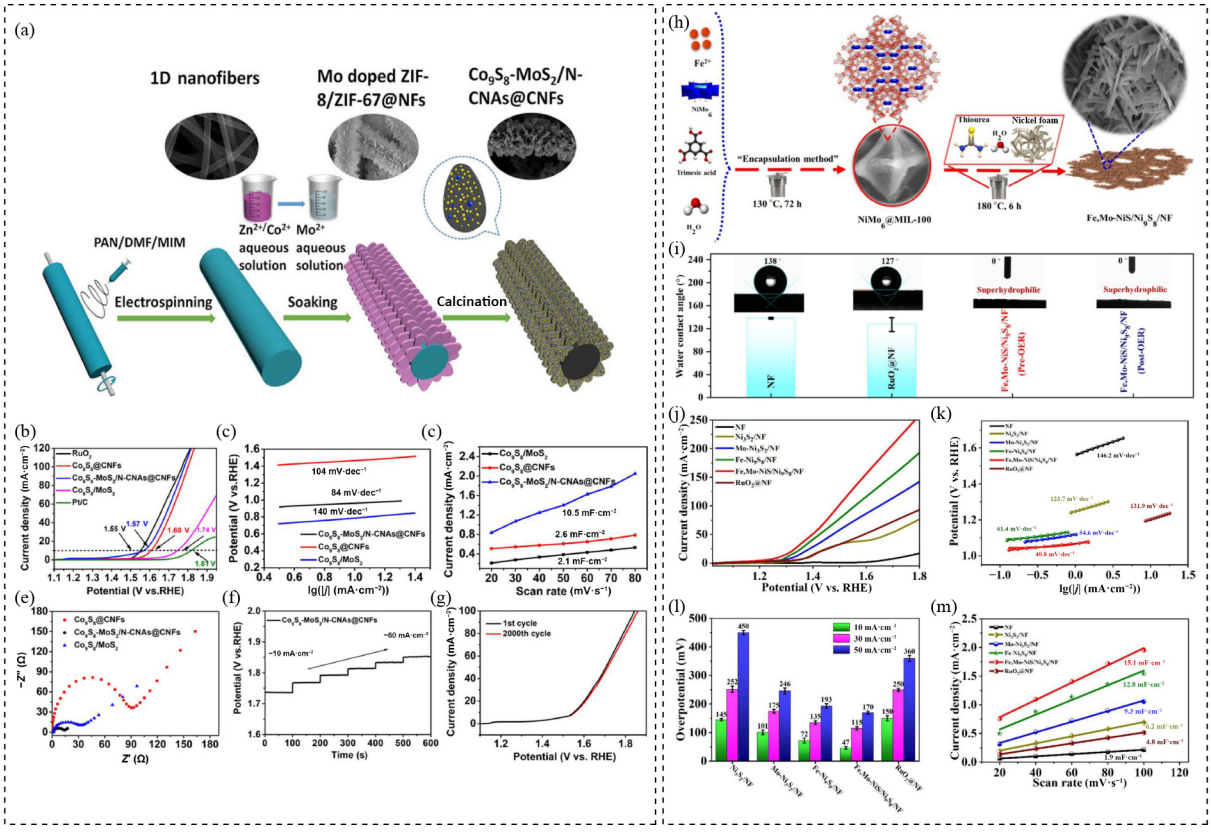

Figure 26 (a) Schematic illustration of the synthesis scheme of Co_9S_8-MoS_2/N-CNAs@CNFs. (b) LSV curves, (c) Tafel plots, and (d) the C_{dl} and relative electrochemically active surface area. (e) Nyquist plots of various catalysts evaluated in 1 M KOH solution for the OER. (f) Multicurrent process of Co_9S_8-MoS_2/N-CNAs@CNFs. (g) OER durability tests of the Co_9S_8-MoS_2/N-CNAs@CNFs catalyst before and after 2000 CV cycles. Reprinted with permission from Ref. [271], © American Chemical Society 2020. (h) Scheme of the synthesis of Fe,Mo-NiS/Ni_9S_8/NF. (i) Contact angles of Fe,Mo-NiS/Ni_9S_8/NF in freshwater before and after OER activity and those of NF and RuO_2@NF. (j) LSV curves and (k) Tafel slopes of NF, Ni_3S_2/NF, Mo-Ni_3S_2/NF, Fe-Ni_9S_8/NF, Fe,Mo-NiS/Ni_9S_8/NF, and RuO_2@NF in 1.0 M KOH. (l) Comparison of η_{10}, η_{30}, and η_{50}. (m) C_{dl}. Reprinted with permission from Ref. [272], © Elsevier Inc. 2025.

their high density of electronic states that affords excellent electrical conductivity, and their excellent resistance to corrosion, all of which collectively contribute to enhanced catalytic activity. In addition, synergistic interactions between POMs and *in situ*-generated oxyhydroxide species during the OER further amplify their catalytic performance [273]. During water electrolysis and oxygen evolution, POM-based materials promote optimized adsorption and desorption of reaction intermediates, thereby accelerating reaction kinetics. Despite these favorable characteristics, several challenges remain. During synthesis, difficulties in controlling particle size and preventing aggregation can considerably reduce the number of accessible active sites, leading to diminished catalytic efficiency. Moreover, although POMs demonstrate appreciable catalytic activity, their overall performance still lags behind that of noble-metal catalysts, particularly in large-scale commercial applications. The OER typically requires high operating voltages, resulting in increased energy consumption and reduced efficiency, which further constrains the practical deployment of POM-based catalysts. Ensuring long-term stability under high current density and prolonged operating conditions is therefore crucial because performance degradation over extended use remains a key obstacle to their industrial implementation [3].

Therefore, despite the promising potential of POMs in catalytic applications, it is imperative to address challenges related to synthesis, efficiency, and stability. Refinement of synthetic strategies, structural optimization, and comprehensive investigations into performance regulation are essential for advancing their application in energy conversion. Future research should focus on strategies such as morphology engineering, heteroatom doping, and the design of heterogeneous interfaces to further improve catalytic activity and durability.

5 POM-based catalysts for overall water splitting

5.1 POM design strategies for achieving dual HER/OER activity

Electrocatalytic water splitting is a pivotal technology for the large-scale production of green hydrogen, with both its efficiency and cost strongly dependent on the performance of catalysts for the HER and OER [274]. The development of bifunctional catalysts that exhibit high activity toward both HER and OER offers considerable advantages over the conventional approach of using separate anode and cathode catalysts with single functionalities [275]. First, bifunctional catalysts reduce dependence on expensive noble metals, thereby lowering overall catalyst costs. Second, their compositional and structural diversity enables optimization of active sites and material properties, allowing catalyst performance to be tailored to specific reaction conditions. Third, the use of a single bifunctional material mitigates issues related to interfacial corrosion or incompatibility between heterogeneous materials—challenges that are particularly severe under strongly acidic or alkaline electrolytic environments—thereby potentially enhancing device durability. Fourth, integrating one catalytic material for both anodic and cathodic reactions simplifies electrolyzer design, reducing manufacturing complexity and associated costs. Finally, the streamlined operational procedures enabled by bifunctional catalysts facilitate their deployment in integrated systems, such as reversible electrolyzer/fuel cell devices that require switching between cathodic and anodic functionalities.

However, current dual-function catalysts—including precious metal alloys, transition metal compounds, and their composites—face several considerable challenges. First, there is a trade-off between catalytic activity and cost: Achieving high catalytic performance typically requires elevated loadings of precious metals (e.g., Pt and Ir), resulting in prohibitive material expenses that hinder large-scale deployment. Second, disparities in reaction kinetics complicate catalyst design. Both HER and OER involve complex, multistep proton–electron transfer processes, with OER particularly demanding owing to the high-energy barrier associated with O=O bond formation. Therefore, a single catalyst must simultaneously optimize H^* binding energy while facilitating efficient adsorption and desorption of oxygen intermediates (e.g., $^*O$ and $^*OOH$), making its design extremely challenging. Third, catalyst stability remains a critical bottleneck. Under extreme operational potentials—especially the high anode potentials required for OER—and in highly corrosive electrolytes, active components are susceptible to structural dissolution, phase transitions, or surface passivation, ultimately leading to performance degradation. Fourth, designing active sites for bifunctional catalysis is inherently complex; achieving efficient synergistic activity at a single site, or accurately engineering two nearby yet non-interfering active sites that enhance each other's performance, remains a formidable challenge.

Therefore, the development of novel dual-functional electrocatalytic materials that simultaneously offer high intrinsic activity, low cost, excellent stability, and well-defined synergistic mechanisms is crucial for advancing water electrolysis technology. With their precisely tunable molecular structures, distinctive redox properties, abundant active metal sites, and potential stability under both oxidative and reductive conditions, POMs have emerged as an ideal molecular platform for the design of high-performance dual-functional HER/OER catalysts.

POM-based electrode materials display a wide range of structures capable of incorporating various metal ions, resulting in diverse POM anion frameworks [216]. This structural versatility enables POMs to act as catalysts with unique active sites, where the distinct multi-metal centers can be individually optimized to promote both HER and OER pathways [276]. For example, tungsten or molybdenum sites in the POM framework can modulate the hydrogen adsorption free energy, whereas transition metal centers such as nickel, iron, and cobalt facilitate the OER. This approach effectively alleviates the pronounced kinetic disparities between HER and OER when using a single catalyst. Additionally, the synergistic interactions between POMs and other transition metal derivatives improve electronic distribution at the material interface and enhance electron transfer at the catalytically active sites—key factors for enhancing the overall catalytic performance of POMs. In this context, Zhou et al. used a straightforward two-step hydrothermal method to *in situ* grow a heterogeneous structure—composed of a Keggin-type multi-metal oxoanion and iron-doped Co–Ni oxide ($Fe_{0.2}Ni_{0.8}Co_2O_4$)—on an NF substrate, denoted as POM-FNCO/NF. This composite demonstrates excellent bifunctional electrocatalytic activity, efficiently promoting both HER and OER. The system achieves 10 $mA{\cdot}cm^{-2}$ for overall water splitting at just 1.58 V, with remarkable long-term stability. These outstanding properties are attributed to the *in situ* growth strategy, which effectively lowers charge transfer resistance at the electrode interface [129]. Similarly, Yang et al. used a Dawson-type POM (P_2Mo_{18}) as a template to synthesize a bifunctional water-splitting catalyst, POM-$ZnFe_2O_4$, via an ion-exchange method. In 1.0 M KOH, the POM-$ZnFe_2O_4$ composite

exhibited superior electrocatalytic performance, reaching 10 $mA{\cdot}cm^{-2}$ at overpotentials of 268 mV for HER and 220 mV for OER—surpassing many existing catalysts, including commercial Pt/C and RuO_2. Furthermore, the catalyst displayed exceptional durability, showing negligible current loss during a 20-h constant-current test. The study revealed that POM incorporation enhanced the composite's conductivity and considerably reduced the Tafel slope. In addition, ESCA measurements indicated that the ECSA of POM-$ZnFe_2O_4$ is substantially larger than that of the individual $ZnFe_2O_4$ or POM components. The resulting increase in ECSA enhances reactant accessibility at the electrode surface, thereby accelerating the electrochemical reactions [233].

Transition metal LDHs are widely recognized as promising electrocatalysts [277–279]. However, studies by Stahl et al. demonstrated that, in NiFe LDH electrocatalysts, water oxidation primarily occurs at Fe^{4+} species located at the edges, corners, or defect sites of the Fe-doped NiOOH lattice [279–281]. Despite their promise, the relatively low conductivity, limited catalytic edge sites, and constrained surface electronic structure of NiFe LDHs restrict their electrocatalytic performance. Modulating the surface electronic configuration of metal centers can adjust the adsorption energies of reaction intermediates, thereby improving electrocatalytic kinetics. Elemental doping has proven effective in this regard. Transition metals such as V, Mn, W, Cr, and Mo have been successfully incorporated into bimetallic NiFe- or CoFe-LDHs to enhance electrocatalytic activity, while high-valence ions from POMs (e.g., W and Mo) can further tune the electronic structure of active centers, promoting water dissociation and lowering the adsorption energy barrier for hydroxide intermediates. Building on this strategy, Liu and coworkers used $K_8(SiW_{11}O_{39})\cdot 13H_2O$ as a structure-directing agent to synthesize a high-performance bifunctional catalyst, NiFe LDH-POM (Figs. 27(a)–27(o)), via a hydrothermal method. In 0.1 M KOH, the catalyst achieved 10 $mA{\cdot}cm^{-2}$ for overall water splitting at overpotentials of 200 mV for OER and 156 mV for HER. Moreover, applying 1.6 V produced a current density of 14 mA cm^{-2}, underscoring the catalyst's superior performance. DFT calculations revealed that W doping altered the adsorption energy of OH in NiFe LDH-POM from −1.79 eV to approximately 1.30 eV, indicating that the incorporation of tungsten ions weakens the binding strength of $^*OH$ at the active sites. This adjustment considerably lowers the adsorption energy barrier for hydroxide intermediates, accelerates oxygen species formation and deprotonation, and ultimately enhances overall reaction kinetics. In summary, tungsten doping not only modulates the electronic structure to reduce the adsorption energy barrier for hydroxides but also considerably improves the electrochemical performance, resulting in exceptional catalytic activity for water splitting [282].

The fundamental principle of dual-active catalysts relies on the partitioning of cooperative active sites and the coupling of electronic states. By independently optimizing the HER and OER pathways across multiple active centers, these catalysts overcome the adsorption energy limitations inherent to single-material systems. POMs, known for their multi-metal cooperativity and structural tunability, are particularly well-suited to address current challenges in electronic state regulation and interface engineering.

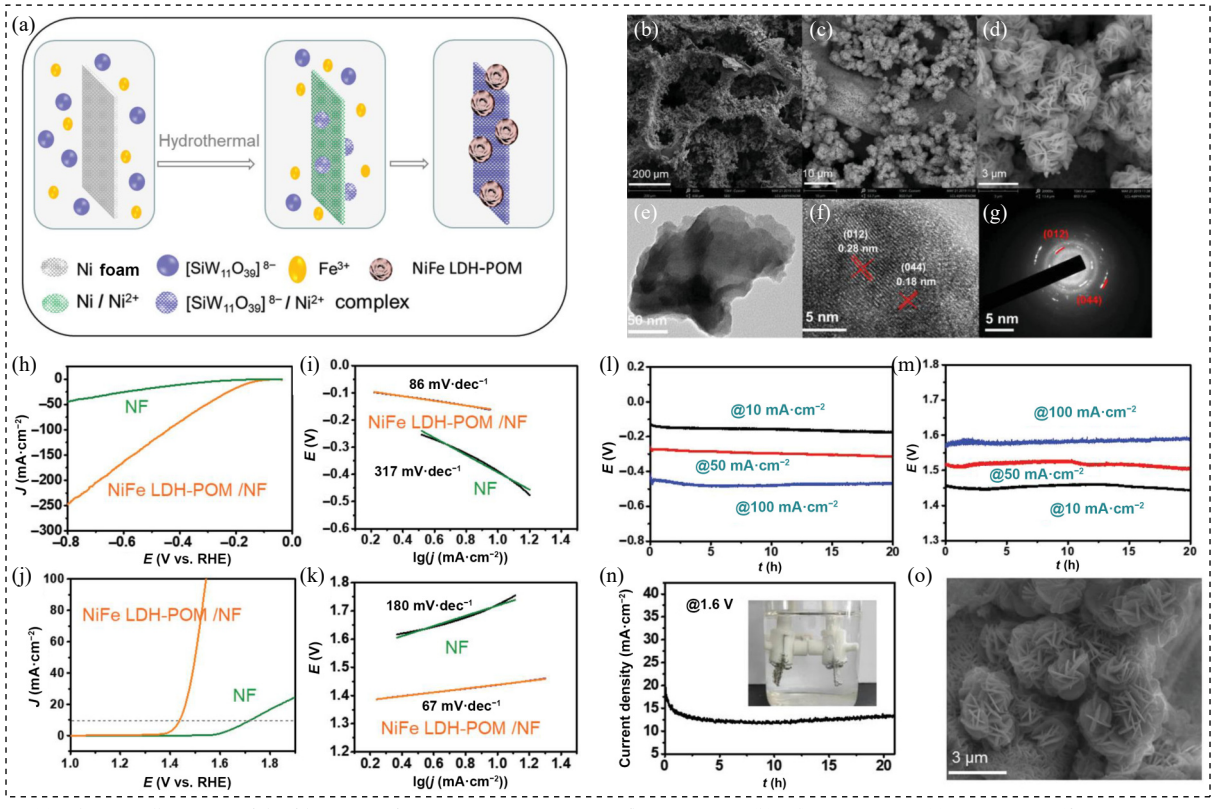

Figure 27 (a) Schematic illustration of the fabrication of 3D NiFe LDH-POM microflowers on NF. (b)–(d) SEM images, (e) TEM image, (f) HRTEM image, and (g) SAED pattern of NiFe LDH-POM/NF. (h) *iR*-corrected polarization curves, (i) Tafel plots of NF and NiFe LDH-POM/NF for HER. (j) *iR*-corrected polarization curves and (k) Tafel plots of NF and NiFe LDH-POM/NF for OER. (l)–(n) HER and OER long-term chronopotentiometry studies of NiFe LDH-POM/NF at a constant current density of 10, 50, and 100 $mA{\cdot}cm^{-2}$, respectively. (m) Overall water splitting by NiFe LDH-POM/NF at potential of 1.6 V (insert: gas bubble release observed at both electrodes). (o) SEM image of NiFe LDH-POM/NF after 20 h sustained electrolysis. Reprinted with permission from Ref. [282], © Wiley-VCH GmbH 2020.

Thus, POM-based catalysts present a promising paradigm for achieving efficient, stable, and cost-effective water electrolysis.

5.2 Evaluation of fully electrolytic cell configurations and performance

The large-scale industrial deployment of water electrolysis for hydrogen production requires the development of bifunctional electrocatalysts that combine high catalytic activity, low cost, and long-term durability (Fig. 28) [283–285]. POMs offer a unique molecular platform for the design of efficient bifunctional catalysts for HER and OER owing to their accurately tunable multi-metal compositions, inherent multielectron transfer capabilities, and intrinsic redox activity. Recent studies have shown that POM-based materials—including POM/carbon composites and POM-based MOFs—exhibit excellent bifunctional activity in half-cell evaluations. Their multi-metal synergistic sites optimize the adsorption energies of key intermediates, such as H^* and $^*OOH$, while their nanostructures expose abundant active sites, and their rigid inorganic frameworks provide potential structural stability. However, most studies have focused on intrinsic activity evaluations under standard three-electrode (half-cell) conditions, which can lead to significant discrepancies when compared to real electrolyzer environments: 1. Charge-transfer limitations: While half-cell tests use conductive substrates (e.g., glassy carbon electrodes), full electrolyzer performance is strongly influenced by the bulk electrical conductivity of the catalyst and the contact resistance at the electrode–collector interface. 2. Mass transport and diffusion effects: Under full-cell operation at high current densities (> 500 mA·cm^{-2}), factors such as ionic permeability of the catalyst layer, efficiency of gas bubble release, and the development of local pH gradients critically affect overall system performance. 3. Anode–cathode interactions: Under dynamic conditions where bifunctional catalysts operate simultaneously at both electrodes, challenges such as competition for active sites, interference from intermediate species, and potential irreversible degradation owing to potential cycling (especially in reversible electrolyzers) can occur. Accordingly, future research should prioritize systematic evaluation of POM-based catalysts in full-cell configurations, including alkaline water electrolyzers, PEM electrolyzers, and AEM electrolyzers.

In recent years, significant research efforts have focused on evaluating water electrolysis catalysts under simulated industrial conditions, with particular emphasis on assessing the scalability of electrode materials in practical electrolyzer systems (Fig. 29) [286]. These studies include: (1) comparing the structure and performance of commonly used commercial electrode catalysts during prolonged operation, focusing on metrics such as full-cell voltage–current density behavior, energy conversion efficiency, and dynamic response characteristics; (2) scaling up electrolyzer testing by increasing the active area from the conventional 1 × 1 cm^2 to areas 10–100 times larger, enabling evaluation of the feasibility and economic advantages of industrial-scale production; (3) using advanced *in situ* spectroscopic and electrochemical techniques to investigate the mechanisms of performance degradation at high current densities (1–2 A·cm^{-2}); and (4) designing electrode materials for industrial applications, including chlorine- and corrosion-

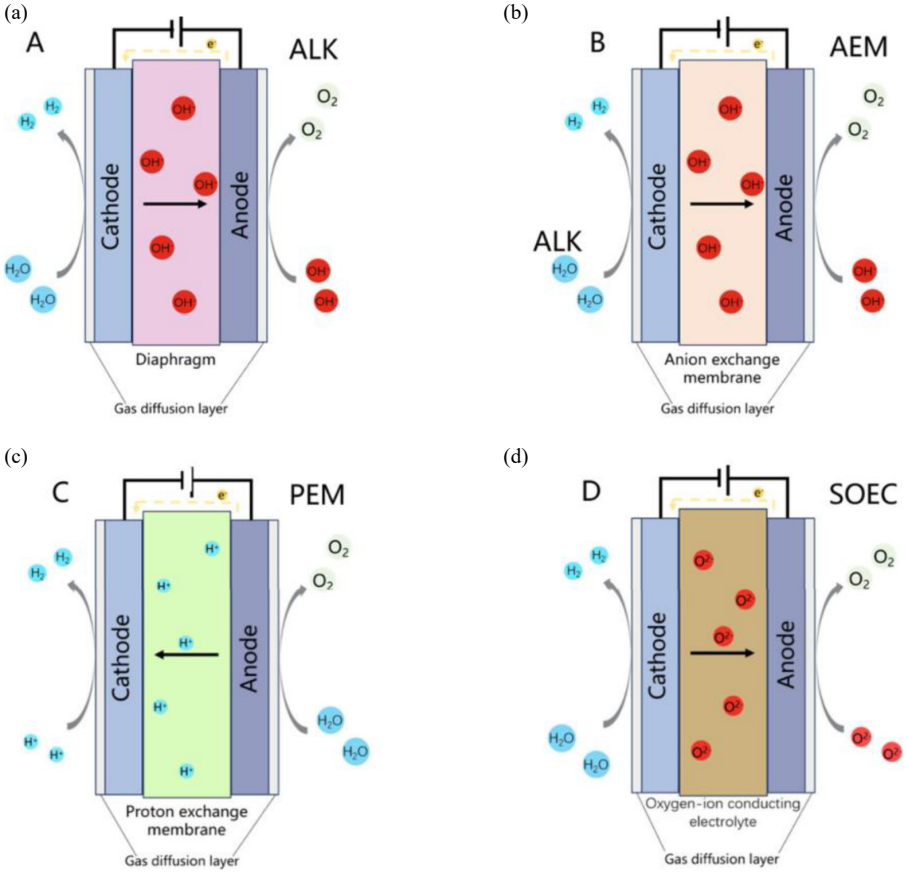

Figure 28 Diagrams of the working principle of four electrolytic water to hydrogen technologies: (a) ALK, (b) AEM, (c) PEM, and (d) SOEC. Reprinted with permission from Ref. [285], © Elsevier Ltd. 2022.

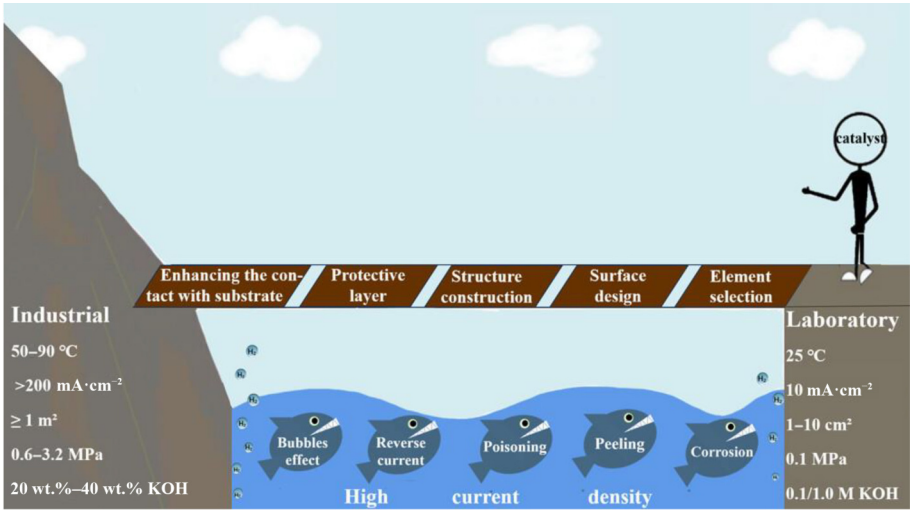

Figure 29 Current problems of catalysts for electrocatalytic water splitting under the high current density and the corresponding strategies propose. Insert, the catalyst working conditions are taken as an example of alkaline electrolyzed water. Reprinted with permission from Ref. [286], © American Chemical Society 2024.

resistant electrodes for seawater electrolysis and materials capable of maintaining stable performance under fluctuating wind and solar conditions. In practical seawater electrolysis, Cl^--induced corrosion and anodic chlorine evolution pose major challenges owing to the high chemical aggressiveness of chloride species and the presence of competitive oxidation pathways. The oxygen-rich coordination shells and high-valence Mo/W centers in POM clusters can effectively suppress Cl adsorption and limit Cl^- penetration at the catalyst–electrolyte interface, thereby mitigating chlorine-induced degradation. Furthermore, POM-derived composites—such as metal carbides, oxynitrides, and POM–MOF hybrids—provide robust bonding environments that enhance resistance to structural dissolution in chloride-containing electrolytes. These properties confer improved stability to POM-based systems in seawater-like conditions, highlighting their potential for chlorine-resistant water-splitting applications.

For POM catalysts, a primary industrial challenge is the tendency of the metal framework to dissolve under high current densities, leading to catalyst poisoning and corrosion. One effective strategy to address this involves modulating the metal microstructure by increasing the contact area with the substrate—for example, using self-supported catalysts rather than binders to ensure strong mechanical bonding. This approach improves resistance to both bubble impact and the detrimental effects associated with high current operation. In addition, the size and structure of the catalyst can be optimized by intercalating POMs into nickel–iron LDH layers or immobilizing them in MOFs or COFs, effectively mitigating leaching. Surface engineering strategies, such as coating the catalyst with a carbon layer, further enhance hydrophilicity, reduce bubble adhesion, and facilitate bubble release, thereby maintaining continuous exposure of active sites.

Wang et al. used acid etching to intercalate PMo_{12} into NiFe LDH, which was then used as the anode in three AEM electrolytic cells with Ni@NiFe LDH assembled as the cathode (Fig. 30(a)) [245]. The cells achieved voltages of 1.50, 1.73, and 1.88 V at 25 °C, and 1.45, 1.61, and 1.70 V at 60 °C, corresponding to current densities of 10, 100, and 200 $mA·cm^{-2}$, respectively. Notably, the cell demonstrated excellent durability by operating stably at 400 $mA·cm^{-2}$ for 90 h. *In situ* Raman and XANES analyses revealed that the incorporation of POMs generated a moderate number of oxygen and metal vacancies, which modulated the local coordination environment and electronic structure, thereby enhancing the electrochemical activity of Ni and Fe. Furthermore, by carefully controlling the defect concentration, POM incorporation effectively improved the long-term stability of the catalyst (Figs. 30(b)–30(d)). Yan et al. synthesized an ultrastructured material, MOF@POM, by grafting POMs onto MOFs using a targeted approach. When used as the anode in an AEM electrolyzer—paired with a 20% Pt/C cathode and a Sustanion X37-50 Grade T separator—the device achieved a current of 70 A (2.8 $A·cm^{-2}$) at 1.98 V and 25 °C. Remarkably, it maintained stable operation for over 5140 h at a current density of 2 $A·cm^{-2}$ and 25 °C, exhibiting an exceptionally low voltage decay rate of 0.02 $mV·h^{-1}$. This performance exceeds that of conventional metal hydroxide catalysts, such as CoFe-LDHs and NiFe-LDHs, which typically experience substantial degradation within 100 h under similar conditions. The article attributes this enhanced stability to several factors: 1. Structural advantages: The hierarchical pore channels in MOF@POM promote rapid bubble release (contact angles < 90°), thereby alleviating bubble blockage commonly observed in NiFe-LDH systems. Comparisons before and after prolonged operation show that MOF@POM preserves its structural integrity during water oxidation, whereas the pristine MOF experiences significant degradation and collapse. This behavior indicates that the cage-like POM structure effectively buffers against electrolyte corrosion, in contrast to the readily oxidized phosphide layer in NiCoP that results in activity decay. 2. Enhanced resistance to metal dissolution: Analysis of metal dissolution rates, together with the activity stability factor derived from oxygen evolution data, shows that MOF@POM exhibits a substantially higher stability factor than CoFe-LDHs and NiFe-LDHs. This result indicates that fewer active sites are lost during water oxidation, confirming that POM grafting considerably enhances the stability of Co and Fe by enabling them to remain active at elevated voltages and suppressing rapid dissolution, thereby extending the catalyst lifetime. 3. Superior electronic conductivity: Electrochemical impedance spectroscopy and ultraviolet photoelectron spectroscopy reveal that MOF@POM exhibits the lowest charge-transfer resistance, supporting its enhanced stability and more efficient electron-transport pathways.

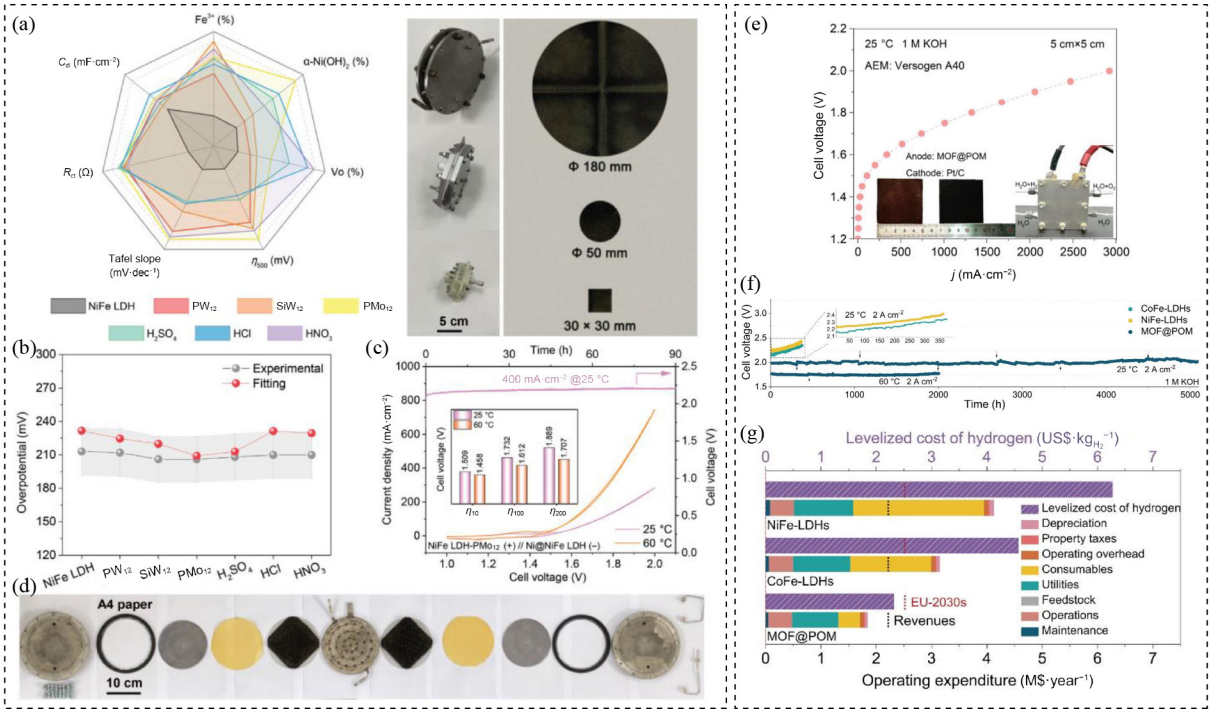

Figure 30 (a) Comparison of performance-determining factors in NiFe LDH-X (NiFe LDH-X are abbreviated as X, X = PW_{12}, SiW_{12}, PMo_{12}, H_2SO_4, HCl, and HNO_3). (b) Comparison of η_{10} values between the fitted results from SICCAS electrocatalytic equation and the experimental ones. (c) Polarization curves of overall water splitting measurement in an electrolysis cell filled with 1 M KOH at 25 and 60 °C with a scan rate of 5 mV·s^{-1}. (d) Stack structure of AEM electrolysis cell for operation. Reprinted with permission from Ref. [245], © Wiley-VCH GmbH 2022. (e) Polarization curves of the 25 cm^2 electrolyzer (electrode area: 5 cm × 5 cm, AEM: Versogen A40, cathode: 20% Pt/C, temparture: 25 °C). (f) Longterm durability of the AEMWE cell at 2 A·cm^{-2}. (g) Economic analysis of the operational costs of different catalysts and the leveled cost of hydrogen production. Reprinted with permission from Ref. [257], © Yue, K. H. et al., some rights reserved; exclusive licensee American Association for the Advancement of Science 2025. No claim to original U.S. Government Works.

4. Excellent thermodynamic stability: Theoretical calculations show that POM grafting improves the stability of $Co_{0.5}Fe_{0.5}OOH$ under high oxidation potentials and alkaline conditions. These computational results are consistent with the experimentally observed activity-decay trends, further confirming that POM incorporation substantially stabilizes peroxo–metal active sites. Notably, TEA indicates that the MOF@POM catalyst has the lowest annual operating costs and, compared with CoFe-LDHs and NiFe-LDHs, offers greater profitability potential [257]. Under a scenario involving a 100 m^2 AEM water electrolyzer operating at 2 A·cm^{-2} for 10 years, MOF@POM can achieve a hydrogen levelized cost (LCOH) of below \$2.5 kg^{-1} H_2, reaching as low as \$2.324 kg^{-1} H_2, thereby meeting the European Commission's 2030 target (Figs. 30(e)–30(g)).

In modern industrial electrolyzer applications, POMs offer notable advantages, particularly through multi-metal synergistic catalysis and exceptional acid–base resistance. First, POMs can form complex systems with various transition metal compounds, providing high conductivity and robust electrochemical stability. This enhancement arises from the ability of POMs to improve both electron and ion transport rates, thereby optimizing overall electrolytic efficiency. In water electrolysis, where reducing overpotential is critical for energy utilization, the incorporation of POMs lowers kinetic barriers in the hydrogen and OERs, accelerating these processes. Second, POMs exhibit superior corrosion resistance compared with conventional metallic electrolytes [258, 287]. Industrial electrolyzers typically operate under strongly acidic or alkaline conditions, which can accelerate corrosion and degrade traditional electrode materials. In contrast, the inherent chemical stability of POMs enables them to withstand harsh pH environments, thereby extending equipment lifetime and improving operational reliability. Moreover, POMs can suppress side reactions such as gas dissolution and crossover, enhancing product purity and overall system efficiency. Despite these advantages, several limitations still constrain their industrial implementation. POM clusters may partially decompose under high temperatures or high current densities, resulting in performance degradation. Under high loadings or fluctuating concentrations, POMs can precipitate or accumulate on electrode surfaces, blocking active sites and diminishing catalytic efficiency. In addition, the high cost of POM synthesis, together with complex fabrication processes, presents economic challenges for large-scale applications. In summary, although POMs offer excellent corrosion resistance and tunable redox chemistry, challenges related to chemical stability, electrode fouling, and cost must be overcome before widespread industrial adoption. Therefore, future efforts should focus on enhancing thermal and electrochemical robustness, improving immobilization strategies, and lowering synthesis costs to enable more efficient, durable, and economically viable electrolytic systems for green hydrogen production.

6 Challenges and future opportunities

6.1 Limitations of current POM catalytic systems

POM-based compounds have demonstrated considerable advantages in electrocatalytic HER and OER owing to their rich redox chemistry, which enables integration with various transition

metals to modulate redox behavior and enhance catalytic performance [221, 288]. Their tunable cluster architectures further allow adjustment of electrochemical properties to suit different catalytic environments. However, several scientific and technical challenges remain for practical applications: 1. Low electronic conductivity: The intrinsically negatively charged metal–oxo cluster frameworks of POMs lack efficient pathways for free electron transport [289]. 2. Slow kinetics in multi-electron transfer processes: Although POMs can accommodate multiple electrons, the limited number of low d-band metal sites on their surfaces leads to sluggish adsorption and desorption of hydrogen species during HER. In addition, the relatively small size of POM monoclusters is unfavorable for facilitating the sequential multistep processes involved in OER. 3. Structural instability under high current density conditions: The high water solubility of POMs can cause dissolution of framework metals such as Mo and W under high current densities, thereby inducing dissociation of the POM structure in extreme operating environments. 4. Challenges in interface control: The oxygenated, negatively charged groups on POM surfaces complicate their immobilization onto supports via electrostatic adsorption or covalent bonding. Furthermore, while confinement-assisted assembly of POMs offers conceptual advantages, it can sometimes provide insufficient protection—resulting in dissolution during electrolysis—or excessive confinement that limits active-site accessibility and participation in the reaction. 5. Most studies on POM-mediated water electrolysis focus on the synergistic effects of multiple metals, often neglecting the dynamic structural evolution during operation. Processes such as intra-cluster electron transfer and POM leaching, which can lead to irreversible transformation into metal hydroxides under high current densities, remain poorly understood.

As a catalyst material for water electrolysis, POM-based compounds require improved conductivity and improved structural stability. Several strategies can be used to achieve these improvements. First, the bonding between POM-based materials and conductive substrates can be reinforced by anchoring them through organic ligands or metal bonds, thereby increasing stability while maintaining high conductivity. Second, beyond strengthening interfacial interactions, the intrinsic conductivity of the compounds can be enhanced by establishing effective conductive pathways via inorganic methods, such as the classical –M–N–M– bridging mode. Additionally, carbon coating techniques can be applied to prevent leaching of POM groups, further contributing to improved conductivity and overall catalytic performance. Third, more flexible structural assembly strategies and metal site-specific coordination, achieved through the selection of functionalized organic ligands, can more effectively activate the catalytic performance of POMs. This approach also allows the incorporation of various transition metals as active sites for water electrolysis, helping to overcome the kinetic limitations inherent to POM materials. Finally, because many reported POM-based materials suffer from cluster collapse following aggressive inorganic modifications, it is crucial to explore milder modification techniques that preserve the integrity of POM clusters. Preserving elements such as Mo and W as ionic clusters to prevent leaching is a promising avenue for future research.

6.2 Future-oriented research trends

6.2.1 Molecular-level regulation

A key strategy for improving the catalytic performance of POMs is accurate molecular-level regulation. Specifically, designing vacancy structures and tuning electronic configurations enables fine control over the local active-site environment [70]. Introducing vacancy structures—such as anionic or cationic defects—modifies local electron density and coordination, optimizing the adsorption energies of critical reaction intermediates (e.g., H^* and OH^*) and accelerating water dissociation kinetics [290]. POMs can generate various vacancy-type species through hydrolysis and related processes, maintaining the integrity of the original framework while exposing coordinatively unsaturated metal sites that function as active electrocatalytic centers. These exposed sites readily bind water molecules, and the resulting metal vacancies exhibit strong coordination capabilities, enabling adsorption of additional metal ions and enhancing catalytic performance through multiple synergistic effects. Moreover, the weakly acidic character of POMs facilitates the formation of metal and oxygen vacancies when combined with other metal compounds; for instance, Wang et al. showed that etching NiFe LDH with POMs under acidic conditions promoted the dissolution and migration of metal oxides. This process facilitates the migration or transformation of specific metal ions, resulting in the formation of corresponding defects and vacancies. During the oxidation of iron, the transition from Fe^{2+} to Fe^{3+} generates iron vacancies, which are crucial for maintaining charge neutrality. XPS and electron paramagnetic resonance analyses confirmed that the etching process increased the concentration of oxygen vacancies in NiFe LDH samples. These vacancies not only enhance catalytic activity but also considerably alter the electronic structure. Furthermore, DFT calculations indicate that oxygen vacancies effectively tune the electronic structure of NiFe LDH, thereby improving its catalytic performance in the OER. Overall, the adjustment of the local coordination environment of metal ions, such as Fe and Ni, through oxygen vacancies plays a key role in enhancing both the electronic properties and catalytic efficiency of these active sites [245].

The accurate design of electronic configurations primarily entails tuning the d-band center and charge distribution by incorporating heterogeneous atoms (e.g., doping with Co or Fe) [291, 292]. Owing to their tunable cluster structures, POM-based materials can more effectively incorporate metal atoms, thereby modifying their electrochemical performance. In particular, the use of POMs as precursors for synthesizing transition metal intermetallic compounds (TMICs) is widespread [293]. Typically, TMIC formation requires high-temperature calcination of the raw materials; however, this approach provides limited control over particle size and microstructure, often yielding larger particles [260]. To enhance catalytic activity, it is essential to reduce TMICs to the nanoscale—or even the atomic scale—to maximize the exposure of active sites. Therefore, the development of effective size-controlled synthesis strategies is essential. For example, using POMs as precursors combined with an assembly-anchoring strategy and amino-containing polymers such as polyethyleneimine prevents POM aggregation, enabling the synthesis of well-dispersed TMICs with particle sizes of 2–3 nm. Acting as an ideal "connector arm," polyethyleneimine limits the number of linked POMs, thereby enabling accurate size control. In addition, its strong interactions with rGO promote effective dispersion of POMs, preventing aggregation during subsequent pyrolysis. This approach facilitates the successful synthesis of well-dispersed WN/rGO composites with uniformly small particle sizes. Moreover, constructing heterojunctions between transition metals and late transition metals enhances catalytic performance. At these heterogeneous interfaces, electron distribution is modulated, optimizing the bonding of

adsorbed hydrogen and oxygen intermediates and generating additional active sites, which together considerably increase reaction rates. The inherent structural tunability of POMs allows accurate control over metal ratios in the heterojunctions prior to pyrolysis, enabling deliberate structural optimization [294]. For example, Fu et al. first synthesized a nickel–vanadium POM precursor to accurately control the V/Ni elemental ratio and subsequently obtained Ni_3N–VN/NF via high-temperature nitridation, which exhibited superior catalytic activity for the HER. Similarly, high-temperature phosphorization yielded Ni_2P–VP_2/NF, showing excellent performance in the OER. In these syntheses, key catalytic factors—including the adsorption energies of intermediates and electrical conductivity—were optimized by carefully modulating the precursor's morphology, size, and composition. Furthermore, theoretical calculations and XPS analyses confirmed that anion regulation affected both the direction of electron transfer and the adsorption energies of intermediates, enabling accurate tuning of catalytic performance [295].

The core strategy for achieving molecular-level control in POM-based electrocatalysts for water electrolysis involves creating a chemical environment rich in highly active sites. This is achieved through vacancy design and defect engineering, which introduce various metal and oxygen vacancies at the molecular scale. Additionally, the accurate tuning of electronic configurations via the incorporation of multiple heteroatoms adjusts the d-band center and charge distribution, optimizing the adsorption and desorption energies of reaction intermediates. Together, these strategies enhance both the intrinsic activity and stability of POM-based electrocatalysts, providing a solid theoretical foundation for efficient, low-energy hydrogen production (Fig. 32 red part).

6.2.2 *Multi-scale interface engineering*

Multi-scale interface engineering of POMs is a key strategy for overcoming both sluggish charge-transfer kinetics and the low utilization of active sites in electrocatalytic water splitting. In particular, composite systems based on POM–MOF hybrids and POM–SACs have achieved breakthrough performance through cross-scale synergistic effects. Owing to the intrinsically low conductivity and high solubility of POMs, their integration with highly conductive materials is crucial to enhance both catalytic activity and stability. A topology-matching assembly strategy that leverages confinement and electronic coupling effects allows the integration of POMs with MOF materials through two primary approaches: 1. In this approach, MOFs encapsulate size-matched POMs within their channels using confinement effects [296–298]. This method requires the pore size to match the POM dimensions within ±0.1 nm—a highly stringent requirement. Poor size matching can either leave active sites exposed, leading to dissolution during electrolysis, or overly constrain the POMs, making their active sites inaccessible for catalysis. 2. Node anchoring: In this approach, POMs form covalent bonds with the metal sites of the MOF, generating a co-assembled POM–MOF superstructure. This design exploits synergistic interactions among metal atoms to establish rapid electron-transport channels between catalytic sites, thereby stabilizing the metal centers and preventing dissolution. Through interfacial synergy, the POM–MOF structure optimizes electron transfer, considerably enhancing both activity and stability in water splitting. During electrolysis, the MOF can undergo *in situ* transformation into ultrathin active layers composed of single-atom transition metal species (e.g., Co, Fe, or Ni hydroxides), while the POM scaffold preserves structural integrity and accelerates electron transport. The resulting composite, analogous to a "rebar–concrete" system, combines the high specific surface area of the MOF with the superior conductivity of POMs, mitigates mechanical stress on the catalytic layer, and enables stable performance under demanding operating conditions.

The single-atom anchoring strategy exploits the molecular tunability of POMs to anchor isolated metal atoms, which are subsequently integrated with conductive substrates through POM interfacial engineering [18, 200]. Using various defect-encapsulation methods, single atoms can be accurately positioned in POM clusters and modified to form catalysts with robust surface chemical bonds. This approach is particularly advantageous for acidic water-splitting systems that rely on noble-metal catalysts. In POMs, heteroatom doping—such as with Pt, Ir, or Ru—through terminal oxygen (O–M) or bridging oxygen (M–O–M) sites, or by embedding single atoms into defective POMs, can fine-tune the electronic structure and reduce noble-metal usage, thereby lowering costs while maintaining high catalytic performance. For instance, Wei et al. reported a strong electronic coupling between vacancy-type SiW_9 and Pt nanoparticles, which accelerates electron transfer from Pt to SiW_9 (Figs. 31(a)–31(d)) [118]. Moreover, POMs can function as proton pumps, enhancing hydrogen-bond network connectivity and proton transfer rates. Through a PCET mechanism, SiW_9 optimizes proton supply and increases proton coverage at Pt active sites. When anchored on Pt nanoparticle surfaces, SiW_9 increases the proportion of asymmetrically hydrogen-bonded water molecules, forming a stronger hydrogen-bond network that further facilitates efficient proton and electron transfer. Under the acidic conditions typical of PEM electrolysis, both POMs and single atoms remain vulnerable to decomposition and catalyst deactivation (Figs. 31(e)–31(g)). Notably, the single-atom anchoring structure, in which POMs act as ligands, effectively stabilizes single-atom nanoparticles and preserves an ultrafine size distribution. By enhancing Coulombic repulsion and steric hindrance, this design prevents single-atom aggregation and improves long-term catalyst stability. In addition, the strong coupling between single atoms accelerates electron transfer, promoting efficient proton capture during the Volmer step and rapid hydrogen evolution in the Tafel step, thereby ensuring consistent catalytic performance (Figs. 31(h)–31(k)).

The essence of multi-scale POM interface engineering lies in the interactions between POM-MOFs and various compounds. Through molecular interface engineering, a superstructure is formed that addresses the dissolution challenges of POMs under high-current conditions, optimizes synergistic effects at the molecular interface, and accelerates charge-transfer rates. Additionally, using charge-capturing and defect-interface engineering strategies, POM–SACs with atomically dispersed active sites can be achieved, increasing the active surface area, facilitating proton transport, and enhancing electron-transfer efficiency. Such interface engineering considerably enhances the electrocatalytic performance of POM compounds in water electrolysis. Future research should incorporate flux calculations to identify optimal POM interface combinations and fine-tune the interfacial electronic structure, thereby advancing the sustainable development of water electrolysis (Fig. 32 blue part).

6.2.3 *Integrated analysis of reaction mechanisms using various techniques*

The complex dynamic behavior of POM-based water electrolysis catalysts—including fluctuations in oxidation states, interfacial

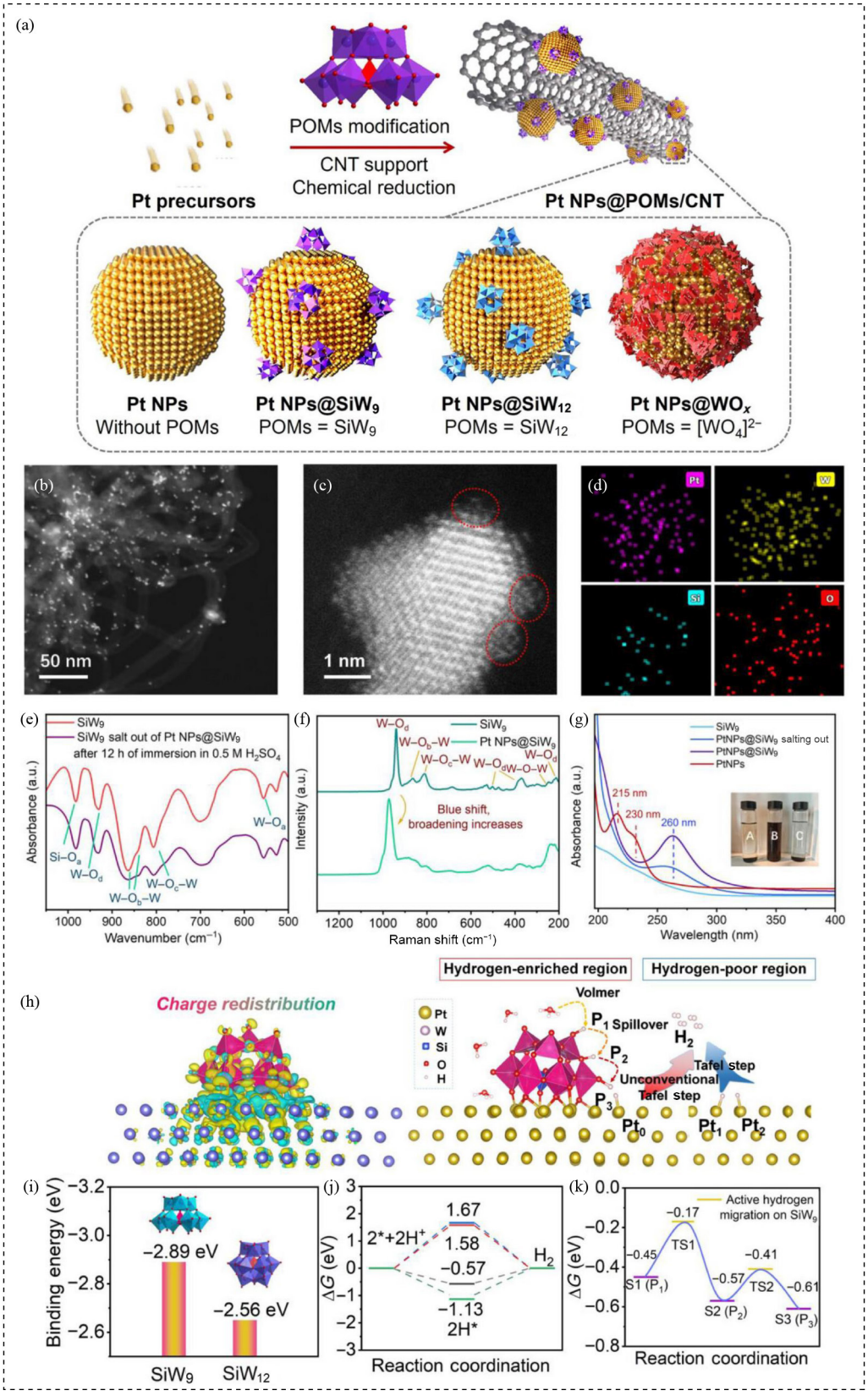

Figure 31 (a) Schematic illustration of the synthetic procedure of Pt NPs anchored by POMs ligands. (b) Dark field TEM image of Pt NPs@SiW_9/CNT. (c) HADDF-STEM image and (d) corresponding EDS mapping images of Pt NPs@SiW_9/CNT. (e) IR spectra of SiW_9 and SiW_9 salting out of Pt NPs@SiW_9 after 12 h of HER at 100 mA·cm^{-2} in 0.5 m H_2SO_4. (f) Raman spectra of SiW_9 and Pt NPs@SiW_9. (g) UV–vis spectra of the SiW_9, Pt NPs, Pt NPs@SiW_9, and Pt NPs@SiW_9 after salting out. (h) Difference charge density: yellow and blue indicate an increase and decrease of electron density, respectively and schematic illustrating the proposed reaction mechanism on Pt NPs@SiW_9. (i) Binding energy of SiW_{12} and lacunary SiW_9 on Pt (111) surface. (j) The free energy profiles of the Tafel step on different sites of Pt NPs@SiW_9. (k) The kinetic energy barriers of hydrogen migration/spillover process for SiW_9. Reprinted with permission from Ref. [118], © Wiley-VCH GmbH 2025.

reconstruction, and multi-element synergy—requires a thorough understanding of the water electrolysis mechanism to guide the design of high-performance, stable electrode materials [287]. In water electrolysis with acid–base materials, structural and chemical changes occur across multiple scales. At the atomic level, in POM clusters, heteroatoms and the metal framework undergo considerable oxidation-state variations, often accompanied by the formation of metal and oxygen vacancies. At the interfacial level, electron transfer and chemical bond reorganization between the POM and its support are prominent. At the system level, factors such as electrolyte mass transport, bubble dynamics, and material dissolution influence the availability of active sites. Therefore, no single diagnostic technique can fully capture these dynamic changes; instead, a coordinated application of multiple *in situ* and operando techniques is required to monitor electron transfer, structural evolution, and intermediate kinetics that govern the underlying mechanism.

The dynamic analysis of the electronic structure relies on the integration of multiple *in situ* spectroscopic techniques, including XAS, ambient pressure X-ray photoelectron spectroscopy (APXPS), and synchrotron radiation Fourier transform infrared (SR-FTIR) spectroscopy. *In situ* XAS tracks real-time variations in the K-edge absorption energy of the active metal, revealing changes in oxidation state and coordination environment [299]. Concurrently, APXPS provides insights into the chemical valence of surface elements and the coverage of adsorbed active species such as oxygen under operating conditions [300, 301]. SR-FTIR captures the vibrational fingerprints of reaction intermediates, while complementary theoretical calculations help elucidate the POM interfacial proton–electron coupling mechanism [302]. Recent studies on POM–MOF superstructures have shown that Yan et al. used *in situ* XANES and EXAFS to monitor changes in the oxidation states and coordination environments of catalyst active sites. During water electrolysis, the oxidation states of Co and Fe increased rapidly with applied potential, indicating that the metal sites evolved from M–O (M = Co or Fe) to M–OH and ultimately to the catalytically active M–OOH phase. This evidence confirms that the catalyst surface undergoes structural transformation under applied potential, converting into its active form. Furthermore, APXPS monitoring of Co, Fe, and Ni oxidation states under water electrolysis conditions revealed that Ni acted as an elastic deformation moderator, stabilizing the active catalytic sites without directly participating in the reaction. In addition, SR -FTIR analysis showed that, as the applied potential increased, characteristic Raman peaks associated with the organic components diminished and, beyond 1.53 V, produced new peaks corresponding to the formation of hydroxyl oxide species. This process occurred alongside significant degradation and structural collapse of the MOF framework. These potential-dependent transformations highlight the activation characteristics of the MOF@POM system during water oxidation. Collectively, the in situ spectroscopic investigations reveal the complex structural evolution and underlying mechanisms of the MOF@POM catalyst during water electrolysis. The facilitated formation and stabilization of active catalytic sites—enabled by the rapid establishment of electron-transfer channels—substantially enhance both catalytic performance and long-term stability. These insights provide a robust theoretical framework and experimental foundation for the rational design of more efficient water electrolysis catalysts [257].

The analysis of morphology and structural evolution requires the combined use of in situ electron microscopy and in situ Raman spectroscopy. *In situ* electron microscopy enables real-time monitoring of structural reconstruction and lattice distortions in POM-based catalysts during synthesis, modification, and electrolysis. In parallel, in situ Raman spectroscopy tracks characteristic vibrational peaks of POMs at varying potentials, facilitating the analysis of redox states and the identification of active sites for both OER and HER [303, 304]. The use of in situ electron microscopy to observe electrolytic structural reconstruction is still an emerging technique. A notable example is provided by Zhao et al., who used in situ liquid electrochemical transmission electron microscopy (TEM) to investigate Rh-doped $NiPS_3$ nanosheets (Ru-$NiPS_3$) under applied current. After a 2-h constant-current test, pronounced reconstruction was observed at the edge regions of the nanosheets. Selected area electron diffraction patterns revealed that, while most of the nanosheets retained their original structure, certain regions transformed into polycrystalline or amorphous states, indicating a progressive amorphization process that was particularly pronounced at the thinner edge regions. Using *in situ* liquid electrochemical transmission electron microscopy, the researchers not only tracked the real-time structural evolution of the materials during electrochemical reactions but also identified the crucial role of an amorphous surface layer in enhancing catalytic performance. These findings highlight that the distribution and functionality of the Rh dopant play a considerable role in improving electrocatalytic activity [305]. It is noteworthy that POM-based materials, particularly those with Mo and W frameworks, are highly prone to transitioning from crystalline to amorphous states during electrolysis. In this context, in situ electron microscopy is indispensable for revealing the real-time evolution of active species during water electrolysis. In contrast, in situ Raman spectroscopy is a more established and widely adopted technique for analyzing active species under operating conditions. Studies typically show that applied voltage induces electronic and conformational changes at material interfaces. For example, during water oxidation with POM-MOFs, increasing the applied voltage leads to the gradual diminution and near disappearance of characteristic Raman peaks associated with organic components (e.g., 1611, 1422, 633, and 376 cm^{-1}) at 1.53 V versus RHE. These peaks are subsequently replaced by new peaks between 465 and 540 cm^{-1}, indicating the formation of hydroxide oxide species, widely recognized as the true active species for OER in water electrolysis[257].

In addition, several techniques enable the simultaneous analysis of water electrolysis catalyst materials. 1. Differential electrochemical mass spectrometry (DEMS): This method uses isotope labeling to investigate electrochemical behavior in combination with complementary analytical techniques, allowing concurrent exploration of reaction mechanisms, including both the AEM and lattice oxygen mechanism (LOM) [306, 307]. Furthermore, in situ DEMS allows real-time monitoring of hydrogen and oxygen evolution rates, enabling calculation of Faradaic efficiency to evaluate catalyst activity and stability during water-splitting hydrogen production [308]. 2. In open electrolytic systems, such as three-electrode cells, high-speed imaging effectively captures bubble dynamics, offering a reliable qualitative method to study bubble growth and detachment during electrolysis [309]. By correlating these observations with electrochemical data, researchers can systematically assess how bubble characteristics influence the electrochemical response. Additionally, high-speed

imaging facilitates the evaluation of material hydrophobicity and hydrophilicity, which is crucial for designing improved catalytic materials [310]. 3. Theoretical calculation methods, such as DFT: By combining multiple analytical approaches to model molecular structures, DFT is used to calculate key thermodynamic parameters, including hydrogen adsorption free energy, water adsorption free energy, and hydroxyl free energy [311]. These values are critical for evaluating catalyst performance and guiding the design of novel catalytic materials. Additionally, DFT-based kinetic analyses provide insights into energy changes along reaction pathways, offering a theoretical foundation for catalyst optimization and the development of new catalytic processes [312].

A comprehensive understanding of multi-acid-driven water electrolysis requires an integrated analytical framework that combines multiple in situ and operando techniques. Future research should focus on the coordinated use of operando XAS, Raman spectroscopy, high-resolution electron microscopy, and DEMS to monitor the dynamic evolution of POM structures, intermediate species, and reaction pathways under realistic electrolysis conditions. Integrating machine-learning algorithms with multi-scale theoretical models will further enable predictive evaluation of catalytic behavior across varying pH values, applied potentials, and local microenvironments, thereby accelerating mechanism-driven catalyst discovery. High-throughput experimental platforms will be essential for rapidly screening POM-derived catalysts and mapping structure–activity relationships. Industrial validation must also be emphasized, with mechanistic models assessed under practical stressors such as fluctuating power inputs and high current densities. Collectively, these strategies are expected to overcome the current "black box" limitations of POM catalysis and provide quantitative guidance for the rational design of next-generation, high-efficiency electrolyzers.

Beyond mechanistic insights, the sustainability of POM synthesis and utilization requires increased attention for large-scale deployment. Most POMs still rely on Mo- and W-based precursors, highlighting the need for resource-efficient and atom-economical synthetic routes. Conventional preparation methods often involve energy-intensive crystallization or high-temperature pyrolysis, emphasizing the importance of developing low-energy, solution-processable, or ambient-temperature methodologies. The intrinsic reversible redox nature of POM clusters offers promising opportunities for catalyst regeneration and closed-loop recycling. Emerging green-chemistry strategies—including biomolecule-assisted assembly, solvent-free fabrication, and the use of benign oxidants—provide viable pathways to reduce the environmental burden of POM production. Incorporating life-cycle assessments and end-of-life considerations will be essential for quantitatively evaluating environmental impacts and guiding the sustainable integration of POM-based electrocatalysts into future green-hydrogen technologies (Fig. 32 green part).

Data availability

Not applicable.

Acknowledgements

We gratefully acknowledge financial support by “Grassland Talents” of Inner Mongolia Autonomous Region, Young Talents of Science and Technology in Universities of Inner Mongolia Autonomous Region (No. NJYT23030), Technology Breakthrough Engineering Hydrogen Energy Field "Unveiling and Leading" Project (No. 2024KJTW0018), “Steed plan High level Talents” of Inner Mongolia University, Carbon neutralization research project (No. STZX202218), the National Natural Science Foundation of China (No. U22A20107), Inner Mongolia Autonomous Region Natural Science Foundation (2023MS02002), Hohhot University Institute Collaborative Innovation Project (No. XTCX2024-02), Guangdong Provincial Key Laboratory of Materials and Technologies for Energy Conversion (No. MATEC2024KF011), the National Key R&D Program of China (No. 2022YFA1205201), and Inner

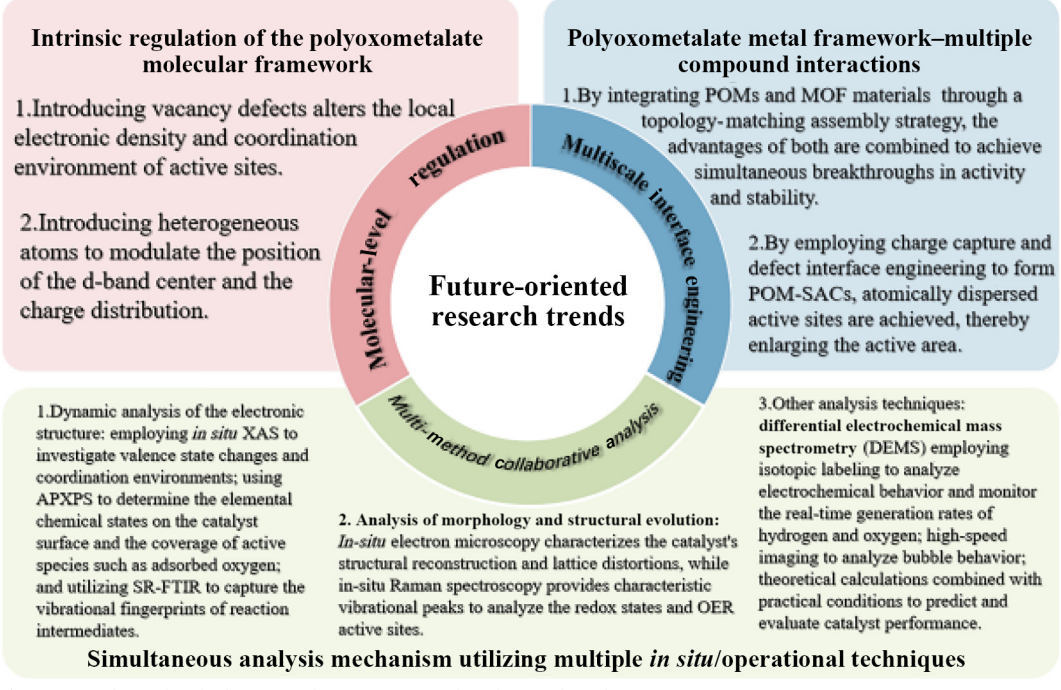

Figure 32 Three future research trends in hydrogen production via POMs-based water electrolysis.

Mongolia Autonomous Region Graduate Research Innovation Project (No. KC2024020B).

Declaration of competing interest

All the contributing authors report no conflict of interests in this work.

Author contribution statement

H. E. Z.: Literature survey, data curation, visualization, writing – original draft. S. M. Y.: Conceptualization, literature survey, framework design of the review, critical analysis, writing – original draft and revision. Y. F. W.: Literature survey, data curation, visualization, writing – original draft. Z. H. Z.: Literature survey, technical discussion, writing – review & editing. Z. L. Z.: Technical discussion, writing – review & editing. K. Y.: Literature survey, visualization, writing – review & editing. Z. C. F.: Literature survey, technical discussion. J. Q. L.: Literature survey, data organization. X. Y. L.: Visualization and graphical refinement. F. C. T. S.: Technical discussion and language polishing. J. W. Z.: Supervision, conceptual guidance, funding acquisition, writing – review & editing.

Use of AI statement

None.

References

[1] Freire, C.; Fernandes, D. M.; Nunes, M.; Abdelkader, V. K. POM & MOF-based electrocatalysts for energy-related reactions. *ChemCatChem* **2018**, *10*, 1703–1730.

[2] Gao, A. L.; Iwano, T.; Uchida, S. Emerging functionalized lindqvist-type polyoxometalate-based compounds: Design, synthesis, and applications. *ChemCatChem* **2025**, *17*, e202500066.

[3] Horn, M. R.; Singh, A.; Alomari, S.; Goberna-Ferrón, S.; Benages-Vilau, R.; Chodankar, N.; Motta, N.; Ostrikov, K.; MacLeod, J.; Sonar, P. et al. Polyoxometalates (POMs): From electroactive clusters to energy materials. *Energy Environ. Sci.* **2021**, *14*, 1652–1700.

[4] Mallouk, T. E. Divide and conquer. *Nat. Chem.* **2013**, *5*, 362–363.

[5] Wang, Y. Q.; Wang, T.; Xu, M.; Li, B. W.; Gao, Z.; Zhang, W. J.; Li, Z. X.; Qu, C. Q.; Feng, M. Polyoxometalate superlattices derived bimetallic sulfides to accelerate acidic and alkaline hydrogen evolution reaction. *J. Colloid Interface Sci.* **2025**, *679*, 760–768.

[6] Ali, A.; Shen, P. K. Nonprecious metal's graphene-supported electrocatalysts for hydrogen evolution reaction: Fundamentals to applications. *Carbon Energy* **2020**, *2*, 99–121.

[7] Zhang, Y. L.; Luo, M. C.; Yang, Y.; Li, Y. J.; Guo, S. J. Advanced multifunctional electrocatalysts for energy conversion. *ACS Energy Lett.* **2019**, *4*, 1672–1680.

[8] Zeng, Y.; Zhao, M. T.; Zeng, H. L.; Jiang, Q.; Ming, F. W.; Xi, K.; Wang, Z. C.; Liang, H. F. Recent progress in advanced catalysts for electrocatalytic hydrogenation of organics in aqueous conditions. *eScience* **2023**, *3*, 100156.

[9] Wang, Z. H.; Wang, X. F.; Tan, Z.; Song, X. Z. Polyoxometalate/metal-organic framework hybrids and their derivatives for hydrogen and oxygen evolution electrocatalysis. *Mater. Today Energy* **2021**, *19*, 100618.

[10] Zhang, L.; Chen, Z. Q. Polyoxometalates: Tailoring metal oxides in molecular dimension toward energy applications. *Int. J. Energy Res.* **2020**, *44*, 3316–3346.

[11] Kang, X.; Zhu, M. Z. Structural isomerism in atomically precise nanoclusters. *Chem. Mater.* **2021**, *33*, 39–62.

[12] Ferrando, R.; Jellinek, J.; Johnston, R. L. Nanoalloys: From theory to applications of alloy clusters and nanoparticles. *Chem. Rev.* **2008**, *108*, 845–910.

[13] Parra-Puerto, A.; Ng, K. L.; Fahy, K.; Goode, A. E.; Ryan, M. P.; Kucernak, A. Supported transition metal phosphides: Activity survey for HER, ORR, OER, and corrosion resistance in acid and alkaline electrolytes. *ACS Catal.* **2019**, *9*, 11515–11529.

[14] Cameron, J. M.; Guillemot, G.; Galambos, T.; Amin, S. S.; Hampson, E.; Mall Haidaraly, K.; Newton, G. N.; Izzet, G. Supramolecular assemblies of organo-functionalised hybrid polyoxometalates: From functional building blocks to hierarchical nanomaterials. *Chem. Soc. Rev.* **2022**, *51*, 293–328.

[15] Zeb, Z.; Huang, Y. C.; Chen, L. L.; Zhou, W. B.; Liao, M. H.; Jiang, Y. Y.; Li, H. T.; Wang, L. M.; Wang, L.; Wang, H. et al. Comprehensive overview of polyoxometalates for electrocatalytic hydrogen evolution reaction. *Coord. Chem. Rev.* **2023**, *482*, 215058.

[16] Sun, C. Y.; Li, W.; Wang, K.; Zhou, W. J.; Wang, H. Q. Polyoxometalates-derived nanostructures for electrocatalysis application. *Rare Met.* **2024**, *43*, 1845–1866.

[17] Dashtian, K.; Shahsavarifar, S.; Usman, M.; Joseph, Y.; Ganjali, M. R.; Yin, Z. Y.; Rahimi-Nasrabadi, M. A comprehensive review on advances in polyoxometalate based materials for electrochemical water splitting. *Coord. Chem. Rev.* **2024**, *504*, 215644.

[18] Ma, T.; Yan, R.; Wu, X. Z.; Wang, M.; Yin, B.; Li, S.; Cheng, C.; Thomas, A. Polyoxometalate-structured materials: Molecular fundamentals and electrocatalytic roles in energy conversion. *Adv. Mater.* **2024**, *36*, 2310283.

[19] Yu, B. Y.; Zhao, X.; Ni, J. F.; Yang, F. Multiscale assembly of polyoxometalates: From clusters to materials. *ChemPhysMater* **2023**, *2*, 20–29.

[20] Huang, X. Q.; Liu, S.; Liu, G.; Tao, Y. W.; Wang, C. R.; Zhang, Y. L.; Li, Z.; Wang, H. W.; Zhou, Z.; Shen, G. D. et al. An unprecedented 2-fold interpenetrated open framework built from Zn_6 ring seamed trivacant polyoxotungstates used for photocatalytic synthesis of pyridine derivatives. *Appl. Catal. B: Environ.* **2023**, *323*, 122134.

[21] Zang, D. J.; Wang, H. Q. Polyoxometalate-based nanostructures for electrocatalytic and photocatalytic CO_2 reduction. *Polyoxometalates* **2022**, *1*, 9140006.

[22] Xu, S. Y.; Wang, P.; Zhang, B. W.; Wang, C.; Low, J.; Ivanov, V. K.; Zhang, Z. M. Nickel-substituted polyoxometalate-CdS single-cluster photocatalysts for efficient plastic waste degradation coupled with H_2 production. *Polyoxometalates* **2025**, *4*, 9140096.

[23] Moors, M.; Warneke, J.; López, X.; de Graaf, C.; Abel, B.; Monakhov, K. Y. Insights from adsorption and electron modification studies of polyoxometalates on surfaces for molecular memory applications. *Acc. Chem. Res.* **2021**, *54*, 3377–3389.

[24] Misra, A.; Kozma, K.; Streb, C.; Nyman, M. Beyond charge balance: Counter-cations in polyoxometalate chemistry. *Angew. Chem., Int. Ed.* **2020**, *59*, 596–612.

[25] Liu, J. X.; Zhang, X. B.; Li, Y. L.; Huang, S. L.; Yang, G. Y. Polyoxometalate functionalized architectures. *Coord. Chem. Rev.* **2020**, *414*, 213260.

[26] Yonesato, K.; Yanai, D.; Yamaguchi, K.; Suzuki, K. Recent advances in polyoxometalate-metal nanocluster hybrids. *Chem.—Eur. J.* **2025**, *31*, e202500877.

[27] Ogiwara, N.; Iwano, T.; Ito, T.; Uchida, S. Proton conduction in ionic crystals based on polyoxometalates. *Coord. Chem. Rev.* **2022**, *462*, 214524.

[28] López, X.; Carbó, J. J.; Bo, C.; Poblet, J. M. Structure, properties and reactivity of polyoxometalates: A theoretical perspective. *Chem. Soc. Rev.* **2012**, *41*, 7537–7571.

[29] Li, M.; Zhang, M. X.; Wang, W. Y.; Cheng, S. Z. D.; Yin, P. C. The applications of small-angle X-ray scattering in studying nano-scaled polyoxometalate clusters in solutions. *J. Nanopart. Res.* **2018**, *20*, 124.

[30] Kondinski, A. Metal-metal bonds in polyoxometalate chemistry. *Nanoscale* **2021**, *13*, 13574–13592.

[31] Wang, D.; Liu, L. L.; Jiang, J.; Chen, L. J.; Zhao, J. W. Polyoxometalate-based composite materials in electrochemistry: State-of-the-art progress and future outlook. *Nanoscale* **2020**, *12*, 5705–5718.

[32] Zhang, Y.; Li, Y. Y.; Guo, H. R.; Guo, Y. Q.; Song, R. Recent advances in polyoxometalate-based materials and their derivatives for electrocatalysis and energy storage. *Mater. Chem. Front.* **2024**, *8*, 732–768.

[33] Maru, K.; Kalla, S.; Jangir, R. MOF/POM hybrids as catalysts for organic transformations. *Dalton Trans.* **2022**, *51*, 11952–11986.

[34] Lian, L. F.; Zhang, H. Y.; An, S.; Chen, W.; Song, Y. F. Polyoxometalates-based heterogeneous catalysts in acid catalysis. *Sci. China Chem.* **2021**, *64*, 1117–1130.

[35] Araújo, H.; Šljukić, B.; Gago, S.; Santos, D. M. F. The current state of transition metal-based electrocatalysts (oxides, alloys, POMs, and MOFs) for oxygen reduction, oxygen evolution, and hydrogen evolution reactions. *Front. Energy Res.* **2024**, *12*, 1373522.

[36] Cui, X. B. Special issue: Research on polyoxometalate materials. *Molecules* **2023**, *28*, 4662.

[37] Wang, S. S.; Yang, G. Y. Recent advances in polyoxometalate-catalyzed reactions. *Chem. Rev.* **2015**, *115*, 4893–4962.

[38] Weinstock, I. A.; Schreiber, R. E.; Neumann, R. Dioxygen in polyoxometalate mediated reactions. *Chem. Rev.* **2018**, *118*, 2680–2717.

[39] Walsh, J. J.; Bond, A. M.; Forster, R. J.; Keyes, T. E. Hybrid polyoxometalate materials for photo(electro-) chemical applications. *Coord. Chem. Rev.* **2016**, *306*, 217–234.

[40] Zhang, M.; Li, H. J.; Zhang, J. H.; Lv, H. J.; Yang, G. Y. Research advances of light-driven hydrogen evolution using polyoxometalate-based catalysts. *Chin. J. Catal.* **2021**, *42*, 855–871.

[41] Yang, G. P.; Liu, Y. F.; Wei, Y. G. Application of polyoxometalates in biomass conversion. *Coord. Chem. Rev.* **2024**, *521*, 216172.

[42] Tian, P.; He, X.; Li, W. X.; Zhao, L.; Fang, W.; Chen, H.; Zhang, F. Q.; Zhang, W. Q.; Wang, W. Zr-MOFs based on Keggin-type polyoxometalates for photocatalytic hydrogen production. *J. Mater. Sci.* **2018**, *53*, 12016–12029.

[43] Jiao, L.; Dong, Y. Y.; Xin, X.; Qin, L.; Lv, H. J. Facile integration of Ni-substituted polyoxometalate catalysts into mesoporous light-responsive metal-organic framework for effective photogeneration of hydrogen. *Appl. Catal. B: Environ.* **2021**, *291*, 120091.

[44] Coyle, L.; Middleton, P. S.; Murphy, C. J.; Clegg, W.; Harrington, R. W.; Errington, R. J. Protonolysis of $[(^{i}PrO)TiMo_5O_{18}]^{3-}$: Access to a family of $TiMo_5$ Lindqvist type polyoxometalates. *Dalton Trans.* **2012**, *41*, 971–981.

[45] Wang, X. L.; Chang, Z. H.; Lin, H. Y.; Tian, A. X.; Liu, G. C.; Zhang, J. W. Assembly and photocatalysis of two novel 3D Anderson-type polyoxometalate-based metal-organic frameworks constructed from isomeric bis(pyridylformyl)piperazine ligands. *Dalton Trans.* **2014**, *43*, 12272–12278.

[46] Gong, P. J.; Li, Y. Y.; Zhai, C. P.; Luo, J.; Tian, X. M.; Chen, L. J.; Zhao, J. W. Syntheses, structural characterization and photophysical properties of two series of rare-earth-isonicotinic-acid containing Waugh-type manganomolybdates. *CrystEngComm* **2017**, *19*, 834–852.

[47] Dong, H. M.; Li, W. H.; Ou, Y. Q.; Gao, D.; Yang, Y. B.; Zhang, Y. H.; Xiao, P. Self-assembly hydrothermal synthesis of silverton-type polyoxometalate-based photocatalysts for enhanced degradation. *Langmuir* **2020**, *36*, 4454–4464.

[48] Zhang, L. Z.; Gu, W.; Dong, Z. L.; Liu, X.; Li, B.; Liu, M. L. Syntheses, structures and properties of a series of photochromic hybrids based on Keggin tungstophosphates. *J. Solid State Chem.* **2009**, *182*, 1040–1044.

[49] Zhang, J. W.; Huang, Y. C.; Li, G.; Wei, Y. G. Recent advances in alkoxylation chemistry of polyoxometalates: From synthetic strategies, structural overviews to functional applications. *Coord. Chem. Rev.* **2019**, *378*, 395–414.

[50] Liu, Y. F.; Hu, C. W.; Yang, G. P. Recent advances in polyoxometalates acid-catalyzed organic reactions. *Chin. Chem. Lett.* **2023**, *34*, 108097.

[51] Ensafi, A. A.; Heydari-Soureshjani, E.; Rezaei, B. Nanostructure polyoxometalates containing Co, Ni, and Cu as powerful and stable catalysts for hydrogen evolution reaction in acidic and alkaline solutions. *Int. J. Hydrogen Energy* **2017**, *42*, 5026–5034.

[52] Ge, J. X.; Hu, J.; Zhu, Y. T.; Zeb, Z.; Zang, D. J.; Qin, Z. X.; Huang, Y. C.; Zhang, J. W.; Wei, Y. G. Recent advances in polyoxometalates for applications in electrocatalytic hydrogen evolution reaction. *Acta Phys.-Chim. Sin.* **2020**, *36*, 1906063.

[53] Zhong, J. W.; Pérez-Ramírez, J.; Yan, N. Biomass valorisation over polyoxometalate-based catalysts. *Green Chem.* **2021**, *23*, 18–36.

[54] Wang, Z. M.; Xin, X.; Li, Z.; Zhang, M.; Zhang, J. W.; Feng, Y. Q.; Zhang, J. H.; Lv, H. J.; Yang, G. Y. Atomically-precise Janus polyoxometalate catalyst with tunable water splitting activity. *Sci. China Chem.* **2023**, *66*, 1771–1780.

[55] Guo, L.; He, L.; Zhuang, Q. H.; Li, B. L.; Wang, C. F.; Lv, Y. F.; Chu, J. F.; Song, Y. F. Recent advances in confining polyoxometalates and the applications. *Small* **2023**, *19*, 2207315.

[56] Samaniyan, M.; Mirzaei, M.; Khajavian, R.; Eshtiagh-Hosseini, H.; Streb, C. Heterogeneous catalysis by polyoxometalates in metal-organic frameworks. *ACS Catal.* **2019**, *9*, 10174–10191.

[57] Ji, Y. C.; Huang, L. J.; Hu, J.; Streb, C.; Song, Y. F. Polyoxometalate-functionalized nanocarbon materials for energy conversion, energy storage and sensor systems. *Energy Environ. Sci.* **2015**, *8*, 776–789.

[58] Zhu, S.; Wu, Y. T.; Ding, L. T.; Zhang, X. H.; Li, L.; Wang, X.; Han, G. Y. Heightening polyoxometalate encapsulation efficiency for biaxial strain-induced catalytic activity boosting. *Energy Storage Mater.* **2024**, *73*, 103777.

[59] Stamate, A. E.; Pavel, O. D.; Zavoianu, R.; Marcu, I. C. Highlights on the catalytic properties of polyoxometalate-intercalated layered double hydroxides: A review. *Catalysts* **2020**, *10*, 57.

[60] Bao, Y. Y.; Chen, Z. Z.; Wang, Y. Z.; Liu, L. Z.; Wang, H. Y.; Li, Z. P.; Feng, F. Co-assembly of graphene/polyoxometalate films for highly electrocatalytic and sensing hydroperoxide. *Front. Chem.* **2023**, *11*, 1199135.

[61] Omwoma, S.; Chen, W.; Tsunashima, R.; Song, Y. F. Recent advances on polyoxometalates intercalated layered double hydroxides: From synthetic approaches to functional material applications. *Coord. Chem. Rev.* **2014**, *258–259*, 58–71.

[62] Zhang, S. S.; Liu, R. J.; Li, S. W.; Dolbecq, A.; Mialane, P.; Suo, L.; Bi, L. H.; Zhang, B. F.; Liu, T. B.; Wu, C. X. et al. Simple and efficient polyoxomolybdate-mediated synthesis of novel graphene and metal nanohybrids for versatile applications. *J. Colloid Interface Sci.* **2018**, *514*, 507–516.

[63] Sun, J. M.; Abednatanzi, S.; Van Der Voort, P.; Liu, Y. Y.; Leus, K. POM@MOF hybrids: Synthesis and applications. *Catalysts* **2020**, *10*, 578.

[64] Wu, J.; Liao, L. W.; Yan, W. S.; Xue, Y.; Sun, Y. F.; Yan, X.; Chen, Y. X.; Xie, Y. Polyoxometalates immobilized in ordered mesoporous carbon nitride as highly efficient water oxidation catalysts. *ChemSusChem* **2012**, *5*, 1207–1212.

[65] Opitz, A. K.; Nenning, A.; Rameshan, C.; Rameshan, R.; Blume, R.; Hävecker, M.; Knop-Gericke, A.; Rupprechter, G.; Fleig, J.; Klötzer, B. Enhancing electrochemical water-splitting kinetics by polarization-driven formation of near-surface iron(0): An *in situ* XPS study on perovskite-type electrodes. *Angew. Chem., Int. Ed.* **2015**, *54*, 2628–2632.

[66] Anyushin, A. V.; Kondinski, A.; Parac-Vogt, T. N. Hybrid polyoxometalates as post-functionalization platforms: From fundamentals to emerging applications. *Chem. Soc. Rev.* **2020**, *49*, 382–432.

[67] Ebrahimi, A.; Krivosudský, L.; Cherevan, A.; Eder, D.

Polyoxometalate-based porphyrinic metal-organic frameworks as heterogeneous catalysts. *Coord. Chem. Rev.* **2024**, *508*, 215764.
[68] Feng, Y. Q.; Zhao, M. Y.; Yang, J. X.; Wang, Z. M.; Bai, P. H.; Liu, Y. K.; Lv, H. J.; Yang, G. Y. Wearing gigantic silver armor on transition-metal-containing polyoxometalates: Formation of supertetrahedral intercluster compounds. *Angew. Chem., Int. Ed.* **2025**, *64*, e202505511.
[69] Cai, H. Q.; Yang, Q. H.; Chen, L. L.; Gao, R. L.; Liao, M. H.; Xing, J. S.; Zhou, W. B.; Pu, N.; Gu, J.; Huang, Y. C. Polyoxometalates-derived Pt–Mo_2C cluster heterostructure for co-catalytic alkaline hydrogen evolution reaction. *Rare Met.* **2025**, *44*, 4701–4711.
[70] Cherevan, A. S.; Nandan, S. P.; Roger, I.; Liu, R. J.; Streb, C.; Eder, D. Polyoxometalates on functional substrates: Concepts, synergies, and future perspectives. *Adv. Sci.* **2020**, *7*, 1903511.
[71] Wang, Z. C.; Zhang, S. S.; Xie, H. Y.; Zhang, N.; Wang, W. J.; Li, S. L.; Xin, X. Dispersing hydrophobic copper nanoclusters in aqueous solutions triggered by polyoxometalate with aggregation-induced emission properties. *Colloids Surf. A: Physicochem. Eng. Asp.* **2023**, *664*, 131147.
[72] Chen, W. J.; Li, H. F.; Jin, Y. Z.; Lei, W. J.; Bai, Q. Y.; Ma, P. T.; Wang, J. P.; Niu, J. Y. Construction of hexameric Ru-substitution POMs to improve photocatalytic H_2 evolution. *Inorg. Chem.* **2023**, *62*, 18079–18086.
[73] Gusmão, F. M. B.; Mladenović, D.; Radinović, K.; Santos, D. M. F.; Šljukić, B. Polyoxometalates as electrocatalysts for electrochemical energy conversion and storage. *Energies* **2022**, *15*, 9021.
[74] Meng, G.; Jin, M. M.; Wei, T. R.; Liu, Q.; Zhang, S. S.; Peng, X. Y.; Luo, J.; Liu, X. J. MoC nanocrystals confined in N-doped carbon nanosheets toward highly selective electrocatalytic nitric oxide reduction to ammonia. *Nano Res.* **2022**, *15*, 8890–8896.
[75] Tang, Y. J.; Zhu, H. J.; Dong, L. Z.; Zhang, A. M.; Li, S. L.; Liu, J.; Lan, Y. Q. Solid-phase hot-pressing of POMs-ZIFs precursor and derived phosphide for overall water splitting. *Appl. Catal. B: Environ.* **2019**, *245*, 528–535.
[76] Hu, M. L.; Wang, Z. N.; Li, M. L.; Pan, K. M.; Li, L. P. Nano-pom-pom multiphasic MoS_2 grown on carbonized wood as electrode for efficient hydrogen evolution in acidic and alkaline media. *Int. J. Hydrogen Energy* **2021**, *46*, 28087–28097.
[77] Liu, Y.; Yue, C. L.; Sun, F. Y.; Bao, W. J.; Chen, L. L.; Zeb, Z.; Wang, C. Z.; Ma, S. Y.; Zhang, C.; Sun, D. F. et al. Superhydrophilic molybdenum phosphide quantum dots on porous carbon matrix for boosting hydrogen evolution reaction. *Chem. Eng. J.* **2023**, *454*, 140105.
[78] Ma, D. F.; He, Z. Y.; Wei, T.; Wang, L.; Li, Y.; Yurievich, K. V.; Anton, R.; Bian, T.; Yan, S. T. Constructing of crystalline CoP/amorphous CoMoP coupling composites for efficient water splitting. *Int. J. Hydrogen Energy* **2024**, *51*, 479–489.
[79] Kang, Q. L.; Lai, D. W.; Su, M. F.; Xiong, B. R.; Tang, W. Y.; Lu, Q. Y.; Gao, F. Tailored dodecahedral polyoxometalates nanoframes with *in situ* encapsulated Co, N, C for oxygen evolution reaction. *Chem. Eng. J.* **2022**, *430*, 133116.
[80] Sun, Z. X.; Wang, R.; Kozhevnikov, I. V. Versatile POMOF-based materials: Synthesis, mechanism, topology and catalytic applications. *Coord. Chem. Rev.* **2025**, *524*, 216304.
[81] Kamata, K.; Sugahara, K. Base catalysis by mono- and polyoxometalates. *Catalysts* **2017**, *7*, 345.
[82] Li, H. Y.; Guo, J.; Li, Z. S.; Wang, J. S. Research progress of hydrogen production technology and related catalysts by electrolysis of water. *Molecules* **2023**, *28*, 5010.
[83] Zheng, Y.; Jiao, Y.; Vasileff, A.; Qiao, S. Z. The hydrogen evolution reaction in alkaline solution: From theory, single crystal models, to practical electrocatalysts. *Angew. Chem., Int. Ed.* **2018**, *57*, 7568–7579.
[84] Hu, C. L.; Zhang, L.; Gong, J. L. Recent progress made in the mechanism comprehension and design of electrocatalysts for alkaline water splitting. *Energy Environ. Sci.* **2019**, *12*, 2620–2645.
[85] Cai, Q. M.; Gao, R. L.; Wang, Y. F.; Xing, J. S.; Zhang, Q. Y.; Zhu, M. Z.; Qin, X. Y.; Liao, M. H.; Huang, Y. C. Ruthenium containing polyoxometalates: From synthesis, structures, properties to functional applications. *Polyoxometalates* **2025**, *4*, 9140083.
[86] Wang, X. S.; Zheng, Y.; Sheng, W. C.; Xu, Z. J.; Jaroniec, M.; Qiao, S. Z. Strategies for design of electrocatalysts for hydrogen evolution under alkaline conditions. *Mater. Today* **2020**, *36*, 125–138.
[87] Xu, H. G.; Zhang, X. Y.; Ding, Y. L.; Fu, H. Q.; Wang, R.; Mao, F. X.; Liu, P. F.; Yang, H. G. Rational design of hydrogen evolution reaction electrocatalysts for commercial alkaline water electrolysis. *Small Struct.* **2023**, *4*, 2200404.
[88] Zhu, J.; Hu, L. S.; Zhao, P. X.; Lee, L. Y. S.; Wong, K. Y. Recent advances in electrocatalytic hydrogen evolution using nanoparticles. *Chem. Rev.* **2020**, *120*, 851–918.
[89] Zhou, B. H.; Gao, R. J.; Zou, J. J.; Yang, H. M. Surface design strategy of catalysts for water electrolysis. *Small* **2022**, *18*, 2202336.
[90] Gao, G. L.; Zhu, G.; Chen, X. L.; Sun, Z. X.; Cabot, A. Optimizing Pt-based alloy electrocatalysts for improved hydrogen evolution performance in alkaline electrolytes: A comprehensive review. *ACS Nano* **2023**, *17*, 20804–20824.
[91] Li, C. Q.; Baek, J. B. Recent advances in noble metal (Pt, Ru, and Ir)-based electrocatalysts for efficient hydrogen evolution reaction. *ACS Omega* **2020**, *5*, 31–40.
[92] Bhunia, K.; Chandra, M.; Kumar Sharma, S.; Pradhan, D.; Kim, S. J. A critical review on transition metal phosphide based catalyst for electrochemical hydrogen evolution reaction: Gibbs free energy, composition, stability, and true identity of active site. *Coord. Chem. Rev.* **2023**, *478*, 214956.
[93] Wu, H. M.; Feng, C. Q.; Zhang, L.; Zhang, J. J.; Wilkinson, D. P. Non-noble metal electrocatalysts for the hydrogen evolution reaction in water electrolysis. *Electrochem. Energy Rev.* **2021**, *4*, 473–507.
[94] Li, K.; Liu, T.; Ying, J.; Tian, A. X.; Wang, X. L. Recent research progress on polyoxometalate-based electrocatalysts in energy generation. *J. Mater. Chem. A* **2024**, *12*, 13576–13604.
[95] Hua, W.; Sun, H. H.; Xu, F.; Wang, J. G. A review and perspective on molybdenum-based electrocatalysts for hydrogen evolution reaction. *Rare Met.* **2020**, *39*, 335–351.
[96] Dey, C. Polyoxometalate clusters: Inorganic ligands for functional materials. *J. Cluster Sci.* **2022**, *33*, 1839–1856.
[97] Sun, R. Z.; Chen, J. X.; Huang, S. L.; Weng, W. T.; Wu, H. P.; Cai, P. W.; Wen, Z. H.; Zheng, S. T. Dissecting structural modification effects on the electrocatalytic hydrogen evolution reaction activity of atomically precise polyoxometalates. *CCS Chem.* **2025**, *7*, 1216–1226.
[98] Liu, Q. D.; Wang, X. Precise assembly of polyoxometalates at single-cluster levels. *Angew. Chem., Int. Ed.* **2023**, *62*, e202217764.
[99] Ueda, T. Polyoxometalates in analytical sciences. *Anal. Sci.* **2021**, *37*, 107–118.
[100] Yang, L.; Xu, M. Z.; Wang, H. N.; Zhang, D. P.; Zhou, Z. Polyoxometalate-based frameworks: Construction strategies and photocatalytic applications. *ChemCatChem* **2024**, *16*, e202400006.
[101] Ameen, S.; Tahir, A.; Haq, T. U.; Khan, A. A.; Butt, M. T. Z.; Hussain, I.; Hussain, S. Z.; Rehman, H. U. Driving sustainable energy: The role of polyoxometalates (POMs) in photoelectrochemical hydrogen production. *Coord. Chem. Rev.* **2025**, *523*, 216265.
[102] Hu, H. B.; Lian, L. F.; Ji, X.; Zhao, W. L.; Li, H. Q.; Chen, W.; Miras, H. N.; Song, Y. F. Polyoxometalate (POM)-based battery materials: Correlation between dimensionality of support material and energy storage performance. *Coord. Chem. Rev.* **2024**, *503*, 215640.
[103] Biboum, R. N.; Keita, B.; Franger, S.; Nanseu Njiki, C. P.; Zhang, G. J.; Zhang, J.; Liu, T. B.; Mbomekalle, I. M.; Nadjo, L. Pd^0@polyoxometalate nanostructures as green electrocatalysts: Illustrative example of hydrogen production. *Materials* **2010**, *3*, 741–754.

[104] Zhang, Y.; Liu, Y. F.; Wang, D.; Liu, J. C.; Zhao, J. W.; Chen, L. J. State-of-the-art advances in the syntheses, structures, and applications of polyoxometalate-based metal-organic frameworks. *Polyoxometalates* **2023**, *2*, 9140017.
[105] Huang, B.; Yang, D. H.; Han, B. H. Application of polyoxometalate derivatives in rechargeable batteries. *J. Mater. Chem. A* **2020**, *8*, 4593–4628.
[106] Zhang, Y.; Liu, J.; Li, S. L.; Su, Z. M.; Lan, Y. Q. Polyoxometalate-based materials for sustainable and clean energy conversion and storage. *EnergyChem* **2019**, *1*, 100021.
[107] Guo, S.; Pan, C. W.; Hou, M.; Hou, Y. T.; Yao, S.; Lu, T. B.; Zhang, Z. M. Dual regulation of sensitizers and cluster catalysts in metal-organic frameworks to boost H_2 evolution. *Angew. Chem., Int. Ed.* **2025**, *64*, e202420398.
[108] Wu, C. X.; Yan, L. K.; Zhang, T.; Su, Z. M. Redox and acidic properties of chalcogenido-substituted mixed-metal polyoxoanions: A DFT study of α-$[PW_{11}O_{39}ME]^{4-}$ (M = Nb, Ta; E = O, S, Se). *Inorg. Chem. Front.* **2015**, *2*, 246–253.
[109] Bibi, R.; Nazir, S.; Shafiq, S.; Zafar, I.; Mohany, M.; Al-Rejaie, S. S.; ul Ain, Q.; Bano, N.; Rani, S.; Shafiq, M. et al. A novel supramolecular Co-EDTA and Ni-anderson polyoxometalate hybrid as a high-performance electrocatalyst for alkaline water splitting. *Mater. Res. Bull.* **2025**, *186*, 113329.
[110] Gautam, J.; Liu, Y.; Gu, J.; Ma, Z. Y.; Zha, J.; Dahal, B.; Zhang, L. N.; Chishti, A. N.; Ni, L. B.; Diao, G. W. et al. Fabrication of polyoxometalate anchored zinc cobalt sulfide nanowires as a remarkable bifunctional electrocatalyst for overall water splitting. *Adv. Funct. Mater.* **2021**, *31*, 2106147.
[111] Li, S. B.; Zhang, L.; Lan, Y. Q.; O'Halloran, K. P.; Ma, H. Y.; Pang, H. J. Polyoxometalate-encapsulated twenty-nuclear silver-tetrazole nanocage frameworks as highly active electrocatalysts for the hydrogen evolution reaction. *Chem. Commun.* **2018**, *54*, 1964–1967.
[112] Qin, H. Y.; Ye, Y. K.; Li, J. H.; Jia, W. Q.; Zheng, S. Y.; Cao, X. J.; Lin, G. L.; Jiao, L. F. Synergistic engineering of doping and vacancy in $Ni(OH)_2$ to boost urea electrooxidation. *Adv. Funct. Mater.* **2023**, *33*, 2209698.
[113] Wang, Y. J.; Cheng, X.; Ma, N. N.; Cheng, W. Y.; Zhang, P.; Luo, F.; Shi, W. X.; Yao, S.; Lu, T. B.; Zhang, Z. M. *In situ* growth of metal-organic layer on polyoxometalate-etching Cu_2O to boost CO_2 reduction with high stability. *Angew. Chem., Int. Ed.* **2025**, *64*, e202423204.
[114] Berardi, S.; Carraro, M.; Sartorel, A.; Modugno, G.; Bonchio, M. Hybrid polyoxometalates: Merging organic and inorganic domains for enhanced catalysis and energy applications. *Israel J. Chem.* **2011**, *51*, 259–274.
[115] Liang, Y.; Zhang, Z.; Su, X. F.; Feng, X.; Xing, S. Z.; Liu, W.; Huang, R.; Liu, Y. W. Coordination defect-induced frustrated lewis pairs in polyoxo-metalate-based metal-organic frameworks for efficient catalytic hydrogenation. *Angew. Chem., Int. Ed.* **2023**, *62*, e202309030.
[116] Jeffries, W. R.; Jawaid, A. M.; Vaia, R. A.; Knappenberger, K. L. Thickness-dependent electronic relaxation dynamics in solution-phase redox-exfoliated MoS_2 heterostructures. *J. Chem. Phys.* **2024**, *160*, 144707.
[117] Wang, X. F.; Cao, T. T.; Xie, T. H.; Huang, Z. G.; Yu, H. G. Keggin-type polyoxometalate based coordination polymers of 3,5-bis(1',2',4'-triazol-1'-yl)pyridine: Synthesis, structures and electrochemical properties. *J. Mol. Struct.* **2025**, *1336*, 142055.
[118] Shen, H. W.; Huang, Y. C.; Zhao, P. C.; Gao, R. L.; Wei, Z. Y.; Gao, X. H.; Liao, M. H.; Dai, W. J.; Liu, X. Z.; Sui, D. S. et al. Ultralow-loading platinum catalysts anchored by lacunary POMs proton pumps for proton exchange membrane water electrolysis. *Adv. Funct. Mater.* **2026**, *36*, e14862.
[119] Yang, L.; Lei, J.; Fan, J. M.; Yuan, R. M.; Zheng, M. S.; Chen, J. J.; Dong, Q. F. The intrinsic charge carrier behaviors and applications of polyoxometalate clusters based materials. *Adv. Mater.* **2021**, *33*, 2005019.
[120] Bagheri, A. R.; Aramesh, N.; Chen, J. S.; Liu, W. N.; Shen, W.; Tang, S.; Lee, H. K. Polyoxometalate-based materials in extraction, and electrochemical and optical detection methods: A review. *Anal. Chim. Acta* **2022**, *1209*, 339509.
[121] Yan, K.; Yu, Z. H.; Wang, Y. Y.; Guo, M. Y.; Xiong, J.; Zhang, R.; Li, X. Y.; Lu, X. B. Polyoxometalates@metal-organic frameworks: Synthesis strategies, nanostructure modulation and application in biomass conversion. *ChemSusChem* **2025**, *18*, e202401456.
[122] Chen, L. L.; Huang, Y. C.; Wang, J. J.; Liao, M. H.; Liu, Z. Y.; Liu, M. Q.; Cai, H. Q.; Wang, L.; Gao, L. D.; Hu, D. W. et al. Growth behavior and electronic regulation of Pt on various Mo-based supports for hydrogen evolution electrocatalysis. *Sci. China Chem.* **2025**, *68*, 1837–1846.
[123] Chen, Y.; Li, F. B.; Li, S. B.; Zhang, L.; Sun, M. A review of application and prospect for polyoxometalate-based composites in electrochemical sensor. *Inorg. Chem. Commun.* **2022**, *135*, 109084.
[124] Zhu, S.; Yang, F. Insights into the host-guest systems of single-walled-carbon-nanotube-confined polyoxometalates. *Cell Rep. Phys. Sci.* **2024**, *5*, 101780.
[125] Wang, C. Z.; Wang, B.; Yang, H.; Wan, Y.; Fang, H. Q.; Bao, W. J.; Wang, W. L.; Wang, N.; Lu, Y. K. A review on polyoxometalates-based materials in addressing challenges faced by electrochemical energy storage systems. *Chem. Eng. J.* **2024**, *483*, 149143.
[126] Hu, Y. L.; Wang, Y. Y.; Zhao, J. W.; Chen, L. J. Recent advances of polyoxometalate-based materials applied for electron-related devices. *Coord. Chem. Rev.* **2024**, *506*, 215724.
[127] Hu, X. Y.; Tian, X. M.; Lin, Y. W.; Wang, Z. H. Nickel foam and stainless steel mesh as electrocatalysts for hydrogen evolution reaction, oxygen evolution reaction and overall water splitting in alkaline media. *RSC Adv.* **2019**, *9*, 31563–31571.
[128] Obodo, R. M.; Shinde, N. M.; Chime, U. K.; Ezugwu, S.; Nwanya, A. C.; Ahmad, I.; Maaza, M.; Ejikeme, P. M.; Ezema, F. I. Recent advances in metal oxide/hydroxide on three-dimensional nickel foam substrate for high performance pseudocapacitive electrodes. *Curr. Opin. Electrochem.* **2020**, *21*, 242–249.
[129] Cui, L. P.; Wang, Y. W.; Yu, K.; Ma, Y. J.; Zhou, B. B. A multi-active site subnano heterostructures catalyst grown *in situ* POM and $Fe_{0.2}Ni_{0.8}Co_2O_4$ onto nickel foam toward efficient electrocatalytic overall water splitting. *Adv. Funct. Mater.* **2024**, *34*, 2408968.
[130] Wu, Q. L.; Yan, X. C.; Jia, Y.; Yao, X. D. Defective carbon-based materials: Controllable synthesis and electrochemical applications. *EnergyChem* **2021**, *3*, 100059.
[131] Zang, D. J.; Gao, X. J.; Li, L. Y.; Wei, Y. G.; Wang, H. Q. Confined interface engineering of self-supported Cu@N-doped graphene for electrocatalytic CO_2 reduction with enhanced selectivity towards ethanol. *Nano Res.* **2022**, *15*, 8872–8879.
[132] Yin, Y. K.; Hou, X. Y.; Wu, B. Z.; Dong, J. J.; Yao, M. G. Heterogeneous structured nanomaterials from carbon and related materials. *Adv. Funct. Mater.* **2024**, *34*, 2411472.
[133] Liu, H. M.; Liu, C.; Zong, X.; Chen, K. T.; Yao, W. D.; Su, Y. H.; Qian, H. Y.; Wang, Y. F.; Chou, S. L.; Hu, Z. Z. et al. Highly efficient water splitting with polyoxometalate coated on deliberately designed porous carbon as a bifunctional electrocatalyst. *ChemistrySelect* **2022**, *7*, e202202382.
[134] Gautam, J.; Liu, Y.; Gu, J.; Ma, Z. Y.; Dahal, B.; Nabi Chishti, A.; Ni, L. B.; Diao, G. W.; Wei, Y. G. Three-dimensional nano assembly of nickel cobalt sulphide/polyaniline@polyoxometalate/reduced graphene oxide hybrid with superior lithium storage and electrocatalytic properties for hydrogen evolution reaction. *J. Colloid Interface Sci.* **2022**, *614*, 642–654.
[135] Sakthinathan, I.; Köhling, J.; Wagner, V.; McCormac, T. Layer-by-layer construction of a nanoarchitecture by polyoxometalates and polymers: Enhanced electrochemical hydrogen evolution reaction. *ACS Appl. Mater. Interfaces* **2023**, *15*, 2861–2872.
[136] Lin, Y. Y.; Zhu, Y. L.; Ma, Q.; Ke, X. L.; Ma, P. W.; Liao, R. F.;

Liu, S. H.; Wu, D. C. Self-supporting electrocatalyst film based on self-assembly of heterogeneous bottlebrush and polyoxometalate for efficient hydrogen evolution reaction. *Macromol. Rapid Commun.* **2022**, *43*, 2100915.
[137] Feng, L.; Liu, Q.; Xu, G. Y.; Ge, M.; Bi, W. T.; Huang, Y.; Zhang, J.; Liu, X. Y.; Chen, S.; Nie, F. J. et al. Manipulating the dynamic proton transport in electrocatalysis at the nanoscale. *ACS Catal.* **2025**, *15*, 4394–4402.
[138] Sun, N. N.; Shah, S. S. A.; Lin, Z. Y.; Zheng, Y. Z.; Jiao, L.; Jiang, H. L. MOF-based electrocatalysts: An overview from the perspective of structural design. *Chem. Rev.* **2025**, *125*, 2703–2792.
[139] Zhang, Q.; Li, F. Y.; Xu, L. Application of polyoxometalates in third-generation solar cells. *Polyoxometalates* **2023**, *2*, 9140018.
[140] Budnikova, Y. H. Recent advances in metal-organic frameworks for electrocatalytic hydrogen evolution and overall water splitting reactions. *Dalton Trans.* **2020**, *49*, 12483–12502.
[141] Shi, W. X.; Fan, H. R.; Liu, W. R.; Qi, Y. Z.; Cui, M. Y.; Lu, T. B.; Zhang, Z. M. Polyoxometalate directional etching for fabricating defect hollow metal-organic framework with hierarchical structure. *Adv. Mater.* **2025**, *37*, 2509925.
[142] Tang, P. Q.; Li, X.; Liu, R.; Wang, Y. R.; Yuan, X. Y.; Qian, Y. Z.; Hao, J. C. Electrochemical performance of polyoxometalate-based composite materials fabricated by a localization-coating strategy. *Colloids Surf. A: Physicochem. Eng. Asp.* **2025**, *720*, 137071.
[143] Nohra, B.; El Moll, H.; Rodriguez Albelo, L. M.; Mialane, P.; Marrot, J.; Mellot-Draznieks, C.; O'Keeffe, M.; Ngo Biboum, R.; Lemaire, J.; Keita, B. et al. Polyoxometalate-based metal organic frameworks (POMOFs): Structural trends, energetics, and high electrocatalytic efficiency for hydrogen evolution reaction. *J. Am. Chem. Soc.* **2011**, *133*, 13363–13374.
[144] Jia, B. B.; Zhang, B. H.; Cai, Z.; Yang, X. Y.; Li, L. D.; Guo, L. Construction of amorphous/crystalline heterointerfaces for enhanced electrochemical processes. *eScience* **2023**, *3*, 100112.
[145] Vrubel, H.; Hu, X. L. Molybdenum boride and carbide catalyze hydrogen evolution in both acidic and basic solutions. *Angew. Chem., Int. Ed.* **2012**, *51*, 12703–12706.
[146] Kawashima, K.; Márquez, R. A.; Smith, L. A.; Vaidyula, R. R.; Carrasco-Jaim, O. A.; Wang, Z. Q.; Son, Y. J.; Cao, C. L.; Mullins, C. B. A review of transition metal boride, carbide, pnictide, and chalcogenide water oxidation electrocatalysts. *Chem. Rev.* **2023**, *123*, 12795–13208.
[147] Anjum, M. A. R.; Lee, M. H.; Lee, J. S. Boron- and nitrogen-codoped molybdenum carbide nanoparticles imbedded in a BCN network as a bifunctional electrocatalyst for hydrogen and oxygen evolution reactions. *ACS Catal.* **2018**, *8*, 8296–8305.
[148] Bird, M. A.; Goodwin, S. E.; Walsh, D. A. Best practice for evaluating electrocatalysts for hydrogen economy. *ACS Appl. Mater. Interfaces* **2020**, *12*, 20500–20506.
[149] Tran, V. V.; Lee, D.; Bui, V. K. H.; Tran, N. T.; Truong, H. B.; Do, H. H. Review-recent advancements in molybdenum carbides for efficient hydrogen evolution reaction. *J. Electrochem. Soc.* **2024**, *171*, 056509.
[150] Chen, L. L.; Huang, Y. C.; Ding, Y. P.; Yu, P.; Huang, F.; Zhou, W. B.; Wang, L. M.; Jiang, Y. Y.; Li, H. T.; Cai, H. Q. et al. Interfacial engineering of atomic platinum-doped molybdenum carbide quantum dots for high-rate and stable hydrogen evolution reaction in proton exchange membrane water electrolysis. *Nano Res.* **2023**, *16*, 12186–12195.
[151] Yan, H. J.; Xie, Y.; Jiao, Y. Q.; Wu, A. P.; Tian, C. G.; Zhang, X. M.; Wang, L.; Fu, H. G. Holey reduced graphene oxide coupled with an Mo_2N–Mo_2C heterojunction for efficient hydrogen evolution. *Adv. Mater.* **2018**, *30*, 1704156.
[152] Li, J. S.; Tang, Y. J.; Liu, C. H.; Li, S. L.; Li, R. H.; Dong, L. Z.; Dai, Z. H.; Bao, J. C.; Lan, Y. Q. Polyoxometalate-based metal-organic framework-derived hybrid electrocatalysts for highly efficient hydrogen evolution reaction. *J. Mater. Chem. A* **2016**, *4*, 1202–1207.
[153] Gao, X. Q.; Chen, Y. T.; Wang, Y. J.; Zhao, L. Y.; Zhao, X. Y.; Du, J.; Wu, H. X.; Chen, A. B. Next-generation green hydrogen: Progress and perspective from electricity, catalyst to electrolyte in electrocatalytic water splitting. *Nano-Micro Lett.* **2024**, *16*, 237.
[154] Niu, S. S.; Yang, J.; Qi, H. F.; Su, Y.; Wang, Z. Y.; Qiu, J. S.; Wang, A. Q.; Zhang, T. Single-atom Pt promoted Mo_2C for electrochemical hydrogen evolution reaction. *J. Energy Chem.* **2021**, *57*, 371–377.
[155] Jia, W.; Zhang, J. L.; Lu, Z. J.; Wang, S. Q.; Feng, S. Z. Pt decorated POMOF-derived constructions for efficient electrocatalytic hydrogen evolution. *Nanoscale* **2020**, *12*, 3902–3906.
[156] Huang, Y. C.; Hu, J.; Xu, H. X.; Bian, W.; Ge, J. X.; Zang, D. J.; Cheng, D. J.; Lv, Y. K.; Zhang, C.; Gu, J. et al. Fine tuning electronic structure of catalysts through atomic engineering for enhanced hydrogen evolution. *Adv. Energy Mater.* **2018**, *8*, 1800789.
[157] Yue, C. L.; Feng, C.; Sun, G. X.; Liu, N.; Hao, H. Y.; Bao, W. J.; Zhang, X. W.; Sun, F. Y.; Zhang, C.; Bi, J. H. et al. Hierarchically stabilized Pt single-atom catalysts induced by an atomic substitution strategy for an efficient hydrogen evolution reaction. *Energy Environ. Sci.* **2024**, *17*, 5227–5240.
[158] Zhao, X. J.; Zhang, Q. J.; Huang, X. Y.; Ding, L.; Yang, W. T.; Wang, C. T.; Pan, Q. H. Polyoxometalate@ZIF-67 derived carbon-based catalyst for efficient electrochemical overall seawater splitting and oxygen reduction. *Int. J. Hydrogen Energy* **2022**, *47*, 2178–2186.
[159] Yang, X.; Cheng, J.; Yang, X.; Xu, Y.; Sun, W. F.; Zhou, J. H. Facet-tunable coral-like Mo_2C catalyst for electrocatalytic hydrogen evolution reaction. *Chem. Eng. J.* **2023**, *451*, 138977.
[160] Liao, M. H.; Zhu, Q. G.; Li, Y. Y.; Yan, Q. Z.; Zhou, S. S.; Dai, J. J.; Huang, Y. C.; Gu, J. Polyoxometalates hydrogels derived porous conductive Pt@Mo_2C carbon aerogels as self-supporting electrocatalysts for enhancing alkaline hydrogen evolution reaction. *Rare Met.* **2025**, *44*, 8609–8618.
[161] Li, J. C.; Wang, X. Y.; Wang, Y.; Zhao, Y. C.; Ma, C. H.; Zhan, T. Z.; Chen, L. H.; Zhao, C. Q.; Lan, J.; Xiao, Z. C. et al. Highly-dispersed Ni, N-doped Mo_2C nanoparticles prepared from organic-derived polyoxomolybdates for efficient electrocatalytic hydrogen evolution. *Int. J. Hydrogen Energy* **2022**, *47*, 28915–28923.
[162] Yang, X.; Cheng, J.; Li, H.; Xu, Y.; Sun, W. F.; Tu, W. F.; Zhou, J. H. "Tip effect" of hexagram-like Co-doped MoC heterostructure for hydrogen evolution reaction. *Appl. Surf. Sci.* **2023**, *627*, 157284.
[163] Zeng, M. Q.; Chen, Y. X.; Li, J. X.; Xue, H. F.; Mendes, R. G.; Liu, J. X.; Zhang, T.; Rümmeli, M. H.; Fu, L. 2D WC single crystal embedded in graphene for enhancing hydrogen evolution reaction. *Nano Energy* **2017**, *33*, 356–362.
[164] Yan, G.; Wu, C. X.; Tan, H. Q.; Feng, X. J.; Yan, L. K.; Zang, H. Y.; Li, Y. G. N-Carbon coated P–W_2C composite as efficient electrocatalyst for hydrogen evolution reactions over the whole pH range. *J. Mater. Chem. A* **2017**, *5*, 765–772.
[165] Ma, T.; Cao, H.; Li, S.; Cao, S. J.; Zhao, Z. Y.; Wu, Z. H.; Yan, R.; Yang, C. D.; Wang, Y.; van Aken, P. A. et al. Crystalline lattice-confined atomic Pt in metal carbides to match electronic structures and hydrogen evolution behaviors of platinum. *Adv. Mater.* **2022**, *34*, 2206368.
[166] Salah, A.; Zhang, L. N.; Tan, H. Q.; Yu, F. Y.; Lang, Z. L.; Al-Ansi, N.; Li, Y. G. Advanced Ru/Ni/WC@NPC multi-interfacial electrocatalyst for efficient sustainable hydrogen and chlor-alkali Co-production. *Adv. Energy Mater.* **2022**, *12*, 2200332.
[167] Yue, C. L.; Liu, N.; Li, Y. P.; Liu, Y.; Sun, F. Y.; Bao, W. J.; Tuo, Y.; Pan, Y.; Jiang, P.; Zhou, Y. et al. From atomic bonding to heterointerfaces: Co_2P/WC constructed by lacunary polyoxometalates induced strategy as efficient hydrogen evolution electrocatalysts at all pH values. *J. Colloid Interface Sci.* **2023**, *645*, 276–286.
[168] Yao, R. Q.; Zhao, H. Y.; Yu, F. Y.; Zhang, W.; Yan, G.; Li, Y. Q.; Wang, Y. H.; Tan, H. Q.; Li, Y. G. Interfacial engineering of Ni/WC

heterostructure electrocatalyst for highly efficient hydrogen evolution reaction in all pH electrolyte. *J. Alloys Compd.* **2024**, *972*, 172827.

[169] Kawashima, K.; Milton, A. E. F.; Archer, J. S.; Collins, D. T.; Serrat, N. L.; Chukwuneke, C. E.; Marquez, R. A.; Smith, L. A.; Mullins, C. B. Incidental and intentional transformation: Transition metal pnictide and chalcogenide electrocatalysts for alkaline hydrogen evolution. *ACS Energy Lett.* **2024**, *9*, 6126–6143.

[170] Anantharaj, S.; Kundu, S.; Noda, S. Progress in nickel chalcogenide electrocatalyzed hydrogen evolution reaction. *J. Mater. Chem. A* **2020**, *8*, 4174–4192.

[171] Jia, H. W.; Meng, L. H.; Lu, Y. L.; Liang, T. Y.; Yuan, Y.; Hu, Y. F.; Dong, Z. K.; Zhou, Y. Z.; Guan, P. Y.; Zhou, L. et al. Boosting the efficiency of electrocatalytic water splitting via *in situ* grown transition metal sulfides: A review. *J. Mater. Chem. A* **2024**, *12*, 28595–28617.

[172] Kumar, P.; García, A.; Praserthdam, S.; Praserthdam, P. A comprehensive review and perspective of recent research developments, and accomplishments on structural-based catalysts; 1D, 2D, and 3D nanostructured electrocatalysts for hydrogen energy production. *Int. J. Hydrogen Energy* **2024**, *88*, 638–657.

[173] Jia, Y. H.; Zhang, Y. C.; Xu, H. Q.; Li, J.; Gao, M.; Yang, X. T. Recent advances in doping strategies to improve electrocatalytic hydrogen evolution performance of molybdenum disulfide. *ACS Catal.* **2024**, *14*, 4601–4637.

[174] Ding, Q.; Song, B.; Xu, P.; Jin, S. Efficient electrocatalytic and photoelectrochemical hydrogen generation using MoS_2 and related compounds. *Chem* **2016**, *1*, 699–726.

[175] Chen, L. L.; Huang, Y. C.; Wang, J. J.; Liao, M. H.; Huang, S. X.; Cai, H. Q.; Wang, L.; Zhao, L. M.; Pu, N.; Fan, Z. J. Platinum-dependent 2H-to-1T phases conversion of MoS_2 nanosheets growing on cross-interlocking porous carbon for boosting hydrogen evolution reaction. *Chem. Eng. J.* **2024**, *498*, 155060.

[176] Kazemi, A.; Manteghi, F.; Tehrani, Z. Metal electrocatalysts for hydrogen production in water splitting. *ACS Omega* **2024**, *9*, 7310–7335.

[177] Ma, C. H.; Zhu, S. S.; Zhao, Y. C.; Wang, X. Y.; Zhan, T. Z.; Chen, L. H.; Wang, J. N.; Ling, Q.; Xiao, Z. C.; Wu, X. F. et al. CoS_2–MoS_2 nanoflower arrays for efficient hydrogen evolution reaction in the universal pH range. *Langmuir* **2024**, *40*, 744–750.

[178] Wang, P.; Wang, T.; Xu, M.; Gao, Z.; Li, H. Y.; Li, B. W.; Wang, Y. Q.; Qu, C. Q.; Feng, M. Keplerate polyoxomolybdate nanoball mediated controllable preparation of metal-doped molybdenum disulfide for electrocatalytic hydrogen evolution in acidic and alkaline media. *Chin. Chem. Lett.* **2024**, *35*, 108930.

[179] Zhen, Q. F.; Pang, H. J.; Hu, S. M.; Jin, Z. X.; Wu, Q.; Ma, H. Y.; Wang, X. M.; Yang, G. X.; Yu, Z. P. Hierarchical heterometallic sulfur/selenide electrocatalysts derived from polyoxometalate for enhanced hydrogen production performance. *Cryst. Growth Des.* **2024**, *24*, 3809–3816.

[180] Hou, Y.; Xin, J. J.; Gómez-García, C. J.; Xiao, B. X.; Pang, H. J.; Ma, H. Y.; Wang, X. M.; Tan, L. C. A facile strategy to create electrocatalysts of highly dispersive Ni–Mo sulfide nanosheets on graphene by derivation of polyoxometalate coordination polymer for advanced H_2 evolution. *ACS Appl. Energy Mater.* **2021**, *4*, 13191–13198.

[181] Theerthagiri, J.; Lee, S. J.; Murthy, A. P.; Madhavan, J.; Choi, M. Y. Fundamental aspects and recent advances in transition metal nitrides as electrocatalysts for hydrogen evolution reaction: A review. *Curr. Opin. Solid State Mater. Sci.* **2020**, *24*, 100805.

[182] Zheng, Y.; Li, X. X.; Pi, C. R.; Song, H.; Gao, B.; Chu, P. K.; Huo, K. F. Recent advances of two-dimensional transition metal nitrides for energy storage and conversion applications. *FlatChem* **2020**, *19*, 100149.

[183] Lv, Z.; Tahir, M.; Lang, X. W.; Yuan, G.; Pan, L.; Zhang, X. W.; Zou, J. J. Well-dispersed molybdenum nitrides on a nitrogen-doped carbon matrix for highly efficient hydrogen evolution in alkaline media. *J. Mater. Chem. A* **2017**, *5*, 20932–20937.

[184] Liu, Z. Y.; Chen, L. L.; Huang, S. X.; Liu, M. Q.; Ye, Q. M.; Huang, Y. C. A strongly coupled Pt–W_2N heterostructure embedded in porous carbon nanoflowers for seawater electrolysis. *Sci. China Mater.* **2025**, *68*, 3626–3637.

[185] Miao, J.; Lang, Z. L.; Zhang, X. Y.; Kong, W. G.; Peng, O. W.; Yang, Y.; Wang, S. P.; Cheng, J. J.; He, T. C.; Amini, A. et al. Polyoxometalate-derived hexagonal molybdenum nitrides (MXenes) supported by boron, nitrogen codoped carbon nanotubes for efficient electrochemical hydrogen evolution from seawater. *Adv. Funct. Mater.* **2019**, *29*, 1805893.

[186] Zhou, W. B.; Huang, Y. C.; Cai, H. Q.; Wang, T.; Li, H. T.; Zhang, C.; Zhao, L. M.; Chen, L. L.; Liao, M. H.; Tang, Z. Q. et al. A strongly coupled cluster heterostructure with Pt–N–Mo bonding for durable and efficient H_2 evolution in anion-exchange membrane water electrolyzers. *Nano-Micro Lett.* **2025**, *17*, 296.

[187] Huang, Y. C.; Zhou, W. B.; Kong, W. C.; Chen, L. L.; Lu, X. L.; Cai, H. Q.; Yuan, Y. R.; Zhao, L. M.; Jiang, Y. Y.; Li, H. T. et al. Atomically interfacial engineering on molybdenum nitride quantum dots decorated N-doped graphene for high-rate and stable alkaline hydrogen production. *Adv. Sci.* **2022**, *9*, 2204949.

[188] Chen, D.; Lu, R. H.; Pu, Z. H.; Zhu, J. W.; Li, H. W.; Liu, F.; Hu, S.; Luo, X.; Wu, J. S.; Zhao, Y. et al. Ru-doped 3D flower-like bimetallic phosphide with a climbing effect on overall water splitting. *Appl. Catal. B: Environ.* **2020**, *279*, 119396.

[189] Song, H.; Guo, M. S.; Wang, J. F.; Liu, Y. Q.; Bi, H. X.; Du, J.; An, W. T.; Ma, Y. Y.; Han, Z. G. Reduced phosphomolybdate as photoassisted electrochemical crystalline sensor for trace Cr(VI) detection. *Polyoxometalates* **2024**, *3*, 9140065.

[190] N, D. B.; S, M. K. K.; P, S. K.; Budagumpi, S.; Kota, S.; Reddy, M. B. M.; Nagaraju, D. H. Advanced transition metal phosphide-based materials for hydrogen evolution reactions: A comprehensive review. *Ionics* **2025**, *31*, 3965–4005.

[191] Xiong, K.; Gao, Y.; Chen, J.; Shen, Y.; Zhang, H. D. Ordered porous Ni *in situ* decorated by thin-layer amorphous nickel-phosphorus via mild electrochemical-phosphorization for enhancing the hydrogen evolution performance. *Chem. Commun.* **2020**, *56*, 611–614.

[192] Wang, D. Z.; Zhang, X. Y.; Zhang, D. Z.; Shen, Y. L.; Wu, Z. Z. Influence of Mo/P Ratio on CoMoP nanoparticles as highly efficient HER catalysts. *Appl. Catal. A: Gen.* **2016**, *511*, 11–15.

[193] Zhang, H. M.; Wang, J. J.; Meng, Y. Q.; Sun, J. F. Recent advances in amorphous metal phosphide electrocatalysts for hydrogen evolution reaction. *Int. J. Hydrogen Energy* **2022**, *47*, 36084–36097.

[194] Xiong, K.; Yu, L. J.; Xiang, Y.; Zhang, H. D.; Chen, J.; Gao, Y. Cerium-incorporated Ni_2P nanosheets for enhancing hydrogen production from overall water splitting and urea electrolysis. *J. Alloys Compd.* **2022**, *912*, 165234.

[195] Aldajani, A. M. O.; Bahri, M.; Kozhevnikova, E. F.; Kozhevnikov, I. V. Polyoxometalates as catalyst precursors for reverse water gas shift. *Appl. Catal. A: Gen.* **2025**, *699*, 120285.

[196] Anjum, M. A. R.; Lee, J. S. Sulfur and nitrogen dual-doped molybdenum phosphide nanocrystallites as an active and stable hydrogen evolution reaction electrocatalyst in acidic and alkaline media. *ACS Catal.* **2017**, *7*, 3030–3038.

[197] Zou, L. L.; Wei, Y. S.; Hou, C. C.; Li, C. X.; Xu, Q. Single-atom catalysts derived from metal-organic frameworks for electrochemical applications. *Small* **2021**, *17*, 2004809.

[198] Zhao, Y. X.; Wen, J. H.; Li, P.; Xiang, Y.; Li, M. Q.; Wang, S. N.; Dou, J. M.; Li, Y. W.; Ma, H. Y.; Xu, L. Q. Polyoxometalate derived bimetallic phosphide electrocatalysts for high-efficiency hydrogen evolution reaction. *Inorg. Chem. Front.* **2024**, *11*, 7512–7524.

[199] Li, J.; Shao, Y.; Liu, G. Y.; Zhang, X. J.; Li, X.; Li, Y. T.; Su, Z. M. Green preparation of high-efficiency mesoporous MoP electrocatalyst for hydrogen evolution. *Int. J. Hydrogen Energy* **2024**, *94*, 1130–1135.

[200] Liu, R. J.; Streb, C. Polyoxometalate-single atom catalysts (POM-SACs) in energy research and catalysis. *Adv. Energy Mater.* **2021**, *11*, 2101120.
[201] Zhao, Y. Q.; Ling, T.; Chen, S. M.; Jin, B.; Vasileff, A.; Jiao, Y.; Song, L.; Luo, J.; Qiao, S. Z. Non-metal single-iodine-atom electrocatalysts for the hydrogen evolution reaction. *Angew. Chem., Int. Ed.* **2019**, *58*, 12252–12257.
[202] Jin, Y. S.; Wang, H. T.; Li, J. J.; Yue, X.; Han, Y. J.; Shen, P. K.; Cui, Y. Porous MoO_2 nanosheets as non-noble bifunctional electrocatalysts for overall water splitting. *Adv. Mater.* **2016**, *28*, 3785–3790.
[203] Bai, C. Z.; Ren, S.; Zhou, Y. L.; Jiang, L. Y.; Yu, Q.; Dong, H. F. Polyoxometalate-single atom catalysts (POM-SACs): Synthetic strategies and energy catalytic applications. *Mol. Catal.* **2025**, *582*, 115203.
[204] Ma, J. Y.; Chang, Z. H.; Xi, X.; Liang, J. J.; Lin, Y. C.; Zhu, Y. L.; Wang, X. L. Reconstruction and immobilization of polymolybdate induced by metal-organic coordination units for enhanced electrocatalytic hydrogen generation. *Inorg. Chem. Front.* **2024**, *11*, 8925–8934.
[205] Abbas, F.; Wei, Y. G. Thermodynamic stability, catalytic activity, kinetics and electronic properties of Polyoxometalate (TM@V-POM) for efficient electrochemical hydrogen evolution reactions: A DFT understanding. *Int. J. Hydrogen Energy* **2025**, *117*, 1–11.
[206] Zhang, Z. R.; Sui, H. Y.; Shi, W. X.; Ren, J.; Yao, S.; Lu, T. B.; Zhang, Z. M. Polyoxometalate-based single-atom catalyst with precise structure and extremely exposed active site for efficient H_2 evolution. *Angew. Chem., Int. Ed.* **2025**, *64*, e202416711.
[207] Rani, S.; AlMasoud, N.; Alomar, T. S.; Nadeem, M.; Bhatti, M. H.; Munawar, K. S.; Tariq, M.; Muhammad Asif, H.; Sohail, M. Synthesis of heterogeneous mesoporous tetrafunctionalalized porphyrin-aliphatic diamine based framework encapsulated vanadium containing POM as electrocatalyst for hydrogen and oxygen evolution reactions. *J. Electroanal. Chem.* **2024**, *967*, 118445.
[208] Chen, S. S.; Ma, C.; Xu, J. B.; Du, X.; Liu, Y. Z.; Sham, T. K.; Zhang, H.; Peng, Y.; Huang, Y. N.; Wågberg, T. et al. Subnanometric Pt–W bimetallic clusters for efficient alkaline hydrogen evolution electrocatalysis. *ACS Nano* **2024**, *18*, 33696–33705.
[209] Li, S. B.; Liang, J. W.; Tan, X. G.; Li, F. B.; Wang, X. M.; Ma, L.; Zhang, L.; Cheng, K. Modulating electrodeposition of ultralow Pt into 2D MoCu-POMOF-derived MoO_2/MoOC for boosted hydrogen evolution reaction. *Int. J. Hydrogen Energy* **2024**, *51*, 1128–1137.
[210] Wen, Y.; Li, C. X.; Wang, J.; Qian, Y. Y.; Shen, F. C. Hierarchically self-supporting phosphorus-doped $CoMoO_4$ nanoflowers arrays toward efficient hydrogen evolution reaction. *ACS Appl. Energy Mater.* **2022**, *5*, 6814–6822.
[211] Yan, Y. Y.; Du, J. Y.; Li, C. Y.; Yang, J.; Xu, Y. K.; Wang, M. L.; Li, Y. P.; Wang, T.; Li, X. S.; Zhang, X. M. et al. H-buffer effects boosting H-spillover for efficient hydrogen evolution reaction. *Energy Environ. Sci.* **2024**, *17*, 6024–6033.
[212] Sultan, S.; Tiwari, J. N.; Singh, A. N.; Zhumagali, S.; Ha, M. R.; Myung, C. W.; Thangavel, P.; Kim, K. S. Single atoms and clusters based nanomaterials for hydrogen evolution, oxygen evolution reactions, and full water splitting. *Adv. Energy Mater.* **2019**, *9*, 1900624.
[213] Guo, T. Q.; Li, L. D.; Wang, Z. C. Recent development and future perspectives of amorphous transition metal-based electrocatalysts for oxygen evolution reaction. *Adv. Energy Mater.* **2022**, *12*, 2200827.
[214] Yoon, H.; Ju, B.; Kim, D. W. Perspectives on the development of highly active, stable, and cost-effective OER electrocatalysts in acid. *Battery Energy* **2023**, *2*, 20230017.
[215] Cao, R. G.; Lee, J. S.; Liu, M. L.; Cho, J. Recent progress in non-precious catalysts for metal-air batteries. *Adv. Energy Mater.* **2012**, *2*, 816–829.
[216] Vilà-Nadal, L.; Cronin, L. Design and synthesis of polyoxometalate-framework materials from cluster precursors. *Nat. Rev. Mater.* **2017**, *2*, 17054.
[217] Zhang, Y.; Guo, H. R.; Ren, J. K.; Li, X. P.; Ren, W. L.; Song, R. MoO_3 crystal facets modulation by doping heteroatom Fe from polyoxometalate for quasi-industrial oxygen evolution reaction. *Appl. Catal. B: Environ.* **2021**, *298*, 120582.
[218] Sood, P.; Joshi, A.; Singh, M. A rare polyoxometalate cluster $[NiW_{12}O_{44}]^{14-}$ based solid as a pre-catalyst for efficient and long-term oxygen evolution. *Nanoscale Adv.* **2022**, *4*, 5015–5020.
[219] Luo, W. J.; Hu, J.; Diao, H. L.; Schwarz, B.; Streb, C.; Song, Y. F. Robust polyoxometalate/nickel foam composite electrodes for sustained electrochemical oxygen evolution at high pH. *Angew. Chem., Int. Ed.* **2017**, *56*, 4941–4944.
[220] Marques, I. S.; Jarrais, B.; Mbomekallé, I. M.; Teillout, A. L.; de Oliveira, P.; Freire, C.; Fernandes, D. M. Synergetic effects of mixed-metal polyoxometalates@carbon-based composites as electrocatalysts for the oxygen reduction and the oxygen evolution reactions. *Catalysts* **2022**, *12*, 440.
[221] Li, N.; Liu, J.; Dong, B. X.; Lan, Y. Q. Polyoxometalate-based compounds for photo- and electrocatalytic applications. *Angew. Chem., Int. Ed.* **2020**, *59*, 20779–20793.
[222] Zhang, S. W.; Ou, F. X.; Ning, S.; Cheng, P. Polyoxometalate-based metal-organic frameworks for heterogeneous catalysis. *Inorg. Chem. Front.* **2021**, *8*, 1865–1899.
[223] Han, X. B.; Wang, D. X.; Gracia-Espino, E.; Luo, Y. H.; Tan, Y. Z.; Lu, D. F.; Li, Y. G.; Wågberg, T.; Wang, E. B.; Zheng, L. S. Fe-substituted cobalt-phosphate polyoxometalates as enhanced oxygen evolution catalysts in acidic media. *Chin. J. Catal.* **2020**, *41*, 853–857.
[224] Zhang, Y.; Guo, H. R.; Yuan, P. F.; Pang, K. L.; Cao, B. X.; Wu, X.; Zheng, L. R.; Song, R. Structural evolution of $CoMoO_4$ to CoOOH by ion electrochemical etching for boosting oxygen evolution reaction. *J. Power Sources* **2019**, *442*, 227252.
[225] Song, Y. F.; Tsunashima, R. Recent advances on polyoxometalate-based molecular and composite materials. *Chem. Soc. Rev.* **2012**, *41*, 7384–7402.
[226] Ibrahim, K. B.; Tsai, M. C.; Chala, S. A.; Berihun, M. K.; Kahsay, A. W.; Berhe, T. A.; Su, W. N.; Hwang, B. J. A review of transition metal-based bifunctional oxygen electrocatalysts. *J. Chin. Chem. Soc.* **2019**, *66*, 829–865.
[227] Xiong, W.; Yin, H. H.; Wu, T. X.; Li, H. Challenges and opportunities of transition metal oxides as electrocatalysts. *Chem. - Eur. J.* **2023**, *29*, e202202872.
[228] Song, J. J.; Wei, C.; Huang, Z. F.; Liu, C. T.; Zeng, L.; Wang, X.; Xu, Z. J. A review on fundamentals for designing oxygen evolution electrocatalysts. *Chem. Soc. Rev.* **2020**, *49*, 2196–2214.
[229] Yang, C. D.; Gao, Y.; Ma, T.; Bai, M. R.; He, C.; Ren, X. C.; Luo, X. L.; Wu, C. Z.; Li, S.; Cheng, C. Metal alloys-structured electrocatalysts: Metal-metal interactions, coordination microenvironments, and structural property-reactivity relationships. *Adv. Mater.* **2023**, *35*, 2301836.
[230] Zhang, A.; Liang, Y. X.; Zhang, H.; Geng, Z. G.; Zeng, J. Doping regulation in transition metal compounds for electrocatalysis. *Chem. Soc. Rev.* **2021**, *50*, 9817–9844.
[231] Enferadi-Kerenkan, A.; Do, T. O.; Kaliaguine, S. Heterogeneous catalysis by tungsten-based heteropoly compounds. *Catal. Sci. Technol.* **2018**, *8*, 2257–2284.
[232] Wang, Y. Y.; Wang, Y.; Zhang, L.; Liu, C. S.; Pang, H. PBA@POM hybrids as efficient electrocatalysts for the oxygen evolution reaction. *Chem. - Asian J.* **2019**, *14*, 2790–2795.
[233] Gautam, J.; Kannan, K.; Meshesha, M. M.; Dahal, B.; Subedi, S.; Ni, L. B.; Wei, Y. G.; Yang, B. L. Heterostructure of polyoxometalate/zinc-iron-oxide nanoplates as an outstanding bifunctional electrocatalyst for the hydrogen and oxygen evolution reaction. *J. Colloid Interface Sci.* **2022**, *618*, 419–430.

[234] Lu, Y. K.; Guo, X. X.; Yang, L. Y.; Yang, W. F.; Sun, W. T.; Tuo, Y.; Zhou, Y.; Wang, S. T.; Pan, Y.; Yan, W. F. et al. Highly efficient CoMoS heterostructure derived from vertically anchored Co_5Mo_{10} polyoxometalate for electrocatalytic overall water splitting. *Chem. Eng. J.* **2020**, *394*, 124849.

[235] Hou, J. G.; Zhang, B.; Li, Z. W.; Cao, S. Y.; Sun, Y. Q.; Wu, Y. Z.; Gao, Z. M.; Sun, L. C. Vertically aligned oxygenated-CoS_2–MoS_2 heteronanosheet architecture from polyoxometalate for efficient and stable overall water splitting. *ACS Catal.* **2018**, *8*, 4612–4621.

[236] He, R. Z.; Huang, X. Y.; Feng, L. G. Recent progress in transition-metal sulfide catalyst regulation for improved oxygen evolution reaction. *Energy Fuels* **2022**, *36*, 6675–6694.

[237] Guo, J. Y.; Haghshenas, Y.; Jiao, Y. R.; Kumar, P.; Yakobson, B. I.; Roy, A.; Jiao, Y.; Regenauer-Lieb, K.; Nguyen, D.; Xia, Z. H. Rational design of earth-abundant catalysts toward sustainability. *Adv. Mater.* **2024**, *36*, 2407102.

[238] Jamal, F.; Rafique, A.; Moeen, S.; Haider, J.; Nabgan, W.; Haider, A.; Imran, M.; Nazir, G.; Alhassan, M.; Ikram, M. et al. Review of metal sulfide nanostructures and their applications. *ACS Appl. Nano Mater.* **2023**, *6*, 7077–7106.

[239] Zhang, Y.; Zhou, Q.; Zhu, J. X.; Yan, Q. Y.; Dou, S. X.; Sun, W. P. Nanostructured metal chalcogenides for energy storage and electrocatalysis. *Adv. Funct. Mater.* **2017**, *27*, 1702317.

[240] Shit, S.; Chhetri, S.; Jang, W.; Murmu, N. C.; Koo, H.; Samanta, P.; Kuila, T. Cobalt sulfide/nickel sulfide heterostructure directly grown on nickel foam: An efficient and durable electrocatalyst for overall water splitting application. *ACS Appl. Mater. Interfaces* **2018**, *10*, 27712–27722.

[241] Han, X. B.; Tang, X. Y.; Lin, Y.; Gracia-Espino, E.; Liu, S. G.; Liang, H. W.; Hu, G. Z.; Zhao, X. J.; Liao, H. G.; Tan, Y. Z. et al. Ultrasmall abundant metal-based clusters as oxygen-evolving catalysts. *J. Am. Chem. Soc.* **2019**, *141*, 232–239.

[242] Limani, N.; Marques, I. S.; Jarrais, B.; Fernandes, A. J. S.; Freire, C.; Fernandes, D. M. Cobalt phosphotungstate-based composites as bifunctional electrocatalysts for oxygen reactions. *Catalysts* **2022**, *12*, 357.

[243] Wang, W.; Cai, M. X.; Wang, T.; Hou, S.; Huang, X. J.; Wang, Z. R.; Lu, Z. Y.; He, P. L. Cobalt polyoxometalates anchored on nife-LDH nanoplates as highly active and stable bifunctional catalysts for overall water splitting. *Adv. Mater. Technol.* **2024**, *9*, 2301607.

[244] Zhang, J. Y.; Zhang, X. F.; Ma, Z.; Fang, K.; Wang, L. Q.; Ni, H.; Zhao, B. POM-intercalated NiFe-LDH as enhanced OER catalyst for highly efficient and durable water electrolysis at ampere-scale current densities. *ACS Catal.* **2025**, *15*, 6486–6496.

[245] Cai, Z. Y.; Wang, P.; Zhang, J. J.; Chen, A. Y.; Zhang, J. W.; Yan, Y.; Wang, X. Y. Reinforced layered double hydroxide oxygen-evolution electrocatalysts: A polyoxometallic acid wet-etching approach and synergistic mechanism. *Adv. Mater.* **2022**, *34*, 2110696.

[246] Li, B.; Wen, H. M.; Cui, Y. J.; Zhou, W.; Qian, G. D.; Chen, B. L. Emerging multifunctional metal-organic framework materials. *Adv. Mater.* **2016**, *28*, 8819–8860.

[247] Cai, G. R.; Yan, P.; Zhang, L. L.; Zhou, H. C.; Jiang, H. L. Metal-organic framework-based hierarchically porous materials: Synthesis and applications. *Chem. Rev.* **2021**, *121*, 12278–12326.

[248] Guan, H. Y.; LeBlanc, R. J.; Xie, S. Y.; Yue, Y. F. Recent progress in the syntheses of mesoporous metal-organic framework materials. *Coord. Chem. Rev.* **2018**, *369*, 76–90.

[249] Sun, M. H.; Huang, S. Z.; Chen, L. H.; Li, Y.; Yang, X. Y.; Yuan, Z. Y.; Su, B. L. Applications of hierarchically structured porous materials from energy storage and conversion, catalysis, photocatalysis, adsorption, separation, and sensing to biomedicine. *Chem. Soc. Rev.* **2016**, *45*, 3479–3563.

[250] Laeim, H.; Molahalli, V.; Prajongthat, P.; Pattanaporkratana, A.; Pathak, G.; Phettong, B.; Hongkarnjanakul, N.; Chattham, N. Porosity tunable metal-organic framework (MOF)-based composites for energy storage applications: Recent progress. *Polymers* **2025**, *17*, 130.

[251] Du, J.; Li, F.; Sun, L. C. Metal-organic frameworks and their derivatives as electrocatalysts for the oxygen evolution reaction. *Chem. Soc. Rev.* **2021**, *50*, 2663–2695.

[252] Sun, F. Z.; Wang, G.; Ding, Y. Q.; Wang, C.; Yuan, B. B.; Lin, Y. Q. NiFe-based metal-organic framework nanosheets directly supported on nickel foam acting as robust electrodes for electrochemical oxygen evolution reaction. *Adv. Energy Mater.* **2018**, *8*, 1800584.

[253] Du, D. Y.; Qin, J. S.; Li, S. L.; Su, Z. M.; Lan, Y. Q. Recent advances in porous polyoxometalate-based metal-organic framework materials. *Chem. Soc. Rev.* **2014**, *43*, 4615–4632.

[254] Xiang, W. L.; Zhang, Y. P.; Chen, Y. F.; Liu, C. J.; Tu, X. Synthesis, characterization and application of defective metal-organic frameworks: Current status and perspectives. *J. Mater. Chem. A* **2020**, *8*, 21526–21546.

[255] Abdelkader-Fernández, V. K.; Fernandes, D. M.; Balula, S. S.; Cunha-Silva, L.; Freire, C. Advanced framework-modified POM@ZIF-67 nanocomposites as enhanced oxygen evolution reaction electrocatalysts. *J. Mater. Chem. A* **2020**, *8*, 13509–13521.

[256] Song, J. X.; Zhu, P. F.; Ma, W. M.; Li, Y. X. PW_6Mo_6/ZIF-67@NF composite with exposed Co nodes as efficient oxygen evolution reaction electrocatalyst. *Int. J. Hydrogen Energy* **2024**, *51*, 327–337.

[257] Yue, K. H.; Lu, R. H.; Gao, M. B.; Song, F.; Dai, Y.; Xia, C. F.; Mei, B. B.; Dong, H. L.; Qi, R. J.; Zhang, D. L. et al. Polyoxometalated metal-organic framework superstructure for stable water oxidation. *Science* **2025**, *388*, 430–436.

[258] Ahmad, W.; Ahmad, N.; Wang, K.; Aftab, S.; Hou, Y. P.; Wan, Z. W.; Yan, B. B.; Pan, Z.; Gao, H. L.; Peung, C. et al. Electron-sponge nature of polyoxometalates for next-generation electrocatalytic water splitting and nonvolatile neuromorphic devices. *Adv. Sci.* **2024**, *11*, 2304120.

[259] Vij, V.; Sultan, S.; Harzandi, A. M.; Meena, A.; Tiwari, J. N.; Lee, W. G.; Yoon, T.; Kim, K. S. Nickel-based electrocatalysts for energy-related applications: Oxygen reduction, oxygen evolution, and hydrogen evolution reactions. *ACS Catal.* **2017**, *7*, 7196–7225.

[260] Jiao, Y. Q.; Yan, H. J.; Tian, C. G.; Fu, H. G. Structure engineering and electronic modulation of transition metal interstitial compounds for electrocatalytic water splitting. *Acc. Mater. Res.* **2023**, *4*, 42–56.

[261] Chandrasekaran, S.; Yao, L.; Deng, L. B.; Bowen, C.; Zhang, Y.; Chen, S. M.; Lin, Z. Q.; Peng, F.; Zhang, P. X. Recent advances in metal sulfides: From controlled fabrication to electrocatalytic, photocatalytic and photoelectrochemical water splitting and beyond. *Chem. Soc. Rev.* **2019**, *48*, 4178–4280.

[262] Li, Y. Q.; Yin, Z. H.; Cui, M.; Liu, X.; Xiong, J. B.; Chen, S. R.; Ma, T. L. Interface engineering of transitional metal sulfide-MoS_2 heterostructure composites as effective electrocatalysts for water-splitting. *J. Mater. Chem. A* **2021**, *9*, 2070–2092.

[263] Jin, M.; Zou, Y.; Shi, B. C.; Liu, T. T.; Tang, Y. J. Laser-induced preparation of anderson-type polyoxometalate-derived sulfide/oxide electrocatalysts for electrochemical water oxidation. *ChemSusChem* **2024**, *17*, e202301862.

[264] Gao, Q. S.; Zhang, W. B.; Shi, Z. P.; Yang, L. C.; Tang, Y. Structural design and electronic modulation of transition-metal-carbide electrocatalysts toward efficient hydrogen evolution. *Adv. Mater.* **2019**, *31*, 1802880.

[265] Humagain, G.; MacDougal, K.; MacInnis, J.; Lowe, J. M.; Coridan, R. H.; MacQuarrie, S.; Dasog, M. Highly efficient, biochar-derived molybdenum carbide hydrogen evolution electrocatalyst. *Adv. Energy Mater.* **2018**, *8*, 1801461.

[266] Wang, Y. F.; Wu, Q. M.; Zhang, B. C.; Tian, L.; Li, K. X.; Zhang, X. L. Recent advances in transition metal carbide electrocatalysts for oxygen evolution reaction. *Catalysts* **2020**, *10*, 1164.

[267] Das, C.; Sinha, N.; Roy, P. Transition metal non-oxides as electrocatalysts: Advantages and challenges. *Small* **2022**, *18*, 2202033.

[268] Tang, Y. J.; Liu, C. H.; Huang, W.; Wang, X. L.; Dong, L. Z.; Li, S. L.; Lan, Y. Q. Bimetallic carbides-based nanocomposite as superior electrocatalyst for oxygen evolution reaction. *ACS Appl. Mater. Interfaces* **2017**, *9*, 16977–16985.
[269] Geng, K. Y.; He, T.; Liu, R. Y.; Dalapati, S.; Tan, K. T.; Li, Z. P.; Tao, S. S.; Gong, Y. F.; Jiang, Q. H.; Jiang, D. L. Covalent organic frameworks: Design, synthesis, and functions. *Chem. Rev.* **2020**, *120*, 8814–8933.
[270] Li, S. S.; Gao, Y. Q.; Li, N.; Ge, L.; Bu, X. H.; Feng, P. Y. Transition metal-based bimetallic MOFs and MOF-derived catalysts for electrochemical oxygen evolution reaction. *Energy Environ. Sci.* **2021**, *14*, 1897–1927.
[271] Zhang, W. M.; Zhao, X. Y.; Zhao, Y. W.; Zhang, J. Q.; Li, X. T.; Fang, L. D.; Li, L. Mo-doped Zn, Co zeolitic imidazolate framework-derived Co_9S_8 quantum dots and MoS_2 embedded in three-dimensional nitrogen-doped carbon nanoflake arrays as an efficient trifunctional electrocatalysts for the oxygen reduction reaction, oxygen evolution reaction, and hydrogen evolution reaction. *ACS Appl. Mater. Interfaces* **2020**, *12*, 10280–10290.
[272] Zeb, Z.; Huang, Y. C.; Chen, L. L.; Gao, R. L.; Gao, X. H.; Sun, M. D.; Cai, H. Q.; Chen, J. C.; Abbas, F.; Liao, M. H. et al. Polyoxometalates metal-organic frameworks-derived transition metal sulfides with rich interfaces for efficient alkaline oxygen evolution reaction. *J. Colloid Interface Sci.* **2025**, *686*, 289–303.
[273] Hu, Q. Y.; Zhou, H. S.; Ding, Y.; Wågberg, T.; Han, X. B. Advances in bridging homogeneous and heterogeneous water oxidation catalysis by insolubilized polyoxometalate clusters. *ACS Catal.* **2024**, *14*, 5898–5910.
[274] Liu, F.; Shi, C. X.; Guo, X. L.; He, Z. X.; Pan, L.; Huang, Z. F.; Zhang, X. W.; Zou, J. J. Rational design of better hydrogen evolution electrocatalysts for water splitting: A review. *Adv. Sci.* **2022**, *9*, 2200307.
[275] Quan, L.; Jiang, H.; Mei, G. L.; Sun, Y. J.; You, B. Bifunctional electrocatalysts for overall and hybrid water splitting. *Chem. Rev.* **2024**, *124*, 3694–3812.
[276] Fareed, I.; Khan, M. D.; Firdous, M.; Maqsood, T.; Farooq, M. U. H.; Tahir, M.; Butt, F. K.; Zou, J. J.; Du, S. F. Fundamentals and perspectives on materials for bifunctional electrocatalysis. *Adv. Sci.* **2025**, *12*, e09902.
[277] Wang, Y. Y.; Yan, D. F.; El Hankari, S.; Zou, Y. Q.; Wang, S. Y. Recent progress on layered double hydroxides and their derivatives for electrocatalytic water splitting. *Adv. Sci.* **2018**, *5*, 1800064.
[278] Yi, H.; Liu, S. Y.; Lai, C.; Zeng, G. M.; Li, M. F.; Liu, X. G.; Li, B. S.; Huo, X. Q.; Qin, L.; Li, L. et al. Recent advance of transition-metal-based layered double hydroxide nanosheets: Synthesis, properties, modification, and electrocatalytic applications. *Adv. Energy Mater.* **2021**, *11*, 2002863.
[279] Gong, M.; Dai, H. J. A mini review of NiFe-based materials as highly active oxygen evolution reaction electrocatalysts. *Nano Res.* **2015**, *8*, 23–39.
[280] Burke, M. S.; Enman, L. J.; Batchellor, A. S.; Zou, S. H.; Boettcher, S. W. Oxygen evolution reaction electrocatalysis on transition metal oxides and (oxy)hydroxides: Activity trends and design principles. *Chem. Mater.* **2015**, *27*, 7549–7558.
[281] Chen, J. Y. C.; Dang, L. N.; Liang, H. F.; Bi, W. L.; Gerken, J. B.; Jin, S.; Alp, E. E.; Stahl, S. S. Operando analysis of NiFe and Fe oxyhydroxide electrocatalysts for water oxidation: Detection of Fe^{4+} by Mössbauer spectroscopy. *J. Am. Chem. Soc.* **2015**, *137*, 15090–15093.
[282] Li, C. L.; Zhang, Z. J.; Liu, R. *In situ* growth of 3D NiFe LDH-POM micro-flowers on nickel foam for overall water splitting. *Small* **2020**, *16*, 2003777.
[283] Zeng, K.; Zheng, X. J.; Li, C.; Yan, J.; Tian, J. H.; Jin, C.; Strasser, P.; Yang, R. Z. Recent advances in non-noble bifunctional oxygen electrocatalysts toward large-scale production. *Adv. Funct. Mater.* **2020**, *30*, 2000503.
[284] Jiao, S. L.; Fu, X. W.; Wang, S. Y.; Zhao, Y. Perfecting electrocatalysts via imperfections: Towards the large-scale deployment of water electrolysis technology. *Energy Environ. Sci.* **2021**, *14*, 1722–1770.
[285] Nejadian, M. M.; Ahmadi, P.; Houshfar, E. Comparative optimization study of three novel integrated hydrogen production systems with SOEC, PEM, and alkaline electrolyzer. *Fuel* **2023**, *336*, 126835.
[286] Gong, S. M.; Meng, Y.; Jin, Z. Y.; Hsu, H. Y.; Du, M. S.; Liu, F. Recent progress on the stability of electrocatalysts under high current densities toward industrial water splitting. *ACS Catal.* **2024**, *14*, 14399–14435.
[287] Gao, D. D.; Trentin, I.; Schwiedrzik, L.; González, L.; Streb, C. The reactivity and stability of polyoxometalate water oxidation electrocatalysts. *Molecules* **2019**, *25*, 157.
[288] Fabre, B.; Falaise, C.; Cadot, E. Polyoxometalates-functionalized electrodes for (photo)electrocatalytic applications: Recent advances and prospects. *ACS Catal.* **2022**, *12*, 12055–12091.
[289] Dada, A. O.; Jones, K. D.; Walsh, D. A.; Newton, G. N. Design and strategies to enhance the electrochemical properties of POM nanomaterials for electrocatalysis. In *Applied Polyoxometalate-based Electrocatalysis*. Fernandes, D. M., Ed.; Wiley-VCH: Weinheim, 2025; pp 27–58.
[290] Li, J. C.; Ma, Y. Q.; Mu, X. G.; Wang, X. J.; Li, Y.; Ma, H. X.; Guo, Z. X. Recent advances and perspectives on coupled water electrolysis for energy-saving hydrogen production. *Adv. Sci.* **2025**, *12*, 2411964.
[291] Wang, Z. Z.; Shen, S. J.; Wang, J. C.; Zhong, W. W. Modulating the D-band center of electrocatalysts for enhanced water splitting. *Chem. -Eur. J.* **2024**, *30*, e202402725.
[292] Wang, P.; Zheng, J.; Xu, X.; Zhang, Y. Q.; Shi, Q. F.; Wan, Y.; Ramakrishna, S.; Zhang, J.; Zhu, L. Y.; Yokoshima, T. et al. Unlocking efficient hydrogen production: Nucleophilic oxidation reactions coupled with water splitting. *Adv. Mater.* **2024**, *36*, 2404806.
[293] Zhao, J. W.; Li, Y. Z.; Chen, L. J.; Yang, G. Y. Research progress on polyoxometalate-based transition-metal-rare-earth heterometallic derived materials: Synthetic strategies, structural overview and functional applications. *Chem. Commun.* **2016**, *52*, 4418–4445.
[294] Yan, H. J.; Tian, C. G.; Sun, L.; Wang, B.; Wang, L.; Yin, J.; Wu, A. P.; Fu, H. G. Small-sized and high-dispersed WN from $[SiO_4(W_3O_9)_4]^{4-}$ clusters loading on GO-derived graphene as promising carriers for methanol electro-oxidation. *Energy Environ. Sci.* **2014**, *7*, 1939–1949.
[295] Yan, H. J.; Xie, Y.; Wu, A. P.; Cai, Z. C.; Wang, L.; Tian, C. G.; Zhang, X. M.; Fu, H. G. Anion-modulated HER and OER activities of 3D Ni–V-based interstitial compound heterojunctions for high-efficiency and stable overall water splitting. *Adv. Mater.* **2019**, *31*, 1901174.
[296] Liu, J.; Goetjen, T. A.; Wang, Q. N.; Knapp, J. G.; Wasson, M. C.; Yang, Y.; Syed, Z. H.; Delferro, M.; Notestein, J. M.; Farha, O. K. et al. MOF-enabled confinement and related effects for chemical catalyst presentation and utilization. *Chem. Soc. Rev.* **2022**, *51*, 1045–1097.
[297] Mialane, P.; Mellot-Draznieks, C.; Gairola, P.; Duguet, M.; Benseghir, Y.; Oms, O.; Dolbecq, A. Heterogenisation of polyoxometalates and other metal-based complexes in metal-organic frameworks: From synthesis to characterisation and applications in catalysis. *Chem. Soc. Rev.* **2021**, *50*, 6152–6220.
[298] Liu, J. L.; Huang, M. Y.; Hua, Z. Y.; Dong, Y.; Feng, Z. R.; Sun, T. D.; Chen, C. X. Polyoxometalate-based metal organic frameworks: Recent advances and challenges. *ChemistrySelect* **2022**, *7*, e202200546.
[299] van Oversteeg, C. H. M.; Doan, H. Q.; de Groot, F. M. F.; Cuk, T. *In situ* X-ray absorption spectroscopy of transition metal based water oxidation catalysts. *Chem. Soc. Rev.* **2017**, *46*, 102–125.

[300] Han, Y.; Zhang, H.; Yu, Y.; Liu, Z. *In situ* characterization of catalysis and electrocatalysis using APXPS. *ACS Catal.* **2021**, *11*, 1464–1484.
[301] Stoerzinger, K. A.; Hong, W. T.; Crumlin, E. J.; Bluhm, H.; Shao-Horn, Y. Insights into electrochemical reactions from ambient pressure photoelectron spectroscopy. *Acc. Chem. Res.* **2015**, *48*, 2976–2983.
[302] Zhou, W. L.; Jiang, J. J.; Cheng, W. R.; Su, H.; Liu, Q. H. *In-situ* synchrotron radiation infrared spectroscopic identification of reactive intermediates over multiphase electrocatalytic interfaces. *Chin. J. Struct. Chem.* **2022**, *41*, 2210004–2210015.
[303] Singha Roy, S.; Nagappan, S.; Satheesan, A. K.; Karmakar, A.; Kundu, S. Surface-enhanced Raman scattering coupled with *in situ* Raman spectroscopy for the detection of the OER mechanism: A mini-review. *J. Phys. Chem. C* **2024**, *128*, 13634–13650.
[304] Yoo, R. M. S.; Yesudoss, D.; Johnson, D.; Djire, A. A review on the application of *in-situ* Raman spectroelectrochemistry to understand the mechanisms of hydrogen evolution reaction. *ACS Catal.* **2023**, *13*, 10570–10601.
[305] Fu, Q.; Wong, L. W.; Zheng, F. Y.; Zheng, X. D.; Tsang, C. S.; Lai, K. H.; Shen, W. Q.; Ly, T. H.; Deng, Q. M.; Zhao, J. Unraveling and leveraging *in situ* surface amorphization for enhanced hydrogen evolution reaction in alkaline media. *Nat. Commun.* **2023**, *14*, 6462.
[306] Mehmood, R.; Zhang, F. X. Recent progress in understanding mechanism of electrochemical oxygen evolution reaction via operando/*in situ* characterizations. *Chem Catal.* **2025**, *5*, 101332.
[307] Zhao, K.; Jiang, X. Y.; Wu, X. Y.; Feng, H. Z.; Wang, X. D.; Wan, Y. Y.; Wang, Z. P.; Yan, N. Recent development and applications of differential electrochemical mass spectrometry in emerging energy conversion and storage solutions. *Chem. Soc. Rev.* **2024**, *53*, 6917–6959.
[308] Pishgar, S.; Gulati, S.; Strain, J. M.; Liang, Y.; Mulvehill, M. C.; Spurgeon, J. M. *In situ* analytical techniques for the investigation of material stability and interface dynamics in electrocatalytic and photoelectrochemical applications. *Small Methods* **2021**, *5*, 2100322.
[309] Kempler, P. A.; Coridan, R. H.; Luo, L. Gas evolution in water electrolysis. *Chem. Rev.* **2024**, *124*, 10964–11007.
[310] Tirumalasetti, P. R.; Weng, F. B.; Dlamini, M. M.; Atabani, A.; Jung, G. B.; Yu, J. W.; Abbas, W.; Hsu, C. Y. A review on performance and two-phase flow in proton exchange membrane water electrolyzers using porous transport layers and high-speed visualization. *Int. J. Hydrogen Energy* **2025**, *144*, 513–521.
[311] Abidi, N.; Bonduelle-Skrzypczak, A.; Steinmann, S. N. Revisiting the active sites at the MoS_2/H_2O interface via grand-canonical DFT: The role of water dissociation. *ACS Appl. Mater. Interfaces* **2020**, *12*, 31401–31410.
[312] Shambhawi; Mohan, O.; Choksi, T. S.; Lapkin, A. A. The design and optimization of heterogeneous catalysts using computational methods. *Catal. Sci. Technol.* **2024**, *14*, 515–532.

Shumao Yuan received his bachelor's degree from Liaocheng University in 2023. He is currently pursuing a joint master's degree under the supervision of Prof. Limin Wu at the Institute of Energy Materials Chemistry, Inner Mongolia University. His research focuses on the design and synthesis of polyoxometalates for electrocatalytic hydrogen evolution and aqueous zinc-ion batteries.

Jiangwei Zhang is currently a "Steed plan High level Talents" Professor, "Grassland Talents", "Inner Mongolia Rejuvenation Talents" of Inner Mongolia, Principle Investigator from College of Energy Material and Chemistry under leadership of Dean Academician Dongyuan Zhao, Inner Mongolia University and Inner Mongolia Advanced Research Institute, Ministry of Education. He received his Ph.D. from Department of Chemistry, Tsinghua University in 2016. He has published 230 innovative publications including in *Science*, *Nat. Catal.*, *J. Am. Chem. Soc.*, *Adv. Mater.*, *Angew. Chem. Int. Ed.*, *Nat. Commun.*, *Energy Environ. Sci.* as corresponding author with H-index = 64. He is consecutively selected as World's Top 2% Scientists in 2024 and 2025. Currently, His researches fuscous on distinctive research in the interdisciplinary field of "Integrating X-ray characterization devices with AI agents to form scientific tools driving the iteration of energy materials."